Summer 2010

Developing new probes for 2DIR spectroscopy

Michael Walt Nydegger
University of Iowa

DEVELOPING NEW PROBES FOR 2DIR SPECTROSCOPY

by

Michael Walt Nydegger

An Abstract

Of a thesis submitted in partial fulfillment
of the requirements for the Doctor of
Philosophy degree in Chemistry
in the Graduate College of
The University of Iowa

July 2010

Thesis Supervisor: Assistant Professor Christopher Cheatum

ABSTRACT

This dissertation presents preliminary work done to characterize new probes for infrared spectroscopy. The probes studied were the C-D stretch transition and the antisymmetric stretch transition of the azide anion. The techniques employed were transient grating spectroscopy and two-dimensional infrared spectroscopy (2DIR). These studies provide information on the lifetime of the chromophores and Fermi Resonances of the chosen oscillators C-D stretch and azide antisymmetric stretch that were observed in the spectra. The first system chosen was a series of deuterated haloforms that include $CDCl_3$, $CDBr_3$ and CDI_3. The vibrational lifetime of all three haloforms was measured in a polar solvent, acetone and a nonpolar solvent, benzene. The results were compared to literature values for their undeuterated haloform counterparts. Upon successful completion of the determination of the lifetimes of the deuterated haloforms, we continued the study of the C-D stretch for deuterated formic acid dissolved in hexane. A 2DIR spectrum of the formic acid –d dimer formed in hexane along with a deperturbation calculation determined the coupling constant between the bright state and dark state. The last system studied was the interaction of 3-azopyridine with a strong acid trifluoroacetic acid (TFA), and a weak acid, formic acid once again 2DIR spectroscopy and a deperturbation calculation determined the coupling constant between bright and dark states.

Abstract Approved: _____
Thesis Supervisor

_____
Title and Department

_____
Date

DEVELOPING NEW PROBES FOR 2DIR SPECTROSCOPY

by

Michael Walt Nydegger

A thesis submitted in partial fulfillment
of the requirements for the Doctor of
Philosophy degree in Chemistry
in the Graduate College of
The University of Iowa

July 2010

Thesis Supervisor: Assistant Professor Christopher Cheatum

Graduate College
The University of Iowa
Iowa City, Iowa

CERTIFICATE OF APPROVAL

PH.D. THESIS

This is to certify that the Ph.D. thesis of

Michael Walt Nydegger

has been approved by the Examining Committee
for the thesis requirement for the Doctor of Philosophy
degree in Chemistry at the July 2010 graduation.

Thesis Committee:
Christopher Cheatum, Thesis Supervisor

Sarah A. Larson

Claudio J. Margulis

Jan U. Rohde

Thomas H. Bogguss

To our unborn children

For the vision is yet for the appointed time; it hastens toward the goal and it will not fail thought it tarries, wait for it; for it will certainly come, it will not delay.

Habakkuk 2:3

ACKNOWLEDGMENTS

To begin with I thank my Lord and Savior, Jesus Christ for His sacrifice for everyone's sins on the cross. I publicly acknowledge that I am a sinner and without Christ's sacrifice on the cross I would be separated from Him forever. I thank God for His gift and for allowing me to accept His gift.

I want to thank my loving wife for her love support and belief in me when I did not believe in myself. I would not want to imagine this time without you. I thank you for being my best friend and the love of my life. Irma, I thank you for all the meals you cooked and all of the hard work you did to make our house feel like home

I thank my parents for their support and encouragement during my life. God could not have made better parents. I thank my sister for being an inspiration to me. You have not had an easy life, however, your faith has never wavered and you continue to persist. Thanks for being an example of persistence.

I would like to thank my advisor Chris Cheatum for his support and faith in me for building the 2DIR experiment not once but twice. Thanks for the cribbage games, and for the times on Macbride fishing. Thanks also for the conversations about everything under the sun and for respecting my opinion as well as teaching me that the words we choose to say as well as write have very specific meaning. I will remember that for it is very important and something I overlook at times.

At this time I would like to thank two very dear friends I have earned here at Iowa, Dr. Kenan Gundogdu and Dr. Jigar Bandaria. Both of you have become younger brothers to me. The day each of you left was a sad day for me. Kenan thanks for teaching me your skill at aligning the experiments as well as the amazing patience you showed me. I value you as a person and friend. Jigar, I am so thankful that God allowed me to be your friend. I will always cherish our time in and out of the lab. You have taught me a great deal about science and I look forward to further conversations with you.

I will have our future children read the Three Investigators' books and tell them about how you and I read them as children half-way around the world.

To Samrat and Mary, you have become valued friend to Irma and I. I thank you for sharing your culture and food with us. Samrat, I already miss our conversations about science, religion and life. May God bless your family this day forth.

Will, I will miss our conversations about sports in particular football. I also will miss working with you on Eleanor, what a machine!!! It is too bad the flood had to split us up.

To my brother in Christ, Brian Hatvick; I thank you for your friendship and prayers. Our conversations and your encouragement during this process have been and will continue to a Blessing. I know God has a plan for your life, for if you hope for what you do not see, with perseverance wait for it eagerly.

Frank Turner, God has blessed me greatly by calling you friend and brother in Christ. What I will miss most about my time at the University of Iowa will be our conversations and prayers together. Working with you in the Spring of 2009, after the flood, has changed my life forever. Words cannot express what a blessing you have been to Irma and me. God be with you always, dear brother!!!!

I would also like to thank all the rest of my colleagues I have encountered in the Cheatum lab: Dr. Sarah Hill, Jameson Kech, Gail Qi and Dominic Hull.

ABSTRACT

This dissertation presents preliminary work done to characterize new probes for infrared spectroscopy. The probes studied were the C-D stretch transition and the antisymmetric stretch transition of the azide anion. The techniques employed were transient grating spectroscopy and two-dimensional infrared spectroscopy (2DIR). These studies provide information on the lifetime of the chromophores and Fermi Resonances of the chosen oscillators C-D stretch and azide antisymmetric stretch that were observed in the spectra. The first system chosen was a series of deuterated haloforms that include $CDCl_3$, $CDBr_3$ and CDI_3. The vibrational lifetime of all three haloforms was measured in a polar solvent, acetone and a nonpolar solvent, benzene. The results were compared to literature values for their undeuterated haloform counterparts. Upon successful completion of the determination of the lifetimes of the deuterated haloforms, we continued the study of the C-D stretch for deuterated formic acid dissolved in hexane. A 2DIR spectrum of the formic acid –d dimer formed in hexane along with a deperturbation calculation determined the coupling constant between the bright state and dark state. The last system studied was the interaction of 3-azopyridine with a strong acid trifluoroacetic acid (TFA), and a weak acid, formic acid once again 2DIR spectroscopy and a deperturbation calculation determined the coupling constant between bright and dark states.

TABLE OF CONTENTS

LIST OF TABLES

Table

LIST OF FIGURES

Figure

LIST OF EQUATIONS

Equation

CHAPTER 1: INTRODUCTION

In order to gain a fundamental understanding of chemical bonding, a detailed look into the vibrational characteristics of molecules is required. For a chemical reaction to occur, a bond must first be broken or dissociate before a new compound can be formed. For a chemical bond to be broken, vibrational energy must be directed or localized into the desired chemical bond's coordinate. This energy must be sufficient to overcome the bond energy that attracts the two atoms together. Upon vibrational excitation of the bond, what happens to its vibrational energy? In other words, what does the excited vibrational state of the molecule resemble? How long does the mode remain excited, in other words, what is the energy flow rate? Does the vibrational energy distribute to other coordinates in the molecule, are other modes of the molecule coupled to the excited coordinate? How does the solvent or bath participate in this? All of these questions can be answered with the use of vibrational spectroscopy. Since the advent of the ultrafast laser, physicists and chemists have the luxury to study vibrational energy on the picosecond to femtosecond time scales. To predict the rates at which energy flows as well as its pathway is the reason why vibrational spectroscopy is an important area of study in chemistry as well as in physics.

To be able to answer the above question and gain more insight into chemical bonding, ideal chromophores must be used. The ideal chromophore has the following characteristics: a large molar absorptivity, sensitive to the solvent, long lifetime, being able to place the chromophore anywhere in the molecule, and finally has a transition in a background free region of the spectrum.

The molar absorptivity sometimes called the extinction coefficient, ε, indicates the strength of the absorption of light by the molecule or chromophore. The extinction coefficient is related to the derivative of the dipole moment with respect to the vibrational coordinate. The dipole moment increases with a greater difference of the

electronegativity between the atom involved in the transition. If the transition can be polarized by the addition of an electronegative group to the oscillator's atoms, the extinction coefficient for the transition can increase. The extinction coefficient can be increased if the transitions of one of the atoms involved in the transition is hybridized. The nonlinear measurements performed, such as transient gratings signal, scales to the fourth power of the molar absorptivity while the 2DIR measurement scales to the fourth power. The ideal chromophore would report on the solvent dynamics to determine the solvent's or bath's role; therefore, the chromophore must have a long lifetime to sample all of the different solvent configurations or environments to measure the solvent dynamics. It would be beneficial to place the chromophore anywhere on or in the molecule so as not to perturb the system. For example, to study the dynamics of the active site of an enzyme, a small enough chromophore that fits inside the active site would be ideal. Lastly, the chormophore's transition would be in a region of the spectrum, (2000-2300) cm^{-1} that is background free.

A possible chromophore would be the C-H stretch that has been studied in a great number of solvents. [1-5] The lifetime of the C-H stretch ranges from 5 ps to over a 100 ps depending on the solvent used; which makes the C-H stretch a candidate chromophore.[6] An advantage as well as a problem with the C-H is its prevalence in molecules. For example, the C-H bonds make up the backbone of enzymes, so exciting the C-H stretch will excite all of the C-H, making it hard to isolate a particular part of the enzyme of interest. The spectral range for the C-H stretch is (3000-3500) cm^{-1}, which happens to be a crowded portion of the infrared vibrational spectrum where other transitions occur such as the O-H and N-H stretch transitions. The molar absorptivity of a C-H stretch is the same as that for the C-D stretch and has been reported as (10-200) cm^{-1}.[7]

The implementation of isotopically labeling chromophores leads to an attractive alternative for chromophores. For example, the C-D, as mentioned above, is a very attractive chromophore because the effect of deuterating the hydrogen, red shifts the C-D

(H) stretch transition by approximately 800 cm^{-1}. This places the transition into a background free part of the spectrum. When deuterating a molecule, the number of modes do not change and the system remains unperturbed. The Romesberg lab has taken advantage of this to study different part of an enzyme.[8-13] There is still the problem with the low extinction coefficient. The use of the C-D stretch for solvent dynamic studies has yet to be determined because the lifetime of the C-D stretch for various molecules and solvent combination has yet to be extensively studied.

The anitsymmetric stretch for a class of anionic chromophores called pseudohalides that include: azide (N_3^-), cyanate (OCN^-), and thiocyanate (SCN^-) yield promise for the ideal chromophore. The antisymmetric stretch of the azide anion, a linear molecule composed of three nitrogen atoms. Being ionic, the pseudohalides have very large extinction coefficients making the antisymmetric stretch of them an attractive chromophore. The extinction coefficient for the azide bound to a number of molecules range from (250-4200) $M^{-1}cm^{-1}$.[7, 14] The antisymmetric stretch lifetime for thiocyanate ranges from (25 -70) ps in polar solvents.[15] The lifetime for azide and cyanate is much shorter, however, limiting the use for solvent dynamics. For comparison the lifetime of azide in D_2O is the same when dissolved in methanol, 2.4 ps.[16] The lifetime for cyanate dissolved in methanol is 3 ps.[16] The thiocyanate has a longer lifetime than azide or cyante in either D_2O or methanol at 18 ps and 11 ps, respectively.[15-17] The pseudohalides are ions, therefore, the generality, of placing it at any desired location of a hydrocarbon such as protein or enzyme, would be difficult. There are studies performed where dynamics of the active site are measured with pseudohalides chromophores.[18-21]

Chapter 2 provides practical guidelines for aligning the ultrafast laser system starting with the optical parametric amplifier (OPA), difference frequency generation (DFG), interferometer; followed by aligning for the signal and lastly the heterodyned measurement. The chapter continues with an introduction and application of the 2DIR

experiment, followed by the origin of the response function. The chapter ends with a description of the Fermi Resonances of vibrational oscillators.

Chapter 3 describes the lifetimes for the deuterated haloforms $CDCl_3$, $CDBr_3$ and CDI_3 dissolved in a polar and nonpolar solvent, acetone and benzene, respectively. A transient grating experiment measures the lifetimes. The vibrational lifetime of the C-D stretch transition is shorter than the corresponding proteated haloforms. The larger number of low order coupled states for the deuterated haloform results in the shorter lifetimes observed.

Chapter 4 describes transient grating and the first one color 2DIR experiments, which characterize the C-D stretch transition for deuterated formic acid dissolved in hexane. The formic acid forms dimers when dissolved in hexane. The C-D stretch of deuterated formic acid has an 11 ps lifetime. The C-D stretch couples strongly to a dark state that contains C-O stretch and the DCO bend of the formic acid dimer ring with a coupling constant of 13 cm^{-1}. Our results suggest that the C-D stretch is a viable probe for 2D IR spectroscopy.

Chapter 5 contains 2DIR spectroscopic information on a synthesized azide pyridine chromophore. The amine of the pyridine ring interacts with a weak acid, formic acid and a strong acid, TFA. The bright state, the azide antisymmetric stretch, couples strongly to dark states composed of ring motions of the pyridine ring. The frequency of the bright state depends on whether the formic acid or TFA interact with the amine on the pyridine ring. The last chapter contains suggestions for further studies pertaining to chapters 4 and 5.

CHAPTER 2: EXPERIMENTAL PROCEDURES AND THEORETICAL BACKGROUND

Experimental Setup for the 2DIR and Transient Grating Experiments

Subpicosecond pulses were used in the experiments contained in this thesis. A commercial Ti:sapphire laser generates pulses centered at 800 nm with a duration of 100 fs at a repetition rate of 1kHz. The energy of each pulse is approximately 1 μJ. A nonlinear technique called optical parametric amplification (OPA) performs down conversion on the 800 nm pulse. The OPA incorporates a type II β-barium oxide crystal cut at 27^{o} to produce signal and idler. Signal and idler combine in a 1 mm thick type II $AgGaS_2$ cut at $\theta = 50^{o}$ for difference frequency generation. Rotation of the face angle of the $AgGaS_2$ crystal will produce pulses between 3-10 μm. The wavelength of light for the C-D stretch transition for the complexes is approximately 4.5 μm. The pulses are nearly transformed limited with a full width half maximum of 150 cm^{-1} yielding a time duration very near to 100 fs. Beam splitters separate the IR beam into three equally energetic arms to produce a three-pulse interferometer with which to perform the transient grating experiment. A reflection off a 3-degree wedged CaF_2 beam splitter is used to create the additional arm used for the local oscillator in the 2D measurement. Corner cube retro reflectors mounted on computer controlled stages control the timing between the pulses. 90-degree off-axis parabolic mirrors focus the three beams unto the sample. The following phase matching condition $\mathbf{-k_1+k_2+k_3}$ dictated the unique direction that produces the signal. Overlapping the 3^{rd} order signal with the local oscillator occurs at a 2" CaF_2 window. Detection of the heterodyned signal takes place with a MCT detector after passing through a monochromator. The homodyne transient grating signal, however, is put onto a MCT detector without going through a monochromator. Both the heterodyned and homodyne transient grating signals with the aid of a gated integrator and

lock in amplifier referenced to a 500 Hz optical chopper, placed in the $\mathbf{k_3}$ path, are isolated and recorded.

The FTIR, transient grating and 2DIR data were analyzed in IGOR (a plotting and data analysis software) to obtain lifetimes for the transient grating and peak positions for the FTIR and 2DIR. For the plotting and finding the peak positions for the 2DIR spectrum a macro was written and can be seen in the appendix. Match the adjustable variable tau1_step in the code to the step size taken for the experiment; also match variable w3_step to the step size in cm^{-1} for the monochromator. Be sure the step size for the monochromator is negative because the monochromator reads from high to low. The lines that read variable low and variable high correspond to the range scanned by the monochromator.

The code to enumerate the state in chapter 3 of this dissertation was written in C++ and also appears in the appendix. The stages are controlled by a computer that runs a in house built Labview code.

Alignment of the Optical Parametric Amplifier (OPA)

The OPA down converts the pulses coming out of the LASER into mid-IR pulses. The pulses are split into three distinct paths in the OPA; the white light path, 1^{st} and 2^{nd} path which are both spatially and temporally overlapped in the β-barium borate (BBO) crystal.

To begin alignment of the optical parametric amplifier (OPA) align the light coming out of the laser passes through all the irises, properly. Place the power meter head just after the cut out hole in the box (see figure 1). The power going into the OPA should be in the range of 800-875 mW. Use the knob on the waveplate outside the OPA to adjust to the proper power (figure 2). Next align the LASER light into the white light portion of the OPA (figure 3). Be sure the first and second pass paths are blocked so as not to burn the β barium borate crystal (BBO). To determine the quality of the white

light place a card behind the lens that focuses the light into the BBO crystal. The white light generated in the sapphire substrate should appear as a rainbow in a ring shape (figure 4) with a bright red ring on the outside. To regulate the quality of the white adjust either the waveplate just after the silica substrate beamsplitter, the iris just prior to the lens that focuses the light into the sapphire substrate (figure 3), or the compression of the laser (figure 5). It may be necessary to adjust all three in order to attain the best white light continuum. If the white light is bright but appears to have defined black rings around the colors or is blurry, adjust the waveplate or iris to remove the black rings or to make it less blurry. After the formation of the white light, focus it into the BBO crystal by adjusting the stage on which sits a lens (figure 3). Once focused into the BBO crystal, adjust the mirror just prior to the iris that controls the quality of the white light and center it through the iris after the BBO crystal (figure 6).

To align the first pass (path), first put the light through the irises to assure straight travel along the holes for both 1^{st} and 2^{nd} paths. Block the white light pass and put a card behind the BBO crystal to determine whether you are focusing too strongly in the first pass. This is observed by monitoring the optical parametric generated light (OPG), which will appear as a bright green halo. The light from the OPG (green halo) surroundings one side of the purplish-blue spot. The purplish-blue spot is the 800 nm light doubled in the crystal and the green halo is the OPG (figure 7). To adjust the power of the first pass change the focusing conditions of the telescope in the first pass (figure 8). The positive lens on the stage will collimate the light. To produce a greater green halo, or more OPG, adjust the stage to so that the lens on the stage moves closer towards the BBO crystal. If you observe white light from only the first pass behind the BBO crystal, block the first pass and move the lens away from the BBO crystal. Prolong generation of white light in the BBO will result in permanently burning the crystal. Adjustment of the telescopes in both the first pass and second pass should not have to be performed too often.

Once the appropriate amount of OPG has been achieved, next unblock the white light and adjust for spatial overlap of the white light and first pass. To do this you will need two point of reference because, there is two adjustments in the first pass that need to be made. The white light being the reference, place the 1st pass (path) onto the white light before and after the BBO crystal. Place a card in front of the BBO crystal, this to align the far mirror in the first pass and center the first pass on top of the white light. This will appear as a large purple circle (5-7 mm) on top of a small (1 mm) bright yellowish-green dot (figure 9). Place the card at the iris just before the second pass timing (figure 6) and adjust the close or near mirror in the first pass till it aligns on top of the white light. Iterate between the two mirrors and the placements of the card, while blocking and unblocking the first pass, to be sure the first pass is collinear to the white light.

Once the first pass and white light pulses have been spatially overlapped, they have to be overlapped temporally. Adjust the first pass timing till a bright green light forms at the iris just prior to the second pass timing (figure 6). If during the entire travel of the first pass timing no green light forms, it stands to reason the spatially overlap of the first pass and white light is poor.

After the appearance of the green light, place the power meter head outside the OPA (figure 10). The power of the first pass with white light, while pumping the OPA with range of 800-875 mW, should in the neighborhood of 4-6mW. In a few rare cases I did achieve greater that 6 mW, however, very rarely. Adjust the pointing of the first pass as well as the first pass timing to achieve the 4-6 mW range. This range is also dependent on how hard one is focusing the first pass or in other words how much OPG is being produced. The power should not fluctuate by more than 0.1 mW.

After maximizing the power of the 1st pass (path) and white light, determine the OPG of the 2nd pass (path) by blocking the 1st pass (path) and the white light and repeating the procedure as performed for the 1st pass (path). Place the card after the BBO

crystal, so between the near mirror of the first pass and the BBO crystal. Upon the card look for the green halo and adjust the telescope in the second pass till a sufficient amount of OPG is formed and no white light is present.

Unblock the first pass and white light to align the second pass. After the first pass and the white light transmit through the BBO crystal the mirror on the 2nd pass timing reflects the white light and the 1st pass at an angle slightly downward back through the BBO crystal and below the entry point of the BBO crystal. Place a card on the side of the BBO crystal closest to the second pass timing as well as below (~2 mm) the entry point of the first pass and white light. It is on this reentry into the BBO crystal that the second pass should be place. Adjust the far mirror so that the second pass aligns on top of the first pass and white light. Place the card after the pick off mirror and before the 800 nm high reflector; adjust the second pass timing till a green light is formed from the first and second pass and the white light.

Place the power meter's head in the location as before (figure 11) to measure the total power of the OPA. Adjust of the 1st and 2nd pass overlaps and timings as will as the OPA rotation angle to optimize the OPA power. The power will range from 170-190 mW.

Alignment of the Difference Frequency Generator (DFG)

The DFG combines both signal and idler into the $AgGaS_2$ crystal and allows adjustment of the spectrum for the experiment. For the DFG to operate properly, the signal and idler have to be both spatially and temporally overlapped. This section is to aid the user in aligning the DFG portion of the experiment.

The OPA generates two pulses, signal and idler whose wavelengths are ~1.1 μm and ~1.7 μm, respectively. The double light from the signal and idler are green and yellow, respectively. Adjustment of the Newport P100-P platform optical mount, sometimes referred to as the pick-off mirror, aligns the light into the DGF by going

through the next iris, as indicated by a arrow in figure12. In figure 12 the white line represents the path of both signal and idler out of the OPA. The optic, just after the iris for aligning into the DFG, is a dichroic mirror, which separates the signal and the idler. The yellow line represents the path of the idler and the green line the path for the signal. The alignment of signal and idler should go through their prospective irises. The timing stage in the path of the signal ensures that both signal and idler are time coincident. Signal and idler will spatially over lap in a dichroic mirror; which reflects the signal and transmits the idler. The iris after the dichroic mirror is to aid in the signal and idler alignment into the DFG crystal. ($AgGaS_2$ type II, $\theta = 50^o$).

First block the path of the idler and pass the signal through the two irises; one before the DFG crystal (figure 12) and one after the DFG crystal (figure 13). Use two mirrors as before in the OPA to align the signal through the irises. This will appear as a pinkish spot after the DFG; and center this on the iris. Next block the signal and repeat the above procedure for the idler, there will appear a yellowish spot after the DFG crystal. The lights seen are not the mid-IR light produced in the DFG crystal but rather from the signal and idler. Unblock the signal and the yellow and pink lights from the signal and idler should be spatially overlapped. The infrared light will pass through a couple of germanium windows (figure 13). The Ge windows serve two purposes, to block the idler and for material compensation. The last Ge window, just prior to the flipper mirror, serves to overlap the red light, from the HeNe LASER, with the IR light produced in the DFG crystal. The red light serves as the tracer, thus the name tracer, traces the path of the IR.

Adjust the flipper mirror (figure 13) so the IR light will be detected on the pyroelectric detector. A BNC cable connects the pyroelectric detector to an oscilloscope which displays the DFG signal. If a DFG signal is not detected the DFG timing stage (figure 12) requires adjustment. If the DFG signal does not appear on the scope after adjusting the timing, one can conclude that the signal and idler are not sufficiently

overlapped. If the signal appears on the scope adjust the following: pointing of the signal, idler, first and second pass, the DFG, 1st, 2nd, timings, the OPA crystal angle, and the compression of the LASER. The DFG signal that appears on the oscilloscope should be maximized. Maximized DFG signal should be 40-80 mV depending on the detector. After the adjustments have been made to maximize the DFG signal, a measurement of the OPA can be performed. The total power out of the OPA should only fall 10-15 mW.

Before moving onto alignment of the interferometer, the red light (HeNe LASER light) and the IR light must be overlapped. The overlap is achieved by use of pyroelectric detectors in the DFG and interferometer boxes. First the gold mirror just after the DFG crystal must be adjusted to optimize the IR light going into the pyroelectric detector just after the flipper mirror. This should be done with the iris just prior to the detector partially shut. Shut the iris to allow approximately 50% of the light to be detected. The flipper mirror should be flipped down to allow the IR and red light into the interferometer. Next place the mirror on the magnetic post should be put in place between axis one and axis two (figure 14). Align the red light through the irises and into the far pyroelectric detector as indicated by figure 15. The far pyroelectric detector should be connected into the 2nd channel of the oscilloscope. Adjustment of the gold mirror, just prior to the Ge window, that overlaps the red light and IR light so as to optimize the signal on the far pyroelectric detector. When the signal is optimized for the far detector, adjustment of the flipper mirror is made to send light into the detector in the DFG box. Iterate the procedure of optimizing between the pyroelectric detector in the DFG box and the far pyroelectric detector till the signal does not change between the two detectors. Place the power meter's head in the beam of the IR light, outside the DFG, the reading should be between 3.5 - 6 mW.

Alignment of the Interferometer

The interferometer controls the timings in the experiment as well as forms the box car geometry (figure 16). Coated ZnSe windows serve as beamsplitter to create three equally energetic axes and a reflection from an 1-inch CaF_2 three-degree wedge generates the local oscillator. All four axes have a retro-reflector atop a computer-controlled stage. An increase in the path length will delay the pulse where a decrease in path length causes the pulse to come sooner.

After the red light and IR light are over lapped; remove the mirror from the magnetic base and center the red light on the irises prior to the periscope. Axis 1 (figure 14) is the first to be aligned. Use the retro-reflector on the computer-controlled stage to adjust the light through the iris in front of the 1 inch round mirror that directs the light into the sample box (figure 17). Place the iris, which has a collar, in the post holder (figure 18) just prior to the 90^o off-axis parabolic mirror. Then adjust the 1" round Au mirror to put the light through the iris. This forces axis 1 into a straight line and serves as the reference for the boxcar geometry. Next place the masking in front of the 2" square Au mirrors as indicated by figure 17. Place the making such that the axis 1 beam hit the masking as shown in figure 16. Adjust the retro-reflector for either axis 2 or 3 to form the boxcar close to the 2" Au mirrors. Place the masking in front of the 90^o off-axis parabolic mirror and adjust the mirror mounts that hold the 2" square Au mirrors so as to form the boxcar.

Alignment of the Sample

The generation of the signal occurs in the sample box when the three beams are incident onto the sample. Several alignment techniques are performed before search for signal. The first being, the pinhole, all three beams must pass through a 100 μm pinhole to ensure good spatial overlap. The second procedure is auto correlation, in which all three of the pulses are adjusted to be temporally overlapped. The last procedure

measures the spectrum for one of the pulses to determine whether the pulse is resonant with the transition vibration in question.

Place the pinhole onto the sample holder. Adjusting the sample holder in all three dimensions, x, y, and z, so all three tracer beams pass through the 100 μm pinhole (figure 19). This approximately locates the sample holder near where all three of the beams are spatially overlapped. Axes 2 and three should be block and the MCT detector (figure 18) should be cooled with liquid N_2. Adjust the position of the pinhole, in all three dimensions, to ensure that the IR light is going through the pinhole to the detector. This is monitored by the signal seen on the oscilloscope. Due to their different wavelengths, the 90^o off-axis parabolic mirror may not focus the red light (tracer) and the IR light the same, adjust the 90^o off axis parabolic Au coated mirror in front of the MCT detector to increase signal. Use neutral density filters to attenuate the signal if saturation of the MCT detector occurs. The amount of signal seen, on the oscilloscope, is approximately 500 mV with neutral density filters totaling 5 O.D. to attenuate the signal. When finished block axis 1 and unblock axis 2, adjust the 2" square mirror to maximize the signal through the pinhole. Repeat for axis 3. If the tracer beams are not present then the red light (tracer) and IR light is not well overlapped. The overlap must be perfect in order to find the 3^{rd} order signal.

Autocorrelation is the next step. Place the chopper in the path of axis 3. The chopper blocks every other pulse and serves to references the signal to zero. The blocked pulse serves as zero. The goal is to find the T = 0 timing for axes 1 and 2 with respect to axis 3. Axes 1 and 3 are the first pair. Take out the pinhole and replace it with the auto correlation crystal ($AgGaS_2$ 5x5x0.3 mm^3 $\theta = 34^o$). Adjust the positioning of the auto correlation crystal till the tracers from axes 1 and 3 coincide to one point on the crystal. Place an iris such that the signal from the autocorrelation crystal pass between axes 1 and 3 (figure 20) as well as place a stack of fused silica in front of the detector. Only the doubled light from the $AgGaS_2$ crystal will transmit through the silica and be detected. If

there is still no signal, adjust the positions of the auto correlation crystal, the 90^{o} off axis parabolic Au coated mirror, and possibly the iris. If signal is still not found a long scan of the computer-controlled stage for axis 1 is required. When signal is found scan axis 1 with use of the Labview code on the computer. A Gaussian peak should arise when scanning the axis 1 stage. If the peak is not at zero, use the move stage XPS code, and move the stage the required number of fs (the code converts distance into femtoseconds) to place the peak at zero. With the auto correlation peak at zero, leave the move stage XPS code running and increase the auto correlation signal, by adjusting the pointings and timings in the OPA and DFG as well as the OPA crystal (BBO). After the auto correlation signal has been maximized scan axis 1 again. If the peak is not at zero use the move stage XPS code to place the peak at zero. Determine the full width-at half maximum of the peak. Divide that value by 1.414 (because it is a 2^{nd} order correlation) to determine the true value. The FWHM should be at or below 100 fs, after the division of 1.414.

Upon completion of the auto correlation for one pair of pulses, the spectrum of the pulse needs to be taken. For this to occur pass a pulse through the monochromator and adjust the waveplate (figure 21). Be sure to place the chopper in the path and scan the monochromator with the computer program KGMonoNew. To set the spectrum at a preferred wavelength or frequency, rotate the monchromator's grating to the desired frequency, and adjust the DFG crystal while observing and increase in signal on the oscilloscope. Take the spectrum, if the FWHM of the auto correlation is 100 fs, and the FWHM of the spectrum is 150 cm^{-1} then the pulse is said to be transformed limited. Upon setting the spectrum, go back to the auto correlation between pulses 1 and 3, and if the T = 0 and the FWHM have not changed move onto pulse pair 2 and 3. If the auto correlation changed, adjust the pointings and timings in the OPA and DFG till an acceptable, less than 100 fs, auto correlation is taken then determine if the spectrum has

changed. Iterate between the spectrum and auto correlation till both are transformed limited.

The auto correlation between 2 and 3 is much simpler. Adjust the iris to be between the pulses 2 and 3. Adjust the 90^{o} off-axis parabolic Au mirror in front of the MCT detector (figure 18) to increase the signal. The 2" square Au mirror in the path of axis 2 requires adjustment to increase the spatial overlap of pulses 2 and 3. Next scan axis 2 to determine temporal overlap as well as the FWHM of the pulse pair 2 and 3. This pulse pair should have a similar FWHM of approximately 100 fs or below.

When the auto correlations of both pulse pairs are done and the spectrum is centered at the appropriate frequency the 3^{rd} order signal needs to be found. Place the sample cell in sample holder and position cell to where all three tracer beams collapse to a point on the cell. Once the sample cell placement has occurred, move the iris to the fourth corner of the boxcar (figure 22) and remove the stack of fused silica in front of the detector. Adjust the 90^{o} off-axis parabolic Au mirror in front of the MCT detector to determine if there is signal. If the signal cannot be found adjust the positioning of the sample cell as well as the iris. Once signal is found, test to be sure it is not scattered light. Scattered light from axis 3 can appear to be signal because during the manufacturing process of the 90^{o} off-axis parabolic Au mirror vertical line appear and can scatter light horizontally which will proceed through the iris and appear as signal. There are two ways to discern between signal and scattered light. Block either axes 1 or 2, not the chopped beam, or move the timing of axis 3 to a few thousands femtoseconds in the negative direction. The signal will disappear from the oscilloscope screen by blocking either of the 2 beams that are not chopped. Signal can be found and there can still contain some scattered light, to alleviate this problem move the sample verticle (y-direction) and horizontally (x-direction). The CaF_2 window, from the sample cell, can scatter light. Moving the iris, horizontally and vertically, will reduce the scattered light. Optimize on the signal after the scattered light has been reduced. Be sure to move axis 3

(capital T) off of T = 0. Do not optimize on the nonresonant signal if possible. For the most part finding signal and not scattered light relies on trial and error and mostly experience. Don't give up and be persistent!!!

The Heterodyne Experiment

The process of heterodyning consists of overlapping the 3rd order signal with a pulse that does not interact with the sample called the local oscillator. The overlap of the 3rd order signal transmits through a 2" diameter 3° CaF_2 wedge while the local oscillator reflects off the 2" diameter 3° CaF_2 wedge. Both signal and local oscillator are routed into the monchromator and detected by a single channel MCT detector.

Once the signal has been found and scattered light reduced to a minimum, block the signal and place the 2" diameter 3° CaF_2 wedge in it holder (figure 23) and the Au mirror that will send the heterodyned signal into the monochromator. Adjust the 2" diameter 3° CaF_2 wedge so that the tracer is centered on to the Au gold mirror. Rotate both 2" diameter 3° CaF_2 wedge and the Au mirror to place the light through the monochromator. This sets the approximate face angle of the 2" diameter 3° CaF_2 wedge. The transmitted signal will diffract through the wedge optic. Next block the local oscillator and allow the signal through to the monochromator. To increase the chance to see the signal, rotate the grating in the monchromator to zero degree. Rotate the Au gold mirror just prior to the 2" diameter 3° CaF_2 wedge and adjust the pointing into the monochromator as well as the waveplate just before the monochromator. Be sure the detected light contains no scattered light buy blocking one of the unchopped beams. Unblock the local oscillator pulse and pass it through the monochromator by rotating the 2" diameter 3° CaF_2 wedge. Do not be afraid to use its tracer as well as the pointing of the local oscillator prior to the 2" diameter 3° CaF_2 wedge. Do not adjust any optic after the 1" Au mirror because the signal already goes through the monochromator. You want to think of placing the local oscillator on top of the signal. To find the time zero for the

local oscillator use the solvent response and scan the stage for the local oscillator. There will appear a interferogram. Move the stage to the center of the interferogram.

After optimizing both signal and local oscillator through the monochromator, rotate the monochromator's grating to the frequency of the transition of interest. The waveplate in front of the monchromator and the pointings of both signal and local oscillator will have to be adjusted. The waveplate in the local oscillator path (arm) adjust the amount of local oscillator light. To improve the heterodyning adjust the pointing of the local oscillator before the 2" diameter 3^{o} CaF_2 wedge. The local oscillator may have to "be walked" so feel free to use two mirrors. Heterodyning can be a bit tricky, and requires patience and most importantly experience. Since there are not adjustments for the 3^{rd} order signal, think of placing the local oscillator on top of the 3^{rd} order signal.

Introduction and Application to 2DIR

Peter Hamm and Manho Lim from Robin Hochstrasser's laboratory at the University of Pennsylvania published the first 2DIR measurement in 1998.[22] The systems they chose to study were the amide I mode N-methylacetamide as well as three small peptides: apamin, scyllatoxin, and bovine pancreatic trypsin inhibitor. The first publishe heterodyned 2DIR measurement came out of the Hochstrasser lab and was performed by Matthew Asplund and Martin Zanni in 2000.[23] The sample consisted of the peptide acyl-proline-NH_2 and amide I served as the chromophore. Since that time the 2DIR measurement has revealed information of the dynamics of proteins.[24-43] The timescale for chemical exchange has been recorded for a number sample using 2DIR.[44-50] Chemical exchange spectroscopy (CES) measures the time scale for the interconversion of distinct molecular structural isomers by taking advantage that the isomers will have different transition frequencies.[51] The systems that have been studied with CES are geometric isomers[44, 45, 49], solvent solute complexes[28, 52], proteins[50].

The 2D-IR experiment is characterized by 3 time periods; evolution (t_1), waiting (T) and detection (t_3), which correspond to the three pulses used in the experiment. The first pulse interacts with the sample and places the oscillators in a coherent superposition state between the ground state, $\nu = 0$, and the first excited state, $\nu = 1$. This interaction initially labels the sample by placing its frequency along the ω_1 axis. The second pulse, which starts the T time, interacts with the sample to collapses the coherence, formed by the first interaction, and placing the population in either the ground state, n = 0, or the first excited state, n = 1. The third pulse (t_3) again places the oscillators in coherent superposition states between both $\nu = 0 \rightarrow \nu = 1$ and $\nu = 1 \rightarrow \nu = 2$, resulting in the signal. The peak positions, amplitudes and line shapes in the 2DIR spectrum record the anharmonicities, couplings and non-linear dependence of the transitional dipole moments on the vibrational coordinates. The peak positions reveal the eigenstates. The magnitude and orientation of the transition dipole moment are reflected in the amplitudes of the 2DIR spectrum. The shapes of the peaks depend on the solute-solvent (bath) interactions. These three observables characterize the eigenstates and solute-solvent interactions.

The diagonal peaks, appearing in red color, arises from the transmission of the $\nu = 0 \rightarrow \nu = 1$ transition. The blue peaks, lying below the diagonal peaks, correspond to overtone modes. The overtone peaks arise from the absorption of the $\nu = 1 \rightarrow \nu = 2$ transition. The difference between the red peak and the blue peak directly below it on the ω_3 axis measures the anharmonicity of that transition. The cross peaks, appearing in a greenish-yellow, arise from the transfer of coherence from one of the fundamental transitions to the other. The excited state absorption peaks originates from the transition involving a combination band and the fundamental transitions.

Theoretical Framework for 4 Wave Mixing Experiments

The theoretical framework for deriving the response function for the four wave mixing experiments is derived based on the theoretical work of Sung and Silbey[53]. The

total Hamiltonian consists of the total material Hamiltonian plus the interaction Hamiltonian.

Equation 1. Total Hamiltonian

$$H=H_M + H_{int}$$

Where H represents the total Hamiltonian and H_M and H_{int} are the total material and interaction Hamiltonians, respectively. The total material Hamiltonian can be written as the summation of system Hamiltonian, bath Hamiltonian, and the system-bath Hamiltonian.

Equation 2. Material Hamiltonian

$$H_M= H_S(\mathbf{P,Q})+ H_B(\mathbf{p,q})+ H_{SB}(\mathbf{P,Q,p,q})$$

The Hamiltonians for the system, bath and system-bath interactions are H_S, H_B, H_{SB}, respectively. Vectors **P** and **p** are the momenta of the system and bath, respectively. The vectors **Q** and **q** correspond to the coordinates for the system and bath, respectively and are interrogated by the applied radiation fields.[54] Both **P**(**p**) and **Q**(**q**) are in reduced mass coordinates. The material Hamiltonian contains information about the system under study.[54] H_M can be partitioned into it components assuming that the system couples to the incident radiation in my case the LASER pulses and not the bath. The system can be completely general but in my case the system corresponds to either the C-D stretch or the azide (N_3^-) asymmetric stretch, and the bath and the solvent (CCl_4, CH_3Cl, D_2O, ect.) are the same. To simplify the math, without losing the integrity of the theory we treat the

bath as a collection or an ensemble of harmonic oscillators where p_ν and ω_ν are the momentum and energy of the ν^{th} bath oscillator.

Equation 3. The Bath Hamiltonian

$$H_B(p,q) = \frac{1}{2}\sum_\nu \left(p_\nu^2 + \omega_\nu^2 q_\nu^2\right)$$

The system bath Hamiltonian, H_{SB}, is written as the summation of the operator for the system's degrees of freedom, $\chi_\nu(\mathbf{P},\mathbf{Q})$. $\chi_\nu(\mathbf{P},\mathbf{Q})$ indicates the coupling between the system and the ν^{th} bath oscillator where ν indexes the bath. In other words, χ_ν is a metric for the force of the bath onto the system's coordinates. The force of the bath onto the system caused fluctuations that lead to shifts the vibrational transition frequency, vibrational relaxation processes and reorientation dynamics.[54]

Equation 4. The System-Bath Hamiltonian

$$H_{SB} = \sum \chi_\nu(\mathbf{P},\mathbf{Q}) q_\nu$$

Equation 5 is the material Hamiltonian where $|a\rangle$ eigenstates of the system. The energy, E, of the eigenstate a and can be written as $E_a^0 = \langle a | H_s | a \rangle$.

Equation 5. Material Hamiltonian with system eigenstates

$$H_M = H_S + H_B = \sum_a |a\rangle E_a^0 \langle a| + \frac{1}{2}\left(p_\nu^2 + \omega_\nu^2 q_\nu^2\right)$$

The system-bath Hamiltonian takes the form of equation 6 after choosing the system's eigenstates as the basis set. The system-bath Hamiltonian is linear in the bath coordinates and recall a and b are the eignestates of the system which make up the basis set.

Equation 6. System-Bath Equation with system eigenstates

$$H_{SB} = \sum_a |a\rangle \left(\sum_v \chi_v^a q_v \right) \langle a| + \sum_{a \neq b} |a\rangle \left(\sum_v \chi_v^{ab} q_v \right) \langle b|$$

The χs, χ_v^a and χ_v^{ab}, are in reality $\langle a \mid \chi_v(\mathbf{P},\mathbf{Q}) \mid a \rangle$ and $\langle a \mid \chi_v(\mathbf{P},\mathbf{Q}) \mid b \rangle$, respectively. The first term in equation 6, the diagonal term, takes into account the fluctuations or dephasing of the system energy levels due to interaction with the bath. The off diagonal term, the second term a≠b, in equation 6 characterizes the induced bath interactions between that of the system's eigenstates. To get an exact and analytical solution, we will assume that the induced bath interactions between that of the system's eigenstates are much smaller than the fluctuations of the system energy levels due to the bath, $\chi_v^{ab} < \chi_v^a$. This assumption simplifies equation 6 to:

Equation 7. Simplified System-Bath Hamiltonian

$$H_{SB} = \sum_a |a\rangle \sum_a \chi_v^a q_v \langle a|$$

The Hamiltonian for the interaction, H_{int}, describes the interaction of the incident radiation field onto the system.[54] $\boldsymbol{\mu}(\mathbf{Q})$ is the transition dipole operator and $\mathbf{E}(\mathbf{r},t)$ is the external electric field that is radiant onto the system or sample.

Equation 8. The Interaction Hamiltonian

$$H_{\text{int}} = -\mu(\mathbf{Q})\cdot \mathbf{E}(\mathbf{r},t) = -\sum_{a} \sum |a\rangle \mu^{ab} \cdot \mathbf{E}(\mathbf{r},t)\langle b|$$

$\boldsymbol{\mu}^{ab}$ is an off diagonal matrix element for the transition dipole matrix and is written as such. Diagonal matrix elements are possible as well, $\boldsymbol{\mu}^{aa}$, which are ultimately the expectation values of the dipole moment operator for the system to be in the $|a\rangle$ eigenstate of the system.

Equation 9. Transition Dipole Matrix Element

$$\mu^{ab} = \langle a|\mu(\mathbf{Q})|b\rangle$$

In the material a time dependent polarization occurs when exposed to an electric field and equation 10 corresponds to this event.

Equation 10. Material Polarization

$$\mathbf{P}(\mathbf{r},t)=\text{Tr}[-\boldsymbol{\mu}(\mathbf{Q})\rho(\mathbf{r},t)]$$

Where $\mathbf{P}(\mathbf{r},t)$ and Tr represents the time dependent material polarization and the trace or sum over all the system's degrees of freedom, respectively. The density matrix operator, $\rho(\mathbf{r},t)$, which obeys the Liouville equation. The spectroscopic observable in our experiments originates from the time dependent material polarization, $\mathbf{P}(\mathbf{r},t)$.

Equation 11. Liouville Equation

$$\frac{\partial \rho(\mathbf{r},t)}{\partial t} = \frac{1}{i\hbar}\left[H_M + H_{\text{int}}\rho(\mathbf{r},t)\right]$$

By solving the Liouville equation for ρ(**r**,t) and substituting the result in equation 6 one can obtain a more formal equation for the material polarization

Equation 12. Formal Material Polarization

$$\begin{aligned}
&\mathbf{P}(\mathbf{r},t) = \sum_{n=1}^{\infty}\mathbf{P}^{(n)}(\mathbf{r},t)\\
&\mathbf{P}^{(n)}(\mathbf{r},t) = \int_0^{\infty} dt_n \int_0^{\infty} dt_{n-1}\ldots\int_0^{\infty} dt_1 \overleftrightarrow{\mathbf{R}}(t_n t_{n-1,\ldots t_1}) \vdots\\
&\mathbf{E}(\mathbf{r},t-t_n)\mathbf{E}(\mathbf{r},t-t_n-t_{n-1})\ldots\\
&\mathbf{E}(\mathbf{r},t-t_n-t_{n-1}\ldots-t_1)
\end{aligned}$$

The tensor $\mathbf{R}(t_n,t_{n-1},\ldots,t_1)$ denotes the nonlinear response from the material. Where ⋮ symbolizes the tensor contraction and n represents the order of the polarization. For example, linear optical properties such as those observed in FTIR the polarization is $\mathbf{P}^{(1)}(\mathbf{r},t)$. $\mathbf{P}^{(3)}(\mathbf{r},t)$ represents the polarization measured in four-wave-mixing processes such as in 2DIR experiments.[54]

Equation 13. Formal Material Polarization Equation for FWM

$$P^{(3)} = \int_0^{\infty} dt_3 \int_0^{\infty} dt_2 \int_0^{\infty} dt_1 \overleftrightarrow{\mathbf{R}}(t_3,t_2,t_1)\mathbf{E}(t-t_3)\mathbf{E}(t-t_3-t_2)\mathbf{E}(t-t_3-t_2-t_1)$$

Where $\mathbf{R}(t_3,t_2,t_1)$ is the response function for the third order polarization measurement.

Equation 14. Third Order Polarization Response Function

$$\overleftrightarrow{\mathbf{R}} = (t_3,t_2,t_1) = \left(\frac{i}{\hbar}\right)^3 \left\langle \left[\left[\left[\mu\left(t_3+t_2+t_1\right),\mu\left(t_2+t_1\right)\right],\mu(t_1)\right],\mu(0)\right]\right\rangle$$

Where $\mu(t) = \exp\left(\frac{iH_M t}{\hbar}\right)\mu(Q)\exp\left(-\frac{iH_M t}{\hbar}\right)$.

Equation 14 has a third order nested commutator and is obtained by integrating equation 13 over the times corresponding to the interactions of the three electric fields of laser pulses with the system. The commutators in equation 14 can be expanded into 8 terms represented by four distinct Liouville pathways, figure 25.[54] Solving the commutators by applying the second cumulant approximation with respect to the energy gap correlation function yields the 3rd order response function, equation 15.

Equation 15: 3rd order response function

$$\mathbf{R}\left(t_3,t_2,t_1\right) = \left(\frac{2}{\hbar^3}\right) = \mathrm{Im}\left\{\begin{array}{l} \sum_{abcd} P_a \mu^{ab}\mu^{bc}\mu^{cd}\mu^{da}\left[\exp\left(-i\omega_{ab}t_3 - i\omega_{ca}t_2 - i\omega_{da}t_1\right)F^{(1)}_{abdc}\left(t_3,t_2,t_1\right)\right] \\ \sum_{abcd} P_a \mu^{ab}\mu^{bc}\mu^{cd}\mu^{da}Tr_B\left[\exp\left(-i\omega_{dc}t_3 - i\omega_{ab}t_2 - i\omega_{da}t_1\right)F^{(2)}_{abdc}\left(t_3,t_2,t_1\right)\right] \\ P_a \mu^{ab}\mu^{bc}\mu^{cd}\mu^{da}Tr_B\left[\exp\left(-i\omega_{bc}t_3 - i\omega_{ca}t_2 - i\omega_{da}t_1\right)F^{(3)}_{abdc}\left(t_3,t_2,t_1\right)\right] \\ \sum_{abcd}\sum_{abcd} P_a \mu^{ab}\mu^{bc}\mu^{cd}\mu^{da}Tr_B\left[\exp\left(-i\omega_{bc}t_3 - i\omega_{ab}t_2 - i\omega_{da}t_1\right)F^{(4)}_{abdc}\left(t_3,t_2,t_1\right)\right] \end{array}\right\}$$

The equation for the response function contains information concerning the vibrational dynamics and orientation dynamics of the sample's dipoles when probed by radiant electric fields.[54] The ω_{xy} is the frequency difference between states x and y, and

μ^{xy} corresponds to the dipole moment operator for transitions between states x and y. The probability, P_a, of starting in state a and written as $P_a=\exp(-\beta E_a)/\Sigma_a\exp(-\beta E_a)$. The F's symbolize the dephasing functions.[55] The solvent or bath induces a frequency shift of ω_{xy}, about the ensemble-averaged value ω°_{xy}, represented by $\delta\omega_{xy}$.[54] These frequency fluctuations are time dependent and written as $\omega_{pq}(t) = \omega^{\circ}_{pq} + \delta\omega_{pq}(t)$.[54] The time scale for the fluctuations are expressed in terms of the energy gap between the different vibrational transitions as auto and cross correlation functions C_{pp} and C_{pq}, respectively.[54] The energy gap correlation function (equation 15) correspond to the fluctuations of the energy gap between levels p and q, relative to the initial state a of the density matrix, over a time period of t.[54] The 2DIR experiment measures the correlations of the fluctuations between the energy gap of different vibrational corrdinates.[54]

Equation 16: Energy gap correlation function

$$C_{pq}(t) = \left\langle \delta\omega_{p,a}(t)\delta\omega_{q,a}(0)\right\rangle$$

Equation 17. Dephasing Functions[55]

$$-\ln F^{1}_{a,b,c,d}(t_3,t_2,t_1) = h_{bb}(t_3)+h_{cc}(t_2)+h_{dd}(t_1)+h^{+}_{bc}(t_3,t_2)+h^{+}_{cd}(t_2,t_1)-f+_{bd}(t_3,t_1;t_2)$$

$$-\ln F^{2}_{a,b,c,d}(t_3,t_2,t_1) = h_{cc}(t_3)+[h_{bb}(t_2)]^{*}+h_{dd}(t_3+t_2+t_1)+[h^{+}_{bc}(t_2,t_3)]^{*}$$
$$- h^{-}_{cd}(t_1+t_2+t_3,t_3)-[f^{-}_{bd}(t_2, t_1+t_2+t_3,t_3)]^{*}$$

$$-\ln[F^{3}_{a,b,c,d}(t_3,t_2,t_1)]^{*} = [h_{bb}(t_3)]^{*}+h_{cc}(t_2+t_3)+h_{dd}(t_1)+h^{+}_{cd}(t_2+t_3,t_1)$$
$$- f^{-}_{bc}(t_3,t_2+t_3;t_2)-f^{+}_{bd}(t_3,t_1;t_2)$$
$$-\ln[F^{4}_{a,b,c,d}(t_3,t_2,t_1)]^{*} = h_{cc}(t_3)+ h_{dd}(t_2+t_1)+ [h_{bb}(t_3+t_2)]^{*}- h^{-}_{bc}(t_3,t_2+t_3)+$$

$$h_{cd}(t_2+t_1, t_3)\text{-}f_{bd}(t_1+t_2,t_2+t_3;t_3)$$

The h and f in the dephasing functions are the line shape functions.

Equation 18. Line shape Functions

$$h_{xy}(t) = \int_0^{\tau} d\tau_2 \int_0^{\tau_1} d\tau_1 C_{xy}(\tau_2 - \tau_1)$$

$$h^{\pm}{}_{xy}(t_2,t_1) = \int_0^{\tau_2} d\tau_2 \int_0^{\tau_1} d\tau_1 C_{xy}(\tau_2 \pm \tau_1)$$

$$f^{\pm}{}_{xy}(t_2,t_1 : t_3) = \int_0^{\tau_2} d\tau_2 \int_0^{\tau_1} d\tau_1 C_{xy}(\tau_2 \pm \tau_1 + \tau_3)$$

For the transient grating and 2D IR experiments three incident electric fields E_1, E_2, and E_3 have a unique wavevector $\mathbf{k}_1$, $\mathbf{k}_2$, and $\mathbf{k}_3$ and are incident onto the sample. The pulses meet in the sample generating the third order signal, $\mathbf{k}_s$. The phase matching conditions for the signal, $\mathbf{k}_s$ are $-\mathbf{k}_1 + \mathbf{k}_2 + \mathbf{k}_3$. Using this phase matching conditions and assuming a rotating wave approximation there are 16 Feynman diagrams derived from the 4 Liouville pathways (Figure 25).[54] The Feynman diagrams are divided into rephrasing and nonrephasing and represents the evolution of the density matrix for all of the time ordering of the pulses (figure 26).[54] The time ordering for the pulse for the rephrasing experiment as known as the photon echo is $-\mathbf{k}_1 + \mathbf{k}_2 + \mathbf{k}_3$. During the evolution period, $e^{i\omega_{pa}\tau_1}$ the phase is acquired by coherences; and is the conjugate of the detection period which is written as $e^{-i\omega_{pa}\tau_3}$.[54] The time ordering for the nonrephasing contribution is $+\mathbf{k}_1 - \mathbf{k}_2 + \mathbf{k}_3$ and $+\mathbf{k}_1 + \mathbf{k}_2 - \mathbf{k}_3$. The nonrephasing diagrams evolve at the same frequency during t_1 and t_3 however they do not rephase macroscopically.[54] The nonrephasing diagrams labeled S_{III} are for multi-leveled systems.[54]

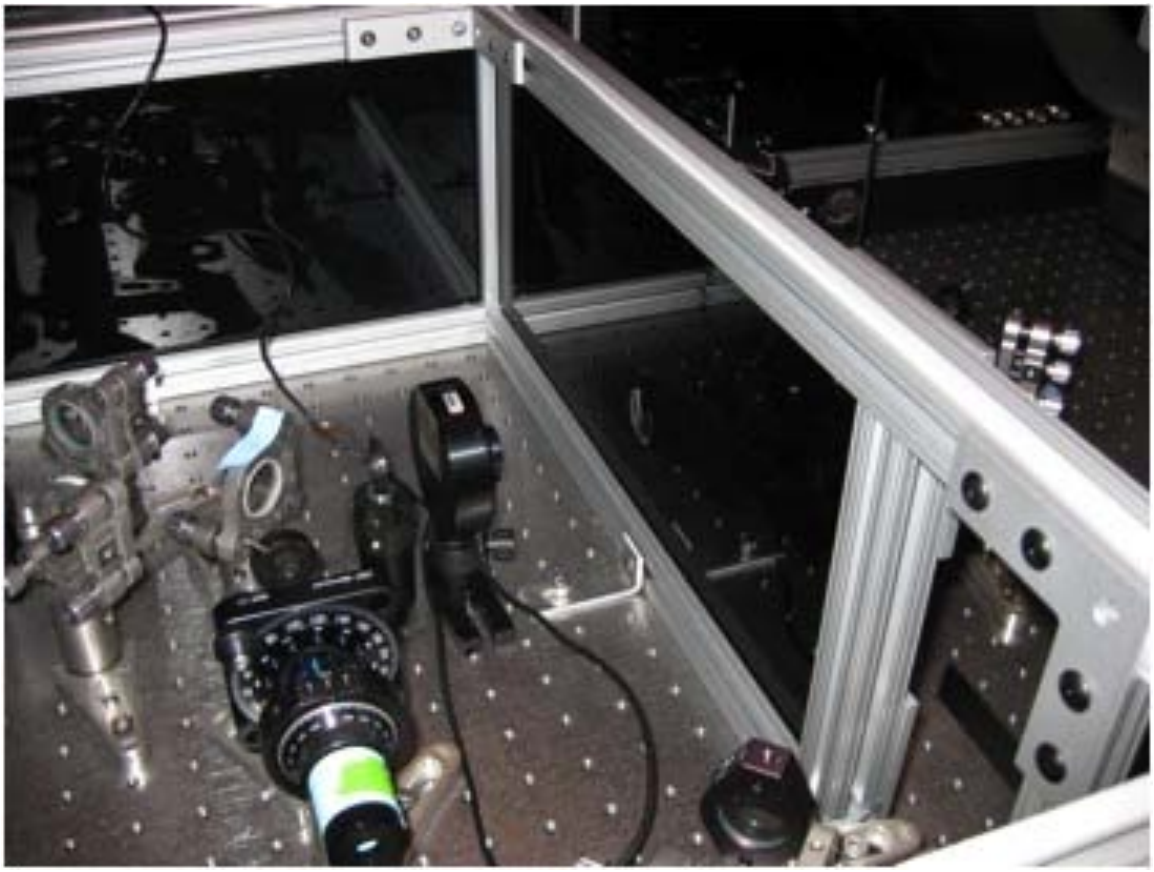

Figure 1. Place of the power meter head

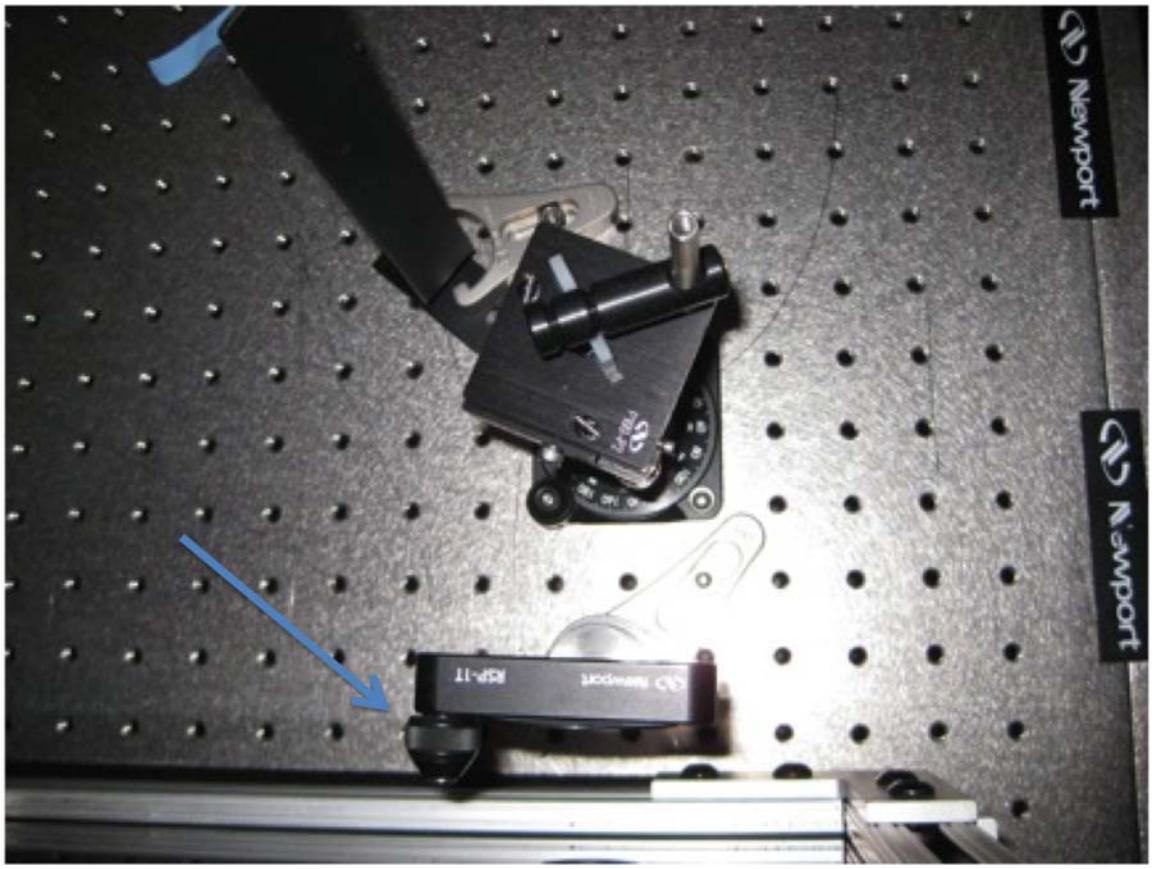

Figure 2. Waveplate Before the OPA. Arrow indicates the knob for waveplate adjustments.

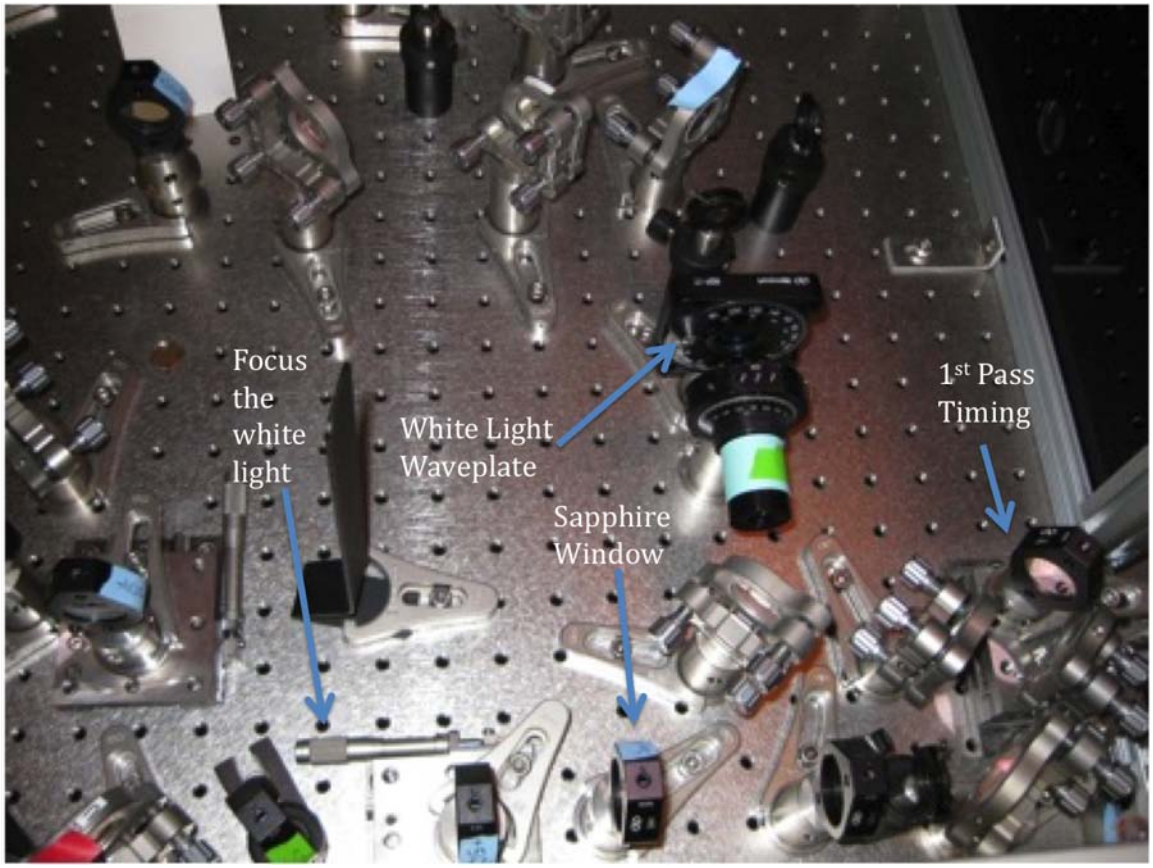

Figure 3. White light path in the OPA

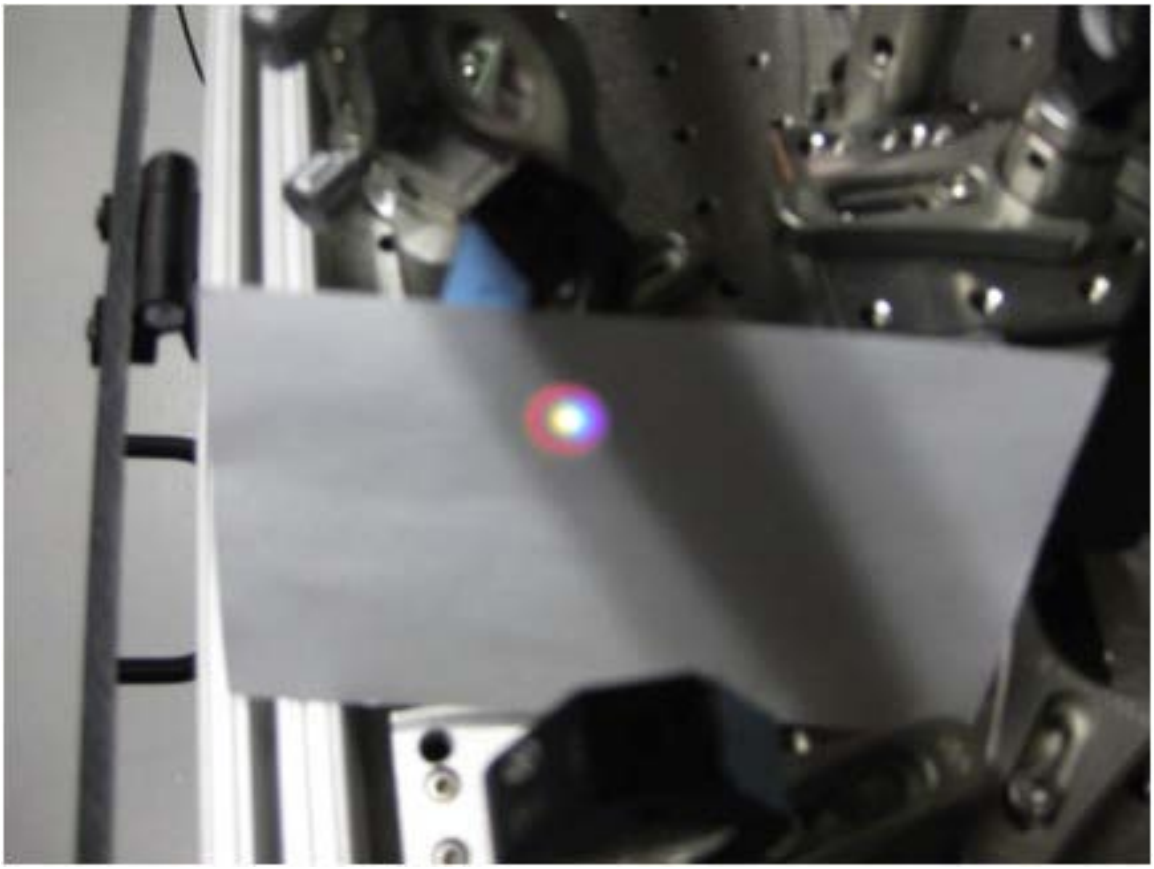

Figure 4. Image of the White Light produced from the Sapphire Window

Figure 5. Compressor controller for the LASER Amplifier

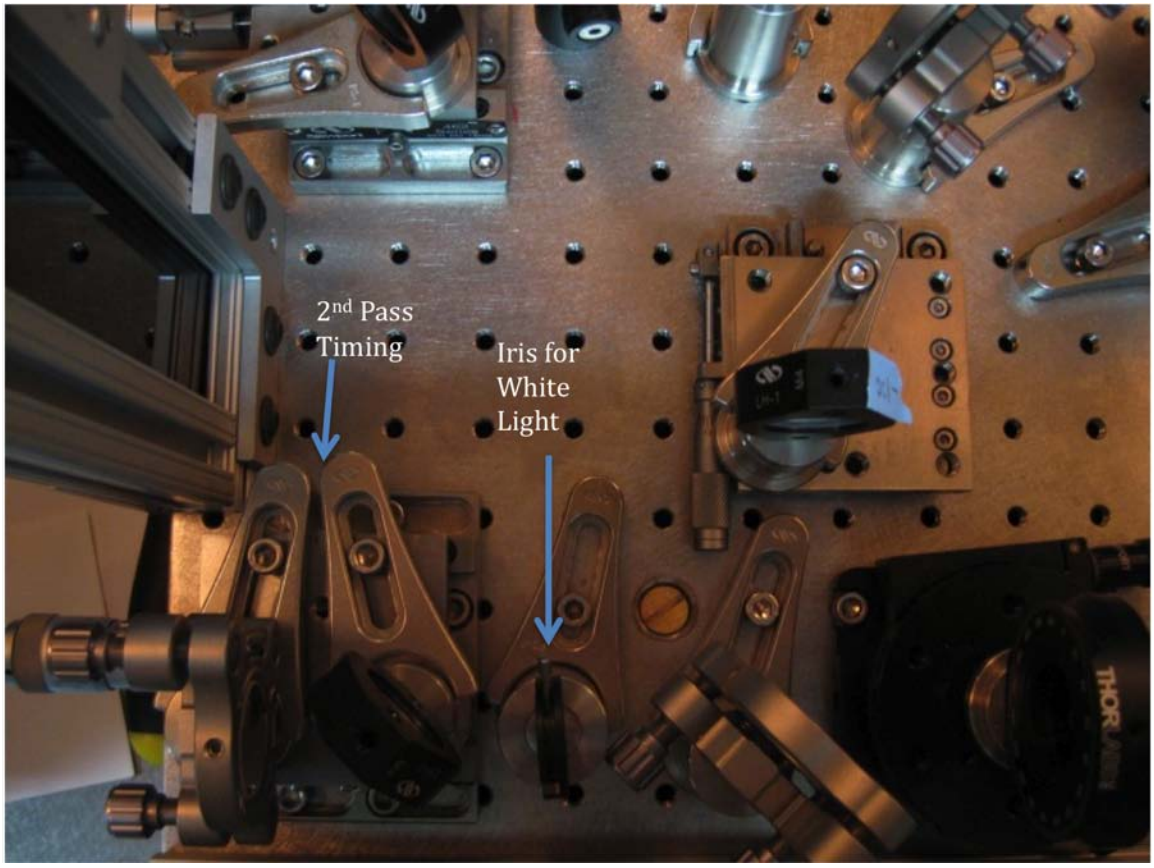

Figure 6. Image of the 2nd Pass Timing and White Light Iris

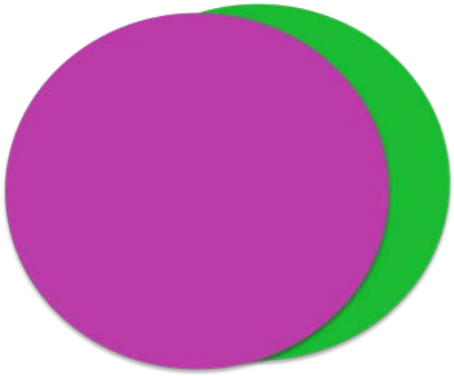

Figure 7. Cartoon of the Green Halo around the first and second pass. The pinkish-purple color is the 800 nm light and the green halo is the OPG.

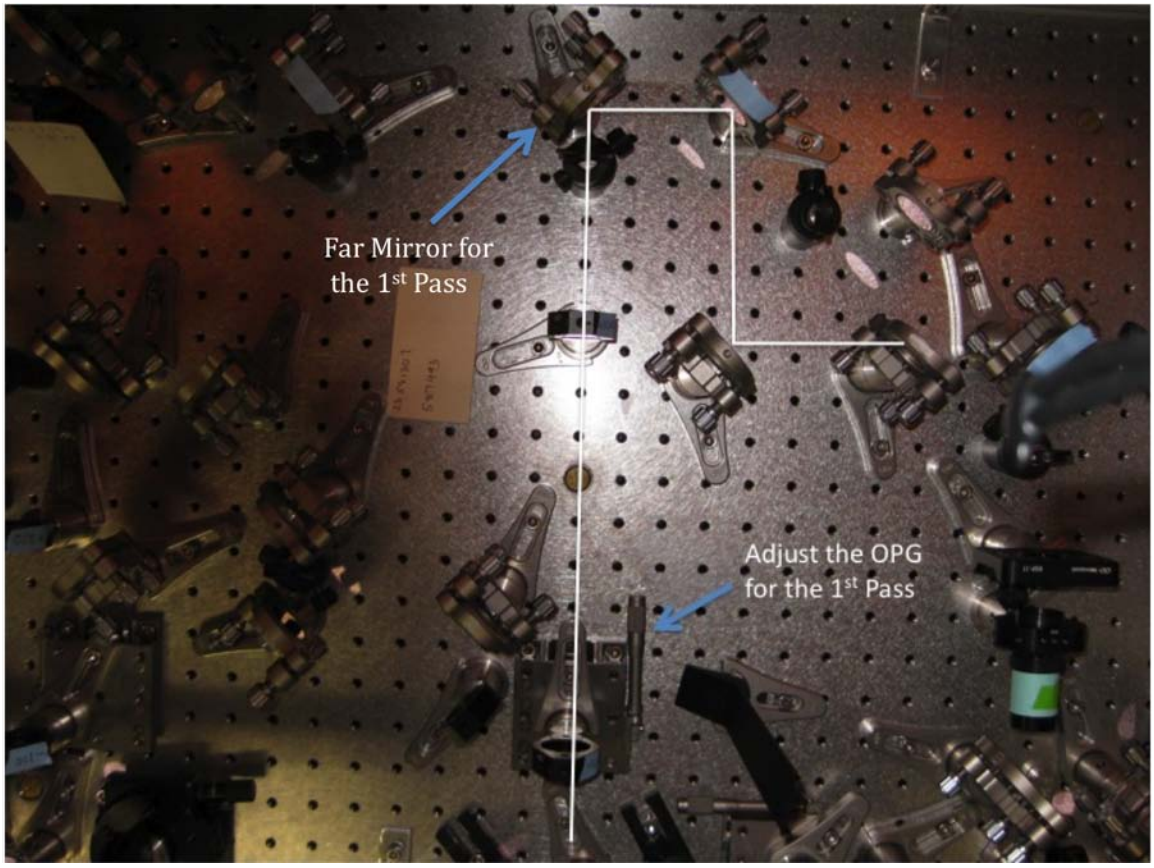

Figure 8. Image of the 1st Pass of the OPA. The white line indicates the path of the 1st pass. The arrows indicate the stage that controls the OPG and the far mirror.

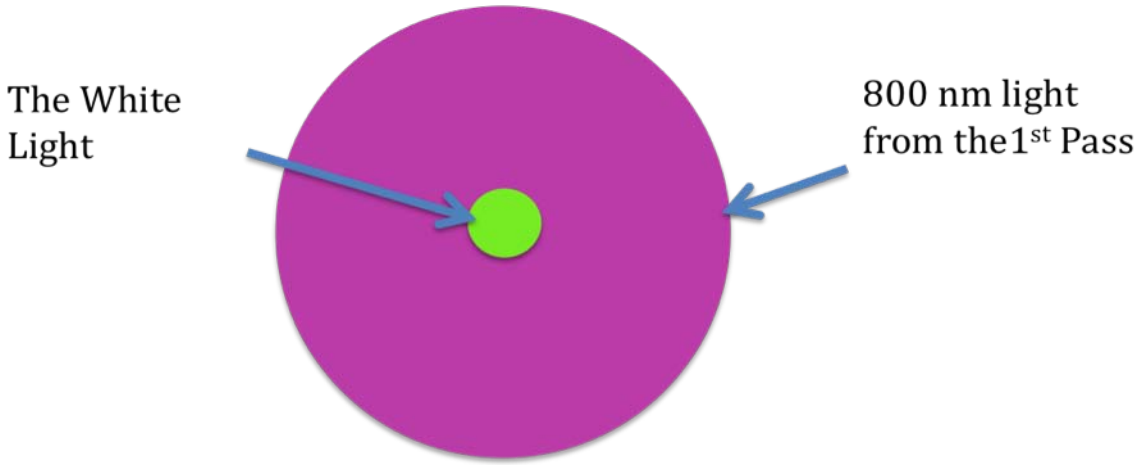

Figure 9. Cartoon of the 1st pass and White Light overlap.

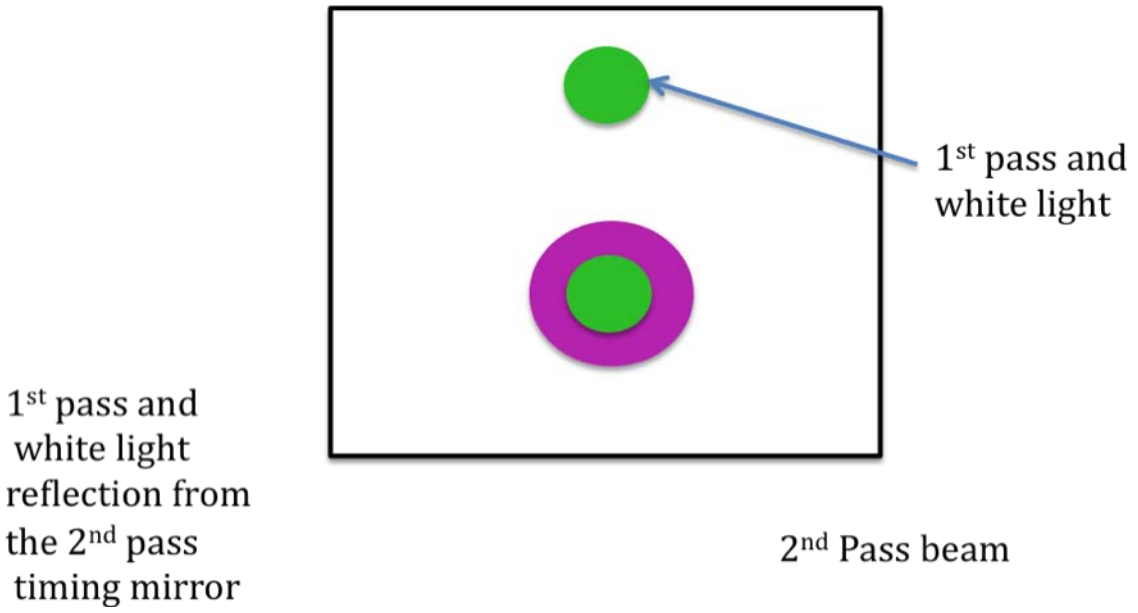

Figure 10. Cartoon showing the alignment for the 1st, 2nd and white light.

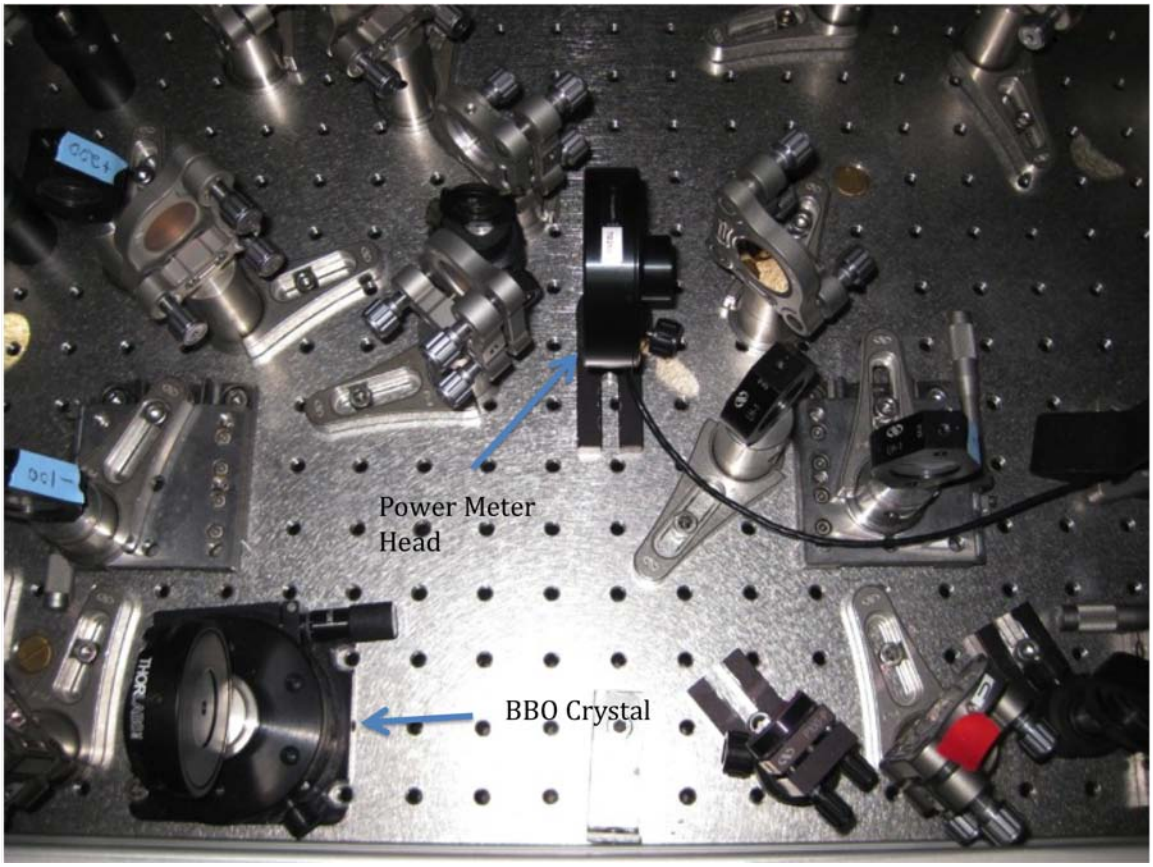

Figure 11. Image of the placement of the power meter's head.

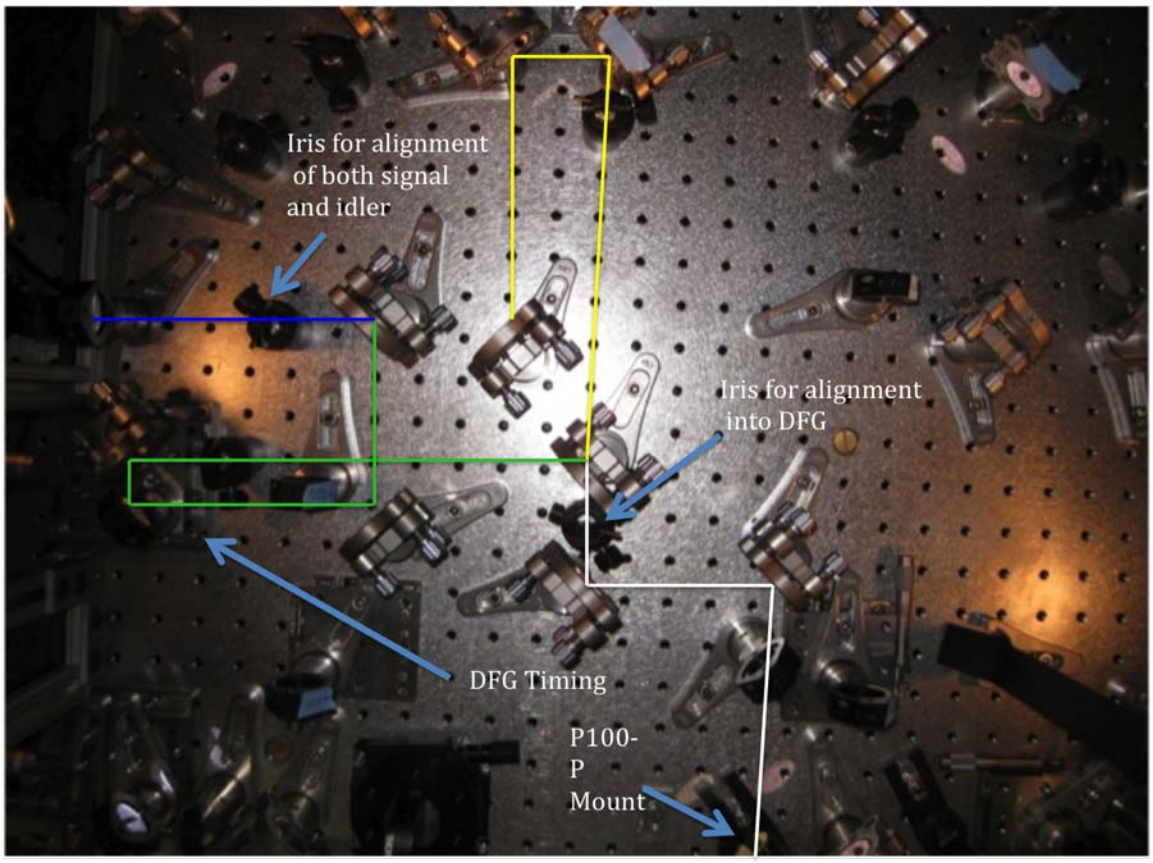

Figure 12. Image of the DFG. The white line is the signal and idler, the yellow line represents the idler, the green line is the signal and the blue line is where signal and idler are spatially and temporally overlapped.

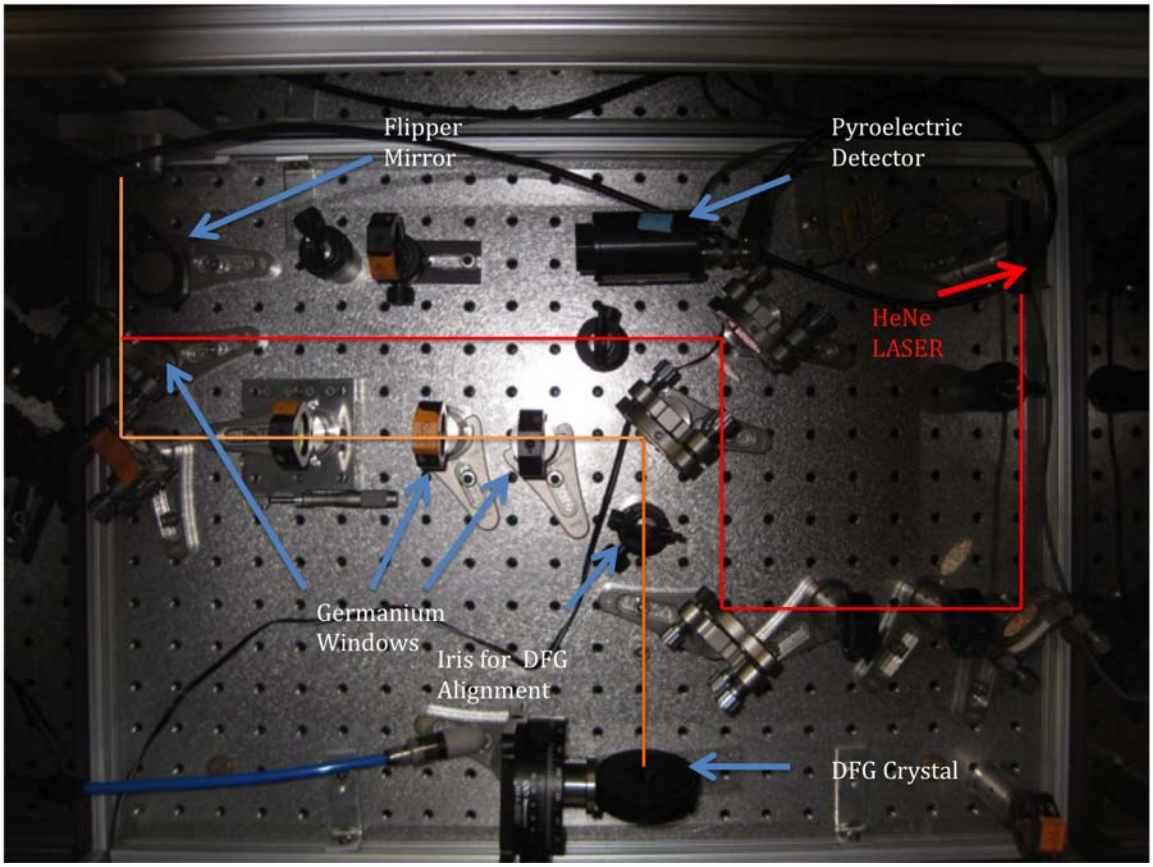

Figure 13. Second portion of the DFG. The orange line the mid infrared light generated from the $AgGaS_2$ crystal. The red line is the HeNe LASER light for tracing the IR light. Indicated by arrows are The $AgGaS_2$ crystal, the Ge windows, flipper mirror, HeNe LASER and the pyroelectric detector.

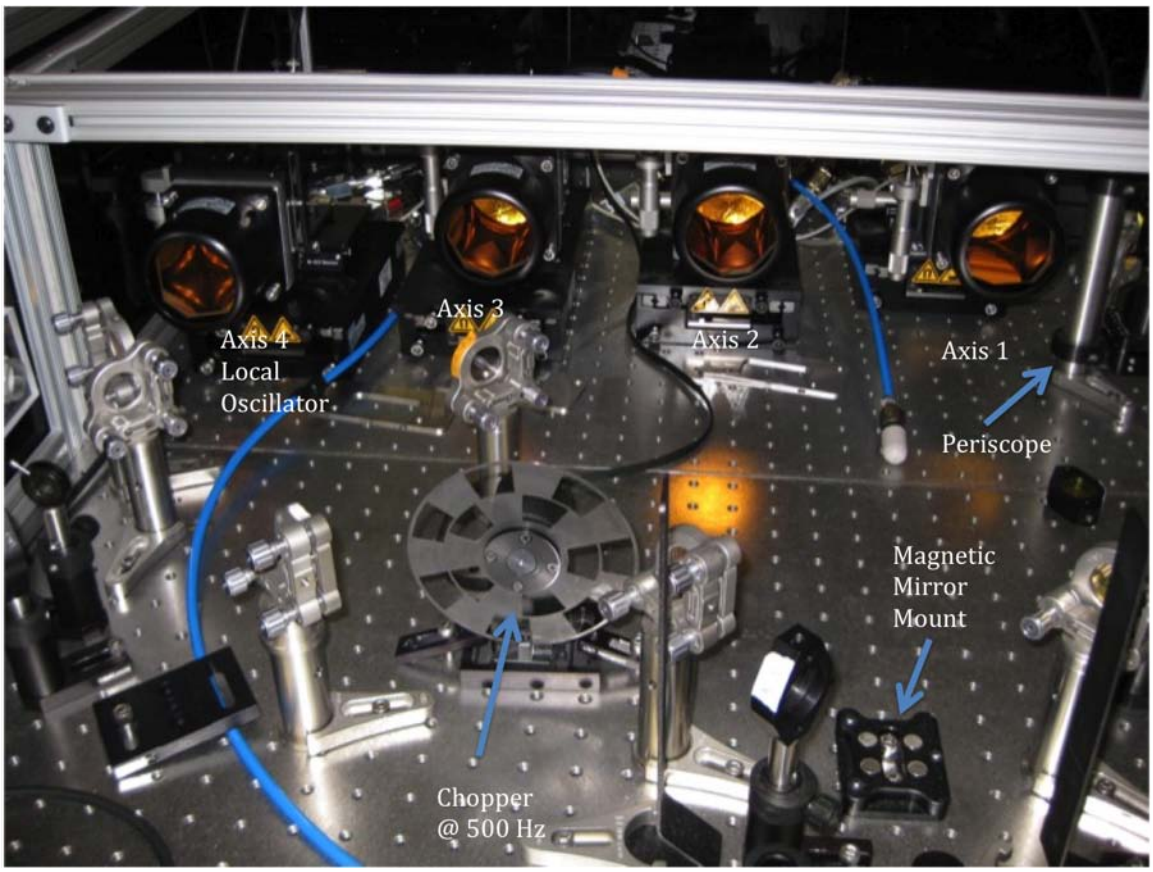

Figure 14. The axes of the interferometer are labeled as well as the periscope, magnetic stage and the chopper.

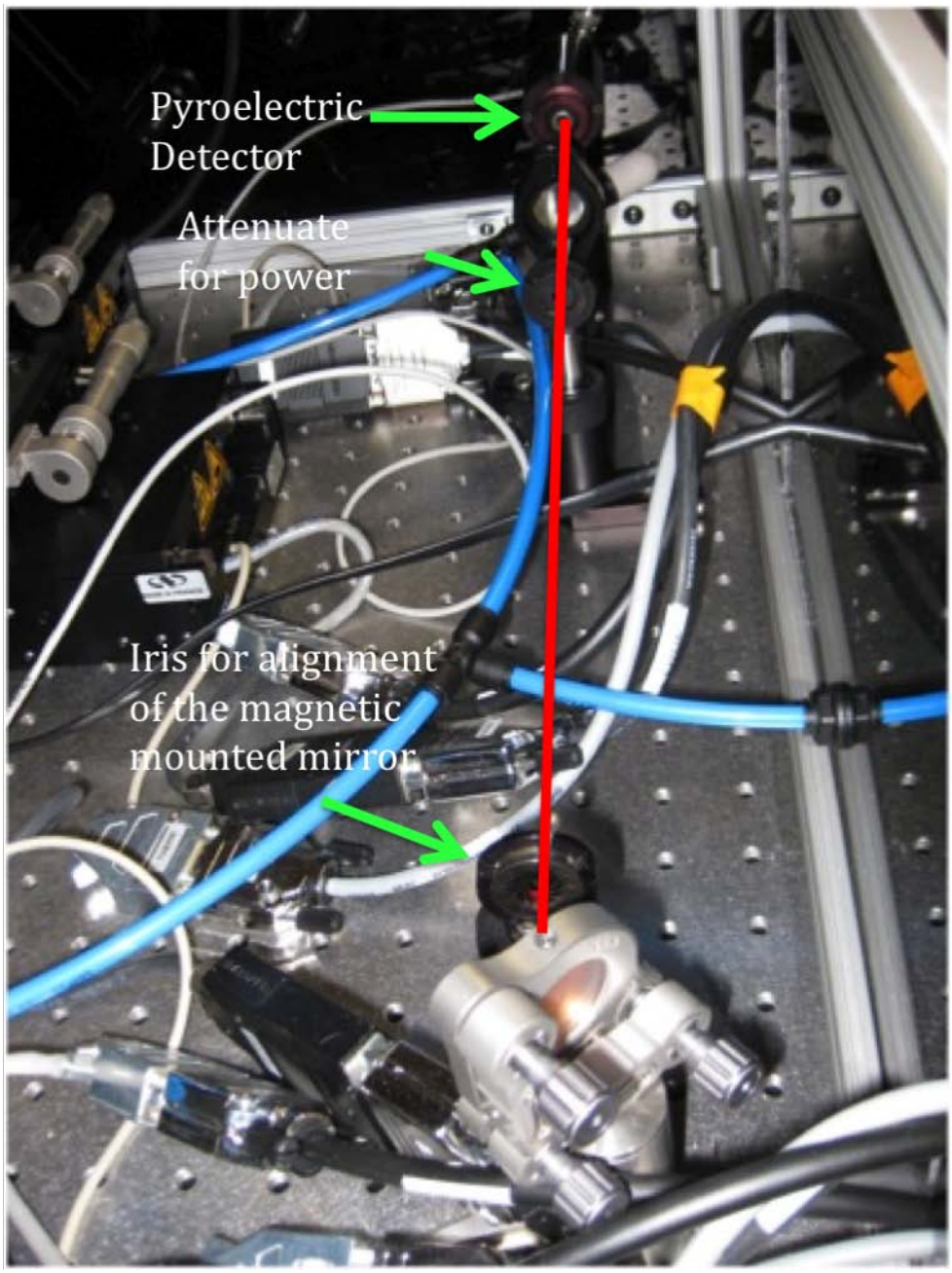

Figure 15. The far path for red light and IR light overlap.

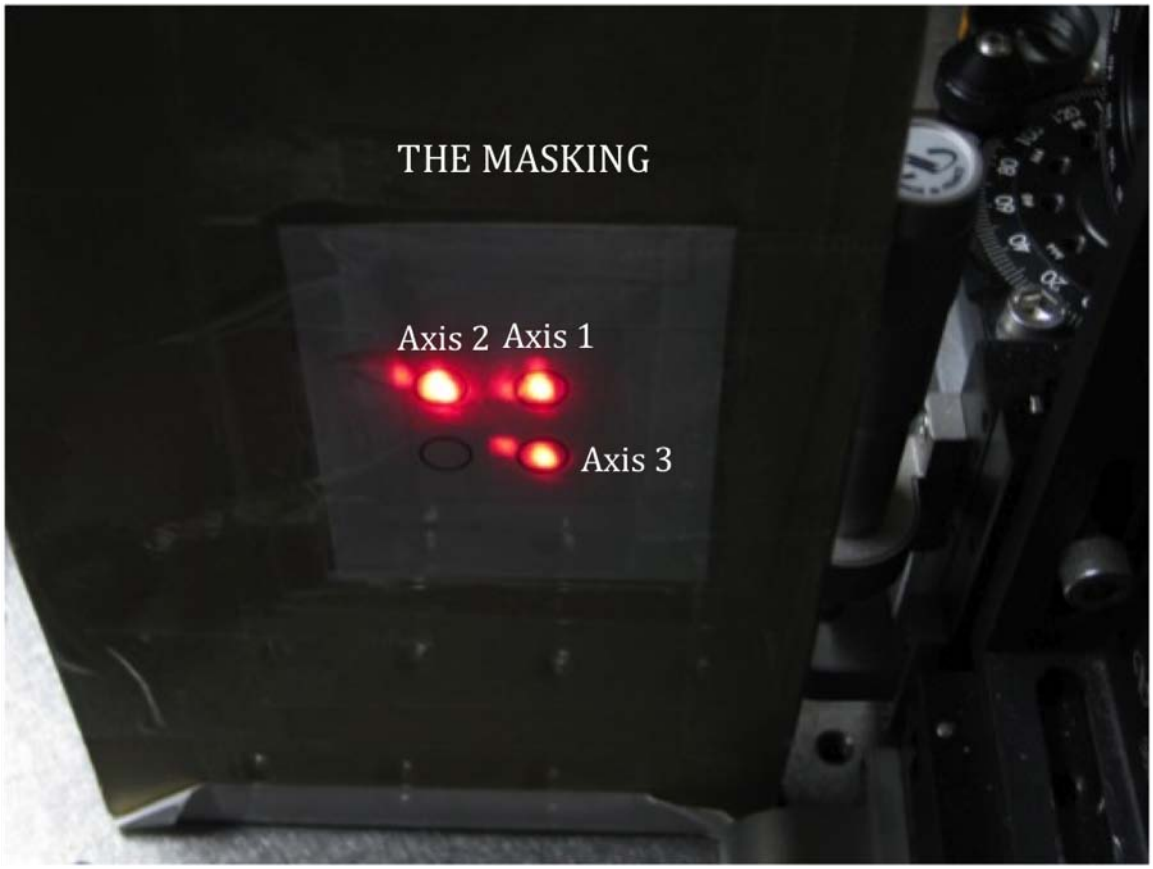

Figure 16. The geometry for the boxcar on the masking.

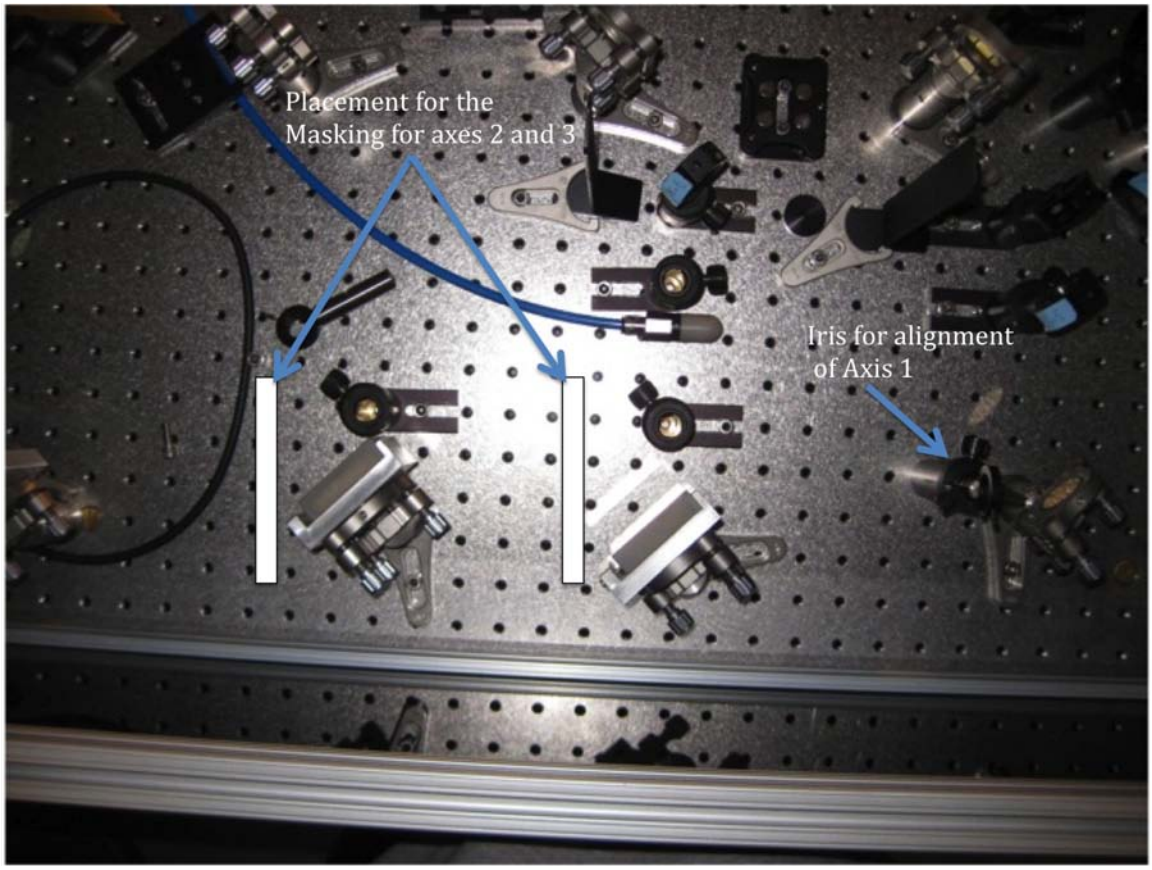

Figure 17. The placement for the masking and the arrow indicates the iris for alignment for axis 1.

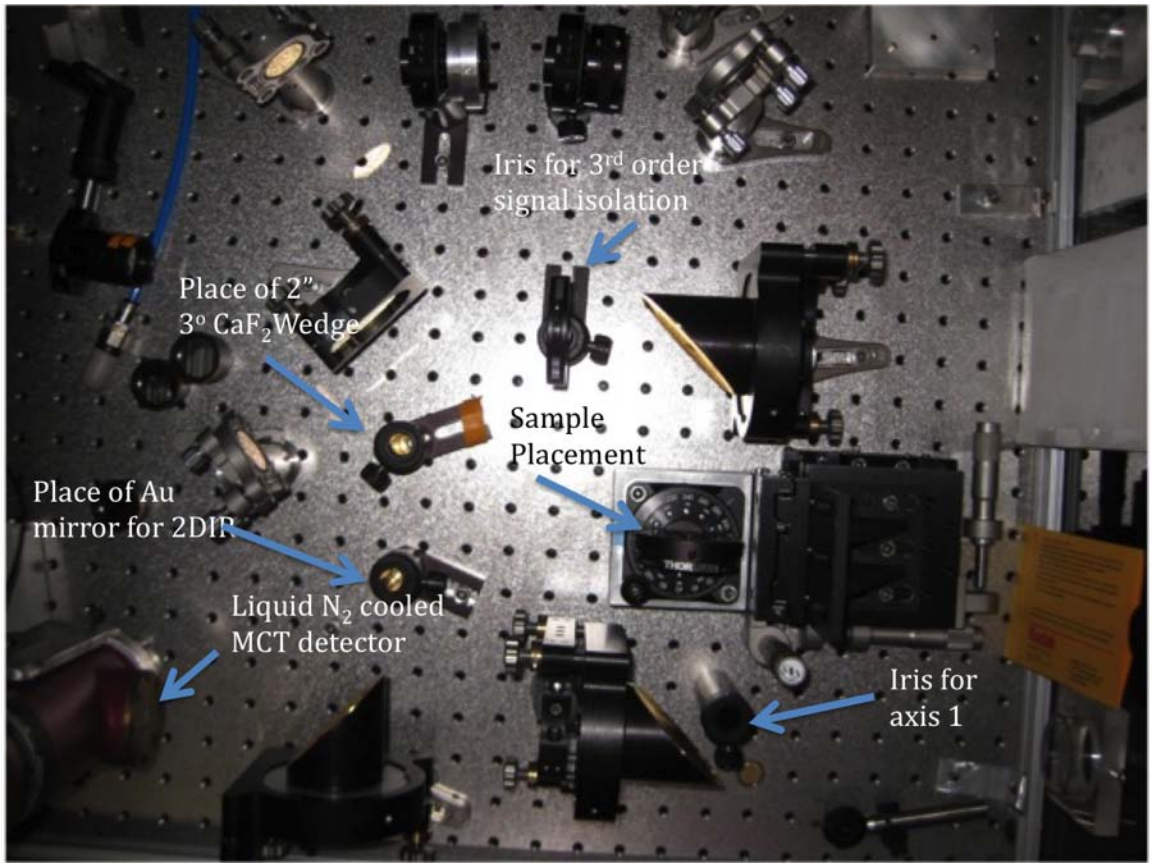

Figure 18. The sample box.

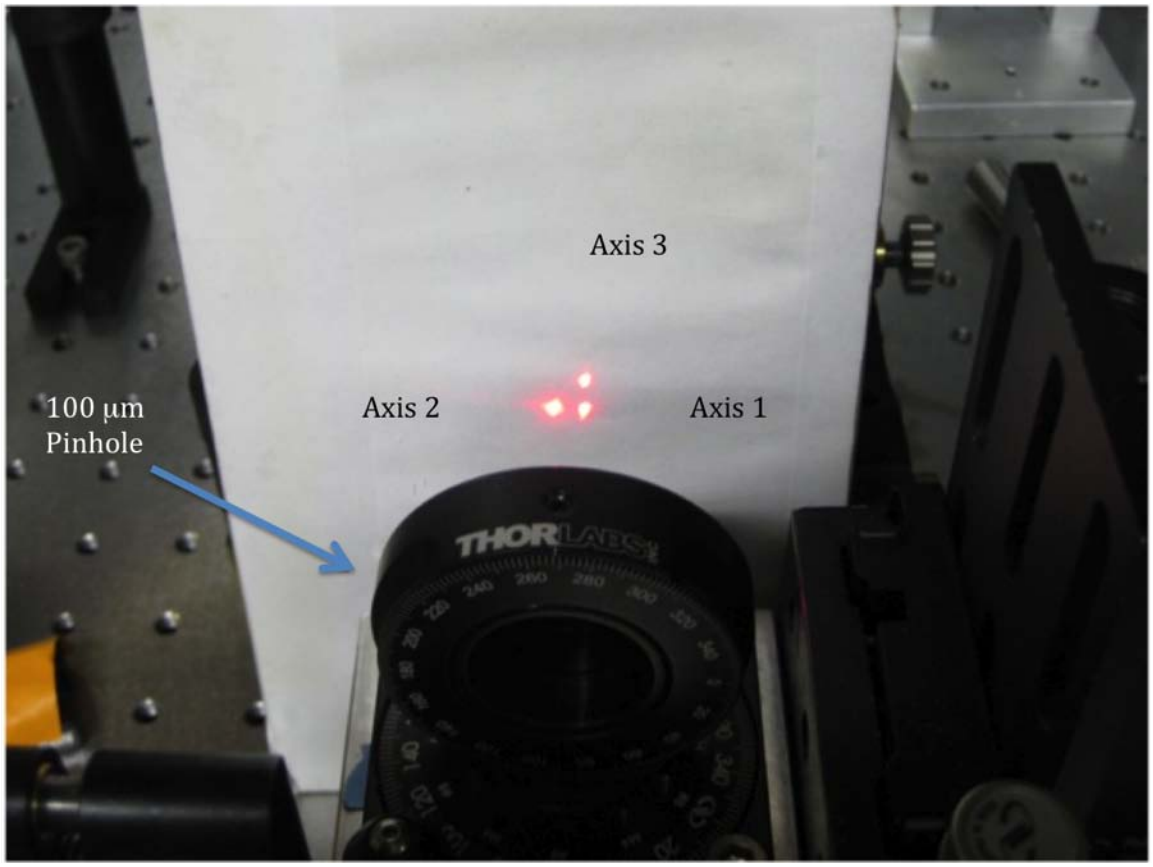

Figure 19. All three axes pass through a 100 μm pinhole. The axes are labeled accordingly.

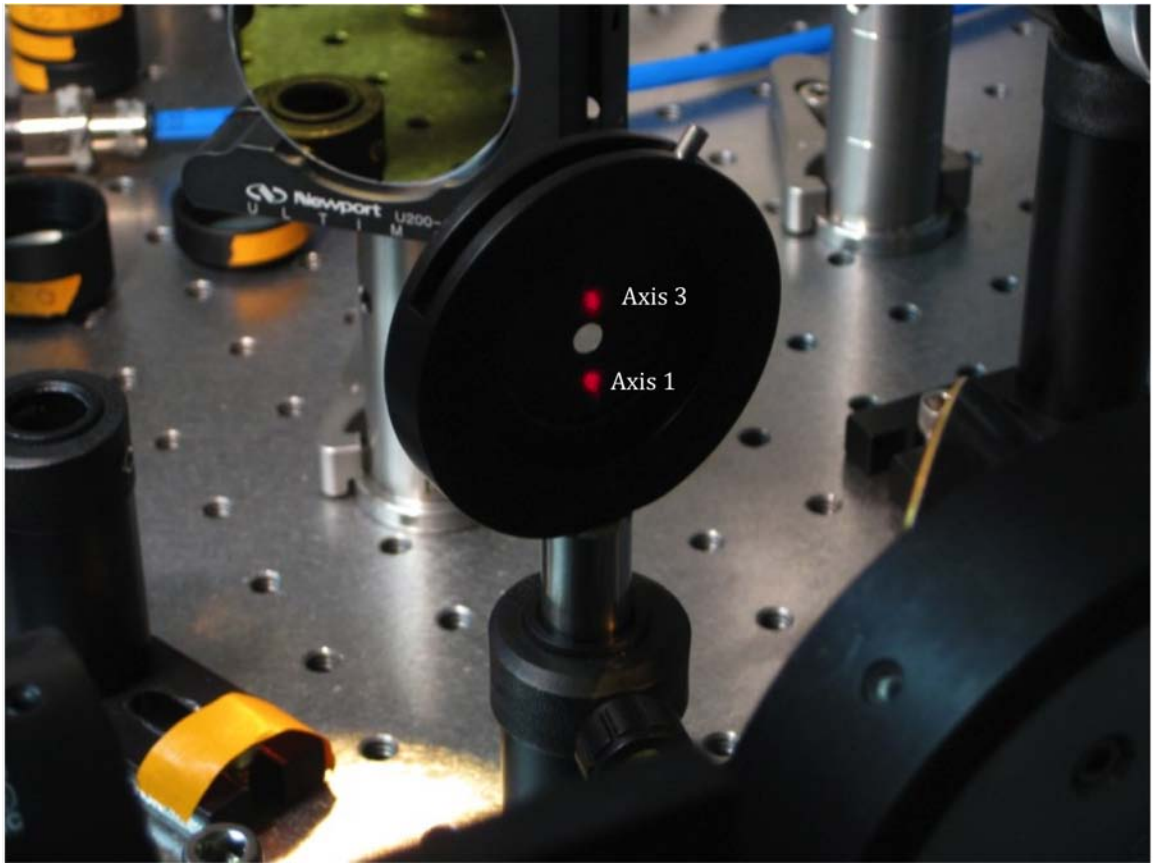

Figure 20. Image of the iris for placement for the auto correlation. The hole in the iris is where the auto correlation signal will pass thru.

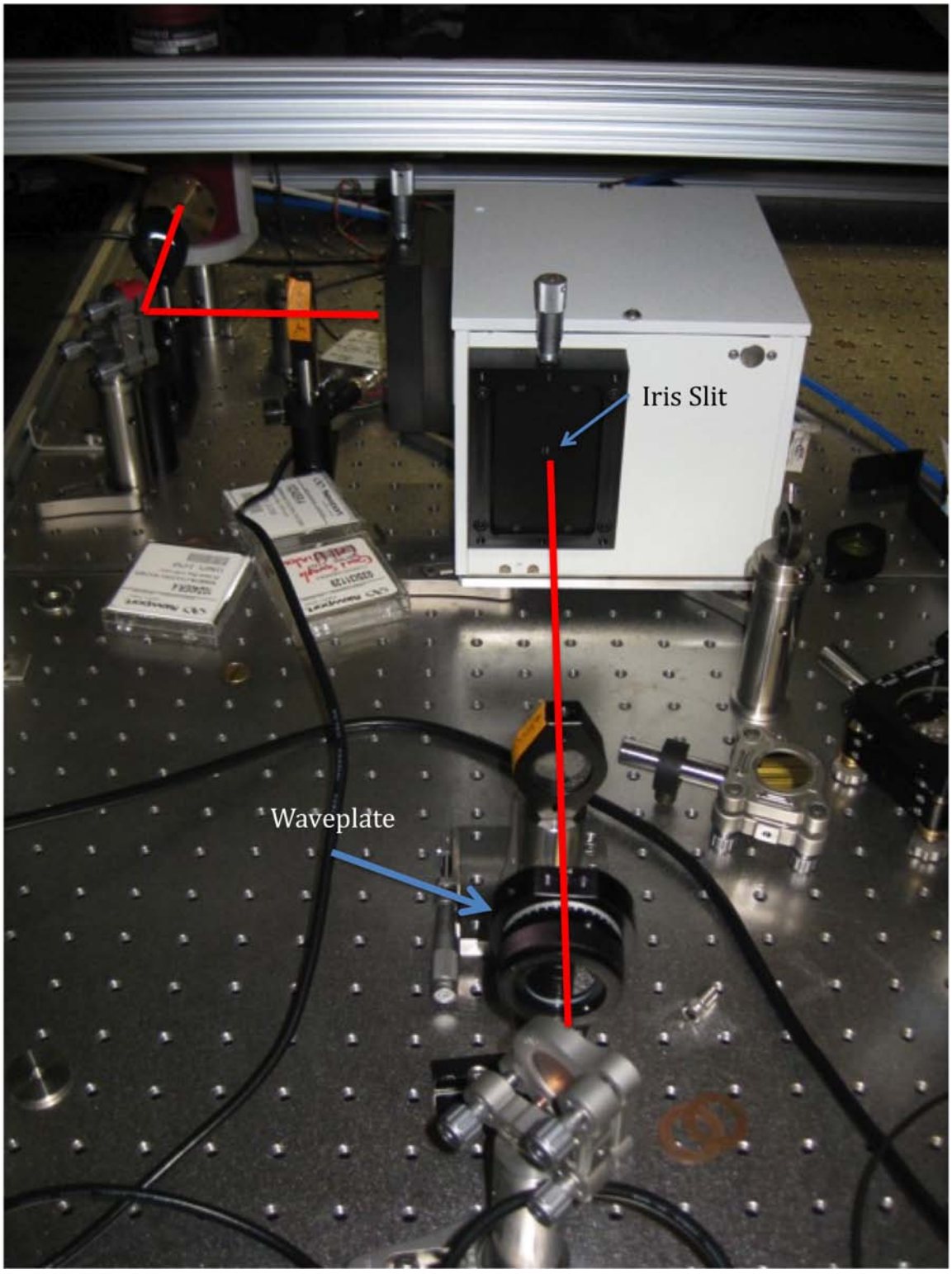

Figure 21. Path of the light going into and out of the monochromator.

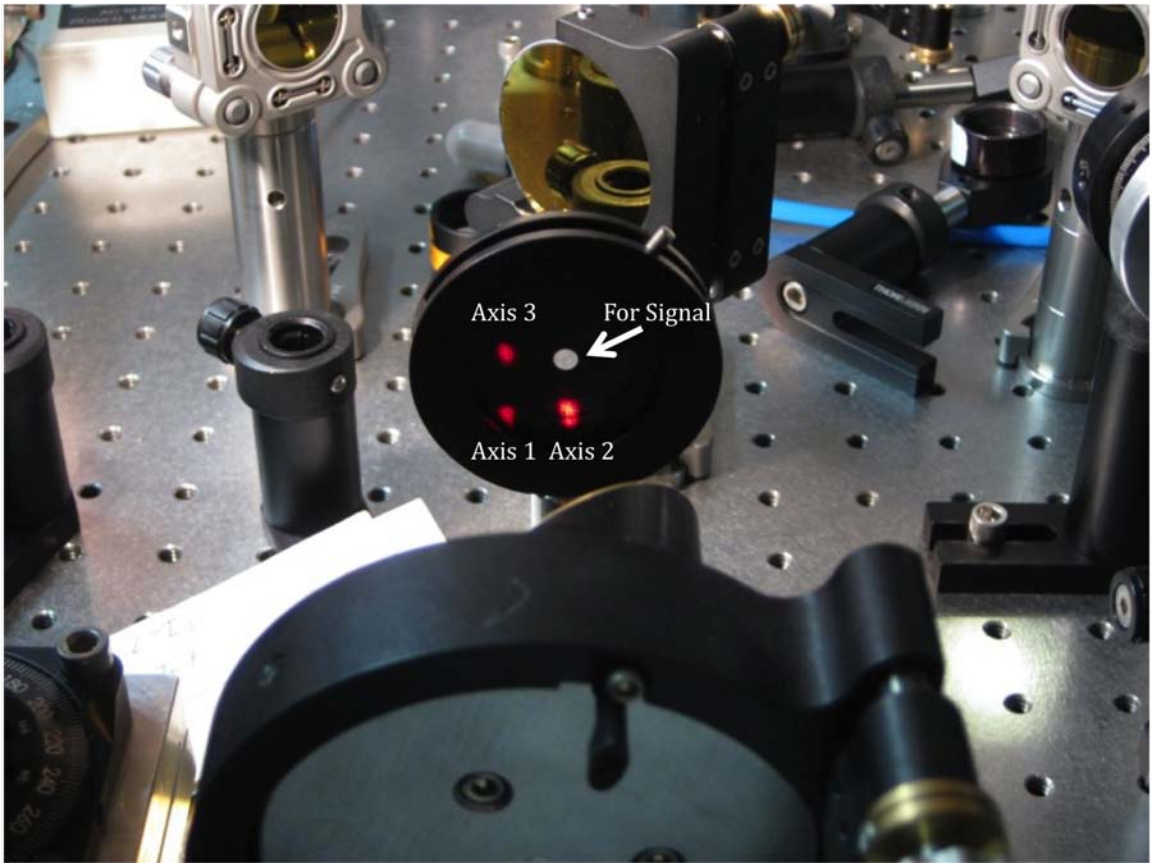

Figure 22. Iris set up for the 3rd order signal.

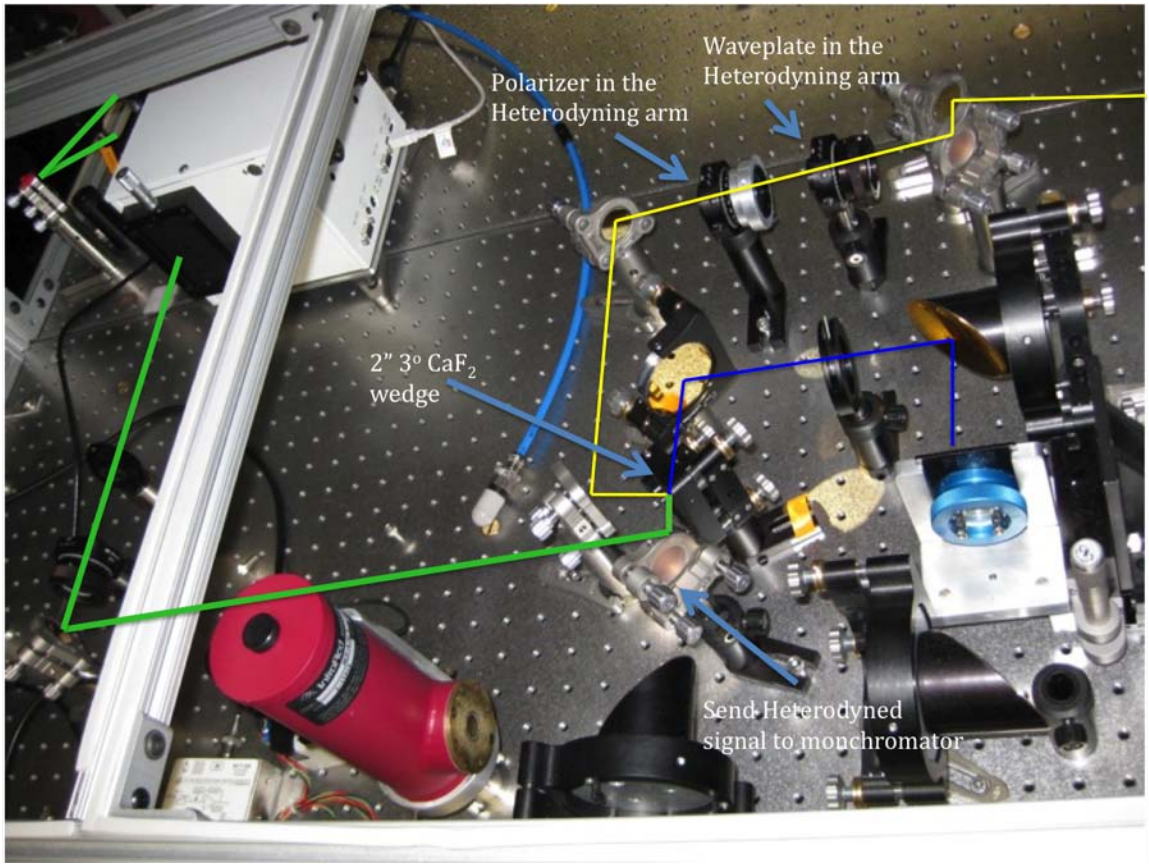

Figure 23. The path for heterodyned measurements. Blue line is the signal, yellow line the local oscillator and the green line the heterodyned signal.

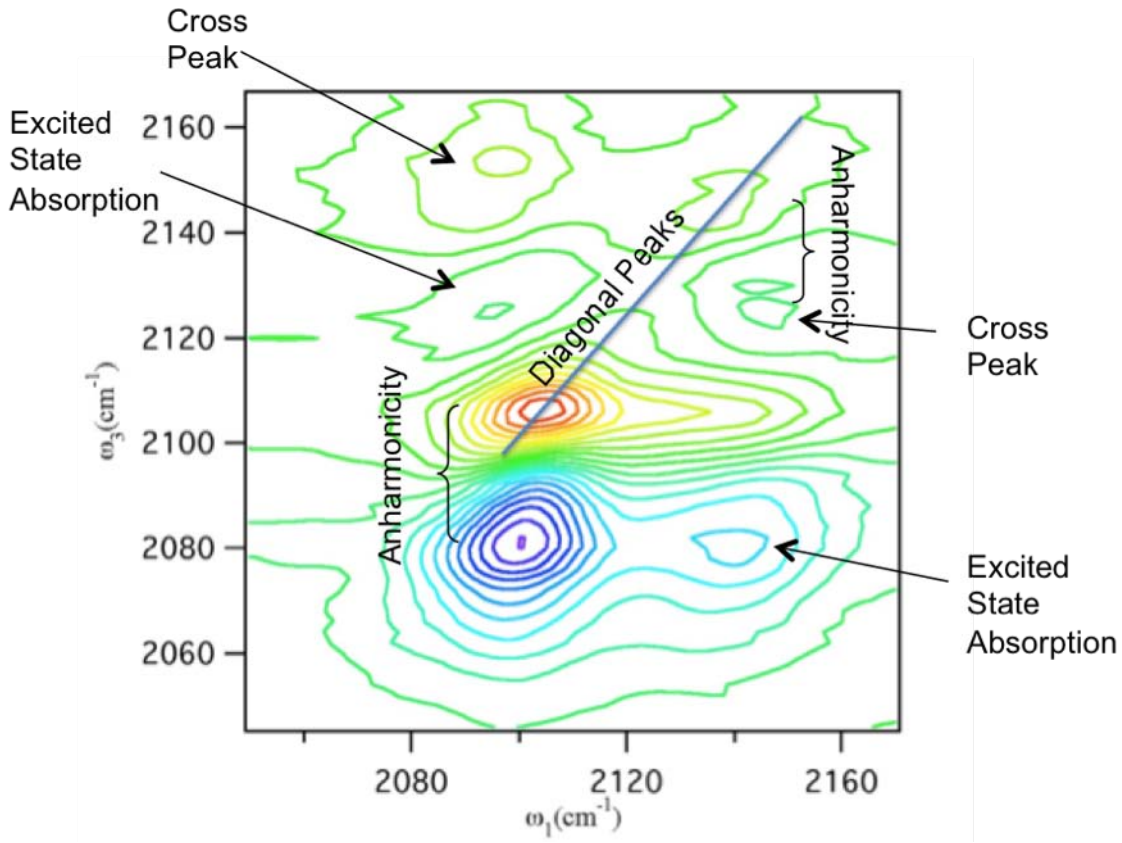

Figure 24. 2DIR spectrum showing diagonal peaks, anharmonicity, cross peaks, and excited state absorption.

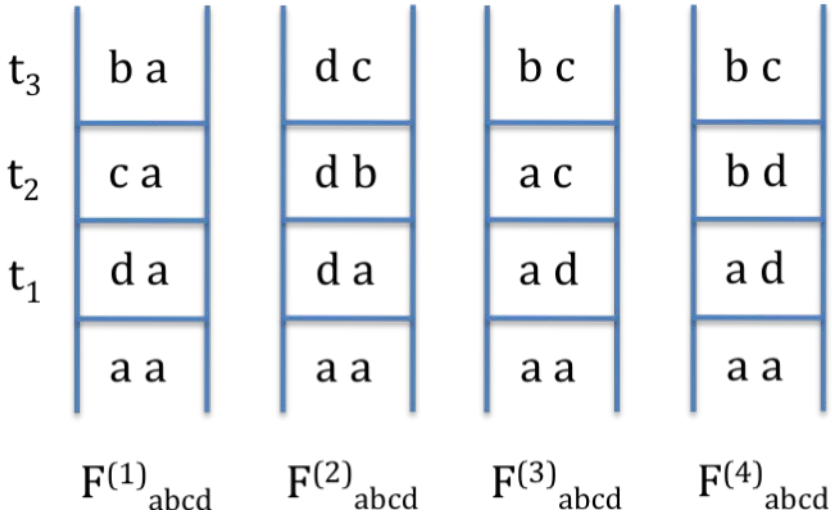

Figure 25. Evolution of the density matrix. The four Liouville pathways. a = 0; b,d = 1; c = 0,2.[53]

$\mathbf{S_I = -k_1 + k_2 + k_3}$

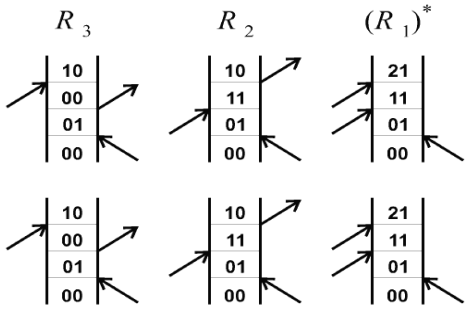

NONREPHASING

$\mathbf{S_{II} = +k_1 - k_2 + k_3}$

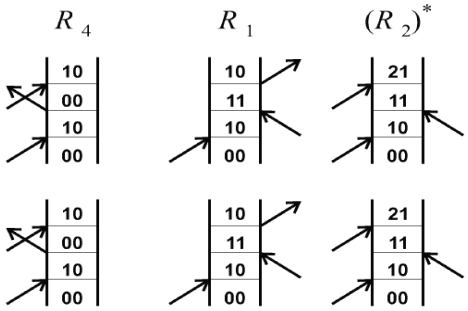

$\mathbf{S_{III} = +k_1 + k_2 - k_3}$

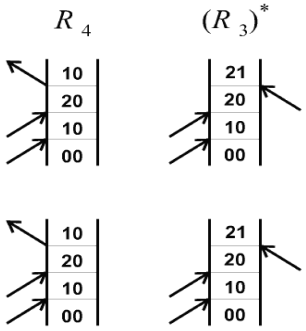

Figure 26. Feyman diagrams for the rephasing and nonrephasing. Adapted from ref. 54.

CHAPTER 3: VIBRATIONAL RELAXATION OF C-D STRETCHING VIBRATIONS IN $CDCL_3$, $CDBR_3$, AND CDI_3

Introduction

Intra- and inter molecular vibrational population dynamics are fundamentally relevant to chemistry. [56] Bond breaking and formation utilize localized vibrational energy to effect chemical change. In addition, vibrational population relaxation reports on intermolecular interactions in condensed phases. Therefore, the time scales of vibrational relaxation and the mechanisms that control energy flow in polyatomic molecules underlie a molecular view of chemistry.

Conventionally, vibrational relaxation is thought to take place via two processes, intra-molecular vibrational energy redistribution (IVR) and intermolecular energy transfer (IET). [6, 57-59] In IVR, energy initially localized in a particular vibration redistributes among the vibrational degrees of freedom of the molecule with relatively little energy transfer to the solvent. Both the coupling between initial and final vibrational states within the molecule and the number of these states that lie in an accessible range of energies, on the order of k_BT, play critical roles in determining the rate of IVR. In IET, energy flows out of the molecule into the solvent degrees of freedom as the molecule relaxes down to its vibrational ground state. The solvent-solute interactions are obviously relevant to the rate of IET. What is less obvious is that the solvent has the potential to play a role in IVR as well.

For large enough molecules true isoenergetic IVR, as would be seen in the gas phase, can dominate the relaxation of the initially excited state. Vibrational relaxation measurements of acetylenic C-H stretches of 10 different methyl acetylenes by Yoo *et al*. indicate such a mechanism and that the solvent makes little or no contribution to the relaxation. [60-62] In contrast, measurements of the relaxation rate of a number of

halomethanes in polar and nonpolar solvents show a rather significant solvent effect on the IVR rate. [1, 6, 57, 63-66] In these molecules, the solvent makes up the energy defect for strongly coupled states. Although both of these relaxation mechanisms have been referred to as IVR, only the former is strictly intramolecular and the latter is more accurately termed solvent-assisted IVR. The solvent-assisted mechanism is what we will refer to as IVR throughout the remainder of this manuscript.

The relaxation of C-H stretching vibrations has been well characterized for a variety of molecules and in several solvents. In fact, the vibrational relaxation of C-H modes has been studied more than the relaxation of any other vibrational mode. The earliest studies on C-H modes go back to the 1970s. [67-69] Subsequent studies of IVR and IET following C-H excitation include experiments on: aromatic molecules,[3, 70, 71] halogenated hydrocarbons, [1, 6, 57, 58, 64, 72-74], acetonitrile [75] methyl acetylenes, [60-62] and alcohols. [76, 77] These experiments have also motivated many theoretical studies providing quantitative insight into the mechanisms of vibrational relaxation. [56, 78-81]

Comparison of the vibrational relaxation of C-H and C-D oscillators for isotopologues of the same molecule can help to clarify the relative importance of the various contributionsto the IVR rate. In the limit of purely statistical IVR, the total state density of the deuterated isotopologue will be significantly less than for the unlabeled molecule suggesting that IVR should be slower for the deuterated molecule. In the limit of state-specific IVR, however, the effect of isotopic substitution will depend on how the strongly-coupled state(s) shift upon isotopic substitution relative to the C-H (D) vibration. The acceptor state(s) could be closer in energy or further away depending on the details of the frequency shifts. Seifert *et. al*. made a comparison of the vibrational relaxation rates of the isotopologues of liquid bromoform, $CHBr_3$ and $CDBr_3$. [82] In this case, deuteration increases the rate of IVR by a factor of two. The authors explain this effect in terms of the shift of the likely acceptor states, which both involve two quanta of C-H (D) bend and a quantum of C-Br stretch, upon deuteration. For $CHBr_3$ these states are more

than 100 cm^{-1} below the C-H vibration, but for $CDBr_3$, the energy mismatch for these states is only about 50 cm^{-1}. Thus, the rate of relaxation increases upon isotopic substitution because of the change in local state structure.

In general, deuterium substitution does not alter the molecular structure but does shift the transition energies for vibrational modes that involve hydrogen stretching or bending. The transition frequencies of other vibrational motions remain the same or change only slightly. Hence, isotope labeling moves the initially prepared state to a lower energy where the local state structure and the density of states are significantly altered but does not perturb the molecular structure or the potential energy surface of the molecule. Therefore, comparison of the relaxation rates of C-D stretching vibrations with those of the unlabeled isotopologues for a sequence of structurally similar molecules in different solvents can clarify the vibrational relaxation mechanism and the role of the solvent in vibrational population dynamics.

In addition to probing the pathways for vibrational energy relaxation, the time-resolved infrared spectroscopy of deuterium labeled molecules is interesting in its own right. Isotope editing is a common tool in the vibrational spectroscopy of biomolecules. For example, isotope labeling studies employing both Fourier Transform Infrared (FTIR) difference spectroscopy and time-resolved IR spectroscopy have been widely used to explore protein dynamics in the amide I region of the IR spectrum. [83] Because C-D stretching vibrations absorb in a spectral region that is relatively free of interfering protein or water absorptions, they are attractive spectroscopic targets. Furthermore, deuterium labeling of particular bonds has the potential to probe specific, local protein structural heterogeneity and dynamics. For example, Chin *et. al*. used IR absorption spectroscopy of deuterium labeled amino acids to study the oxidation state of the cofactor in cytochrome c. [8] More recently, Sudo *et. al*. studied the structure of photo-intermediates of deuterium labeled retinal in rhodopsin using IR absorption spectroscopy. [84] The measurements we present here contribute to the basic understanding of the C-D

vibrational dynamics and lay the foundation for developing time-resolved vibrational spectroscopy of C-D oscillators. The time-resolved spectroscopy of C-D stretches has many potential applications as a probe of local structure and intermolecular interactions including studies of biomolecules similar to those described above.

We present infrared transient grating measurements of the vibrational relaxation of C-D stretching states in deuterated haloforms, CDI_3, $CDBr_3$ and $CDCl_3$ dissolved in acetone and benzene. Several research groups have investigated the vibrational relaxation of the C-H modes in the isotopologues of these molecules. We make direct comparison to those results and gain insight into the mechanism of IVR for the C-H (D) stretch in haloforms and the effect of solvent on the relaxation rate.

Results and Discussion

Figure 27 shows the infrared absorption spectra of the deuterated haloforms in acetone (solid), benzene (dashed) and $CHCl_3$ (dotted). The C-D vibrational transition is centered near 2250 cm^{-1}. The feature at 2210 cm^{-1} in the spectra of the benzene samples is a weak benzene absorption, likely a combination band. The transition intensity of the C-D oscillators is strongly solvent dependent. The absorption corresponding to the C-D stretch of chloroform is more than three times stronger in acetone than it is in benzene and an order of magnitude greater than it is in $CHCl_3$. For bromoform the ratio is closer to two between acetone and benzene and closer to four between acetone and $CHCl_3$. For iodoform the transition strength is about two times stronger in acetone compared to benzene and an order of magnitude grater than it is in $CHCl_3$. Because of these variations, the grating signal, which scales as the power of the molar absorptivity, is much larger for the haloforms dissolved in acetone than in benzene. In addition, the absorption linewidth, like the transition strength, for each of these molecules, is greater in acetone (about 14 cm^{-1}) than it is in benzene (about 8 cm^{-1}). These characteristics of the infrared absorption spectra are indicative of strong solvent-solute interactions. [57]

Figures 28 and 29 show the transient grating data for deuterated chloroform (top), bromoform (middle), and iodoform (bottom) in acetone and benzene, respectively. For comparison, the solvent response is also shown (dashed line). The initial rise of the signal before zero delay corresponds to a free induction decay that begins well before the pulses start to overlap. [85, 86] The large peak at zero delay, which is truncated in the figures, is the non-resonant response of the solvent, a characteristic of four-wave mixing experiments, and persists only for the duration of pulse overlap. To extract the vibrational energy relaxation rate, we analyze the decay of the signal after the nonresonent response. In benzene, there is an additional subpicosecond solvent response arising from excitation of the weak combination band at 2210 cm^{-1}. We do not fit this decay separately and thus it is included in the subpicosecond component of the measured grating decay of our samples. The decays of the grating signals are nonexponential for all measurements, each consisting of a subpicosecond component and a picosecond timescale component. The reported time constants are insensitive to the exact starting point of the fit so long as it begins after the decay of the nonresonant response. Because the homodyne detected signal is proportional to the magnitude square of the signal electric field, and the signal is nonexponential, we fit the data to a squared bi-exponential decay, i.e.

Equation 19. Squared biexponential decay equation

$$S(t) \cong \left| a e^{-\frac{t}{\tau_1}} + b e^{-\frac{t}{\tau_2}} \right|^2$$

Nonexponential population decays have been observed previously. [22, 87-89] There are several possible explanations for nonexponential population dynamics. First, solvent memory effects, which occur when the relaxation dynamics are not averaged over all

solvent configurations, can cause nonexponential decay. Both benzene and acetone form complexes with haloforms. At early times, i.e. less than the lifetime of these complexes, the transient grating signal may contain contributions from inhomogeneous vibrational dynamics. On longer time delays, once the solute has dynamically averaged over solvent configurations, the signal would then reflect homogenous vibrational dynamics. A second possible explanation for the nonexponential decay is strong coupling to nearby dark states, in which, the excited mode rapidly equilibrates with strongly-coupled states and then relaxes out of these states. Hamm *et. al*. [22] and Maekawa *et. al*. [88] attribute similar nonexponential population decays to such a mechanism. Finally, it is also possible that the coherent artifact contributes to the early part of the transient resulting in a nonexponential decay. Regardless of its origin the fast contribution to the decay is not indicative of the solvent assisted IVR. Therefore, we identify the slow component in the fits as the measured IVR time.

In principle, the grating decay is sensitive to both IVR and IET. Because of the nature of sequential kinetics, one would only expect to observe a distinct IET contribution to the transient grating decay if the IET rate is substantially slower than the IVR rate. If IET is faster than IVR, then no population builds-up in the intermediate states. If IET takes place on the same time scale as IVR, then IVR and IET are not separable. If IET is slower than IVR, then the transients should exhibit a long time decay due to IET. Based on the previous measurements of IET in the unlabelled isotopologues, we expect that the IET rate to be slower than IVR, especially in benzene. [6, 90] One important caveat is that the changes in IVR mechanisms and in the isotopic composition of the solvent can also lead to differences in IET process. We do not observe a long decay component in our transients indicating that either IET occurs on short time scale, similar to or faster than IVR or it makes little contribution to the transient grating decay. It is likely that the contribution from IET is weak. IET contributes to the signal because the C-D stretch transition of the daughter modes populated via IVR is anharmonically

shifted by a small amount and may have a slightly different transition moment. During the IET process, the C-D transition returns to its original position and intensity contributing an additional decay to the transient grating signal. In our case the IET contribution to the transients is weak because the spectroscopic perturbations of the C-D stretch are small. The ground state bleach and the absorption of vibrationally hot molecules, which have opposite phases, destructively interfere. If the C-D frequency and the transition moment for the vibrationally hot molecules were the same as the ground state molecules, then IET would make no contribution to the grating decay. The fact that we do not observe a slow decay in our transients suggests that IET does not significantly contribute to the signal. Nevertheless, the potential contribution of IET to the observed decay limits the accuracy of our results.

Table 1 summarizes the IVR times for each molecule in both acetone and benzene. The reported errors in the lifetimes represent the fit errors. In parenthesis we report the IVR lifetimes for the CH relaxation from previous measurements.

We have focused on deuterated iodoform, bromoform and chloroform in part because the vibrational relaxation of the unlabeled isotopologues has been studied extensively. Previous measurements show that the vibrational relaxation of these molecules is primarily state-specific and strongly solvent dependent with lifetimes ranging from a few picoseconds to about 100 ps. [6, 90] Our aim in measuring the relaxation of the deuterated isotopologues of these molecules is to further explore the relaxation mechanism and the solvent effect and how these features change in response to a perturbation, deuterium substitution. This perturbation is interesting both as a probe of the mechanisms of vibrational relaxation, for which these molecules are now a benchmark, and because of the ongoing interest by our group and others in using deuterium labeling as a way to probe intra- and intermolecular interactions.

IVR Mechanism

State-specific relaxation involves one or a few states strongly-coupled to the initially prepared state that serve as the important pathways for the depopulation of the initial state. This relaxation mechanism stands in contrast to statistical relaxation, which assumes that all of the states nearby in energy equally contribute to the depopulation of the initially prepared state. Based on Fermi's golden rule, the rate constant for statistical relaxation is expected to scale with the total density of states at the energy of the initially prepared state. This statistical assumption underlies transition state theory and other statistical models of chemical reaction dynamics, so the breakdown of statistical behavior is an important phenomenon in the context of chemical reaction dynamics.

The C-D stretching state is lower in energy than the corresponding C-H state, and, as a result, the density of states for the deuterated molecule is lower. Figure 30 schematically depicts the low-ordered-coupled states within 200 cm^{-1} of the C-D stretching state enumerated via a harmonic state count using the normal modes from Table 2 sorted by coupling order for each of the three compounds. In each case, we have also calculated the density of states of the deuterated and undeuterated (in parenthesis) molecules. The state count is not quantitatively correct first because we do a harmonic state count to enumerate the states and second because we use the gas phase frequencies. [91] For CDI_3, the gas phase frequencies are not available in the literature, so we estimate the frequencies. We use the experimental value for the C-D stretch from the FTIR spectrum, and, for the remaining modes, we scale the CHI_3 frequencies by an amount consistent with the frequency shifts in $CDCl_3$ and $CDBr_3$ upon deuteration. [91] Nevertheless, the argument is only qualitative and, therefore, is independent of the exact values of the fundamental frequencies. As expected, the density of states at the energy of the C-D stretch decreases compared to that for the C-H stretch for all of these molecules. Based on a statistical relaxation model, we would predict that the relaxation rate for the deuterated isotopologues should be slower than for the C-H relaxation and that the

relaxation rate for the molecules should vary monotonically with $k_{CHCl3} < k_{CHBr3} < k_{CHI3}$. Our results show exactly the opposite trends. In each case the relaxation rate of the C-D vibration is similar to or faster than the corresponding C-H vibration, and iodoform exhibits the slowest relaxation followed by bromoform and then chloroform. Thus, our results are inconsistent with a statistical relaxation mechanism. This conclusion is in agreement with previous studies of C-H relaxation. [6, 57, 60-62, 90]

The state structure of the low-order-coupled states in haloforms determines the IVR dynamics. Previous studies of the C-H relaxation have focused on the 4th-order-coupled states, particularly those that include two quanta of C-H bending excitation, as the likely candidates for the primary relaxation pathway. [6, 73, 81] This analysis is supported both by the IVR rates correlate well with the energy defect of those states and by IR-pump/Raman-probe measurements that indicate that CH bending and C-X stretching modes are excited as the C-H population decays. [58] Following this reasoning, we analyze the 4th-order-coupled states for the deuterated haloforms, listed in Table 3 and identify correlations between the observed IVR rates and variations in the state structure.

In chloroform the number of 4th-ordered-coupled states increases from 9 for the undeuterated molecule to 30 for the deuterated isotopologue. For $CHCl_3$, all of the 9 states involve 2 quanta of CH bend ($2\nu_4$). In contrast, for $CDCl_3$, there are an additional 9 states with no CD bend character and 12 with only 1 quantum of CD bend. There are no analogues to these states nearby in energy to the C-H stretch. Thus, for chloroform, the number of low-order-coupled states that can serve as relaxation pathways significantly increases upon deuteration. Although the effect is most dramatic in chloroform, a similar analysis holds for the other haloforms. For bromoform, the number of states increases from 6 (H) to 15 (D). Of these additional states, 6 have 1 quantum of CD bend and the other 3 involve 2 quanta of CD bend. In the case of iodoform the 4 states near the C-H stretch are composed of 3 quanta of CH bend. For CDI_3 there are an

additional 6 states with 2 quanta of CD bend. Clearly, the bend mode, because it is the highest frequency mode after the C-H (D) stretch plays a critical role.

Not only does the number of states of 4th-order-coupled states change upon deuteration, the energetic state structure is also different. In $CDCl_3$, the new states that are not present for $CHCl_3$ have a better energy match to the C-D stretching state compared to the ones that serve as the dominant relaxation pathway in $CHCl_3$. For example, the state with 3 quanta of CCl_3 antisymmetric stretch ($3\nu_5$) forms a 4-fold degenerate set of states that is not an important 4th-order-coupled state for $CHCl_3$ because its energy defect is approximately 800 cm^{-1}. For $CDCl_3$, however, it is only 19 cm^{-1} off resonance with the C-D stretch. In addition, there are two states with 1quantum of CD bend and 2 quanta of CCl_3 symmetric stretch ($\nu_4 + 2\nu_2$) at 2232 cm^{-1}, which is only 34 cm^{-1} away from the C-D stretching state. The corresponding state in $CHCl_3$ is 454 cm^{-1} away from the C-H stretch. In contrast, the state that is to the dominant IVR pathway for $CHCl_3$, two quanta of CH bend and a quantum of CCl_3 symmetric stretch ($2\nu_4 + \nu_2$), which is 86 cm^{-1} away from the C-H stretch, is not shown in Figure 30 because it is 221 cm^{-1} above the C-D stretch. There is, however, a new state with 2 quanta of CD bend and a quantum of CCl_3 symmetric deformation ($2\nu_4 + \nu_3$) only 69 cm^{-1} away from the C-D stretch. This analysis indicates that not only should IVR in $CDCl_3$ be faster than the corresponding C-H relaxation both because of the increased number of states and improved energy match, but also the relaxation should proceed through different states for $CDCl_3$ than for $CHCl_3$. The difference between the IVR processes of $CHCl_3$ and $CDCl_3$ may also result in a difference IET as well. Thus isotope labeling completely changes the relaxation pathways and time scales.

In $CHBr_3$, just as with $CHCl_3$, the dominant relaxation pathway involves two quanta of C-H bend and a quantum of C-Br antisymmetric stretch, $2\nu_4 + \nu_5$, which lies 65 cm^{-1} above the C-H stretching state. The corresponding state in $CDBr_3$ is 81 cm^{-1} away from the C-D stretch, but the analogous combination with the symmetric stretch, $2\nu_4 +$

ν_2, is only 30 cm^{-1} above the C-D stretching state. Thus, the IVR mechanism of the deuterated isotopologue is essentially the same as in the unlabeled molecule, but the relaxation rate increases because the states that serve as the relaxation pathway have a smaller energy defect for the C-D than for the C-H. These observations are consistent with previous work on bromoform and its deuterated isotopologue in mixtures of $CHBr_3$ with $CDBr_3$. [82]

A similar analysis in iodoform explains the dramatic enhancement in the IVR rate upon deuteration. In CHI_3, the only 4^{th}-order-coupled state within 200 cm^{-1} of the C-H stretching state is the second overtone of the C-H bend, $3\nu_4$, which is 190 cm^{-1} above the C-H stretch. In CDI_3, the corresponding mode is only 50 cm^{-1} above the C-D stretch, and an additional state, $2\nu_4 + \nu_5$, moves to within 137 cm^{-1} of the C-D stretching state. As a result, the relaxation of the C-D is an order of magnitude faster than for the C-H.

Solvent Effect on Relaxation

As has been demonstrated previously, vibrational relaxation is strongly solvent dependent. [1, 6, 57, 63-66] Previous studies of the C-H relaxation of haloforms indicate that, in general, strong specific solvent-solute interactions lead to faster IVR kinetics. One explanation of the solvent effect is that the solvent serves to make-up the energy defect between the initial state and the low-order-coupled states that form the dominant relaxation pathways. Increasing the strength of the solvent-solute interactions improves the solvent's ability to cover the energy defect between the states, thereby increasing the rate of IVR.

The linewidths and intensities of the C-D transitions in the IR absorption spectra (shown in Figure 27) are all sensitive to variations in the strength of the solvent-solute interactions. In acetone, the lineshapes of the C-D transition is significantly asymmetrically broadened relative to the benzene lineshapes, consistent with stronger solvent-solute interactions in acetone leading to heterogeneous broadening of the

lineshape. The intensities of the transitions vary with two trends: For a given molecule, the transition is always stronger in acetone than in benzene, and, for a given solvent, the iodoform transition is the strongest and the chloroform transition is the weakest with bromoform falling in between these two. These intensity variations arise because, for the haloforms, the dipole moment as a function of the C-H (D) bond length is near its maximum. [79] Thus the intensity of the C-H (D) transition, which, is proportional to the first derivative of the dipole moment with respect to the vibrational coordinate, is near zero. Any perturbation, however, such as a solvent-solute interaction, can alter the shape of the dipole moment function so that the equilibrium bond length no longer corresponds to the maximum. Then the derivative, and thus the transition intensity will increase. Consequently, the intensity of the C-D transition correlates with the strength of the solvent-solute interactions.

Previous studies of iodomethanes in these solvents suggest that the dominant solvent-solute interaction in these systems involves a charge-transfer complex in which the solvent donates electron density into an anti-bonding orbital of one of the C-X bonds of the haloform. [57, 90] Consistent with the trends in the absorption spectra, these interactions would be strongest for iodoform and weakest for chloroform and acetone would serve as a better electron donor than benzene. For CH_2I_2, *ab initio* calculations predicted a 2 kCal/mol interaction with acetone. [57] Complexes of this type, sometimes referred to as halogen bonded complexes, are well known in supramolecular chemistry. [92, 93] Such complexes likely contribute to the strong solvent-solute interactions for bromoform and iodoform in acetone and benzene. Chloroform, however, is known to form weak hydrogen bonds to acetone. Less is known about the benzene chloroform interactions. Although they should be weak, the C-D transition intensity does increase on going from $CHCl_3$ to benzene as the solvent.

In benzene, our data show the trend we expect based on the arguments in the previous section about state structure. Chloroform shows the fastest IVR followed by

bromoform, then iodoform. For the C-H relaxation of chloroform, the IVR rate in benzene is the same, within experimental error, as it is in CCl_4. [6] In contrast, the IVR rates for bromoform and iodoform are greater in benzene than in CCl_4 suggesting that the solvent-solute interactions are significant for bromoform and iodoform but that they do not affect the relaxation rate for chloroform in benzene. Assuming that is still the case for the C-D relaxation, then the 2.6 ps lifetime we observe for $CDCl_3$ in benzene represents the lifetime in a weakly interacting solvent, and we would predict that the relaxation rate should be similar in other weakly interacting solvents like CCl_4. Of course, the benzene chloroform interactions do perturb the C-D transition intensity so we cannot rule out a solvent effect on the lifetime as well. For bromoform and iodoform, benzene is clearly not a weakly interacting solvent. Although the IVR rate of these molecules is slower in benzene than in acetone, we would predict that the IVR would be slower still in more weakly interacting solvents like CCl_4. This prediction is consistent with previous measurements of the IVR lifetime of $CDBr_3$ in $CHBr_3$ of 24 ps, which is a factor of two longer than the 12.3 ps lifetime we observe.

In acetone, we observe the same trend in IVR lifetimes for bromoform and iodoform as is seen in the C-H relaxation. In each case, the relaxation of the molecule in acetone is faster than the corresponding decay in benzene. For chloroform, however, we see an unexpected result. The lifetime of the C-D stretch is *longer* in acetone than in benzene by about a factor of 4. This result is in contrast to the behavior for the C-H relaxation and to our expectation based on the infrared absorption spectra, which both suggest that acetone is the more strongly interacting solvent. One way to rationalize the solvent effect in acetone is by reconsidering the details of the state structure. The states with the smallest energy defect, $3\nu_5$ and $\nu_4 + 2\nu_2$, are 19 and 34 cm^{-1} below the C-D stretch state respectively. In acetone, the C-D frequency is higher in energy than in benzene by about 10 cm^{-1}. Because of this shift, the C-D stretching state moves away from the nearby states that are the likely relaxation pathways, consistent with the

observation that the lifetime of that state increases. As the energy defect gets larger, the relaxation becomes slower. Although the solvent effect on the vibrational lifetime of $CDCl_3$ is counter to what we expected, such behavior is possible in a state-specific relaxation mechanism. To our knowledge this is the first example of a system where the vibrational lifetime increases as a result of strong solvent interactions.

Conclusion

We have studied the vibrational energy relaxation of deuterated chloroform, bromoform and iodoform molecules in acetone and benzene. Comparing our findings with previous studies of the C-H relaxation shows that isotope labeling changes the state structure of the low-order coupled states nearby in energy to the C-D stretch without changing the chemical characteristics of the molecule. In deuterated molecules, there are more low-ordered-coupled states compared to the unlabeled isotopologue. In bromoform and iodoform, the relaxation proceeds through essentially the same types of states for both isotopologues and the vibrational relaxation rate of the deuterated molecules is faster because of the improved energy defect with the important acceptor states. In chloroform, new relaxation pathways become available in the deuterated molecule that were not present in the unlabeled molecule, and these new states are nearly energetically resonant with the C-D stretching state leading to fast relaxation for the deuterated isotopologue.

There are significant solvent effects for the haloforms in benzene and acetone. For bromoform and iodoform, these effects can be understood in terms of the formation of charge-transfer complexes between the solute and the solvent molecules, i.e halogen bonds. For chloroform in acetone, it is likely that hydrogen bonding is more favorable than halogen bonding. The strength of the complexation is different for each of these molecules in the two solvents, and these differences are reflected in both the IR absorption spectra of the C-D vibrations and the observed IVR rates. The most surprising result is that the relaxation

rate for chloroform is slowest in the more strongly interacting solvent, acetone. This result is not only unexpected, it is also unprecedented.

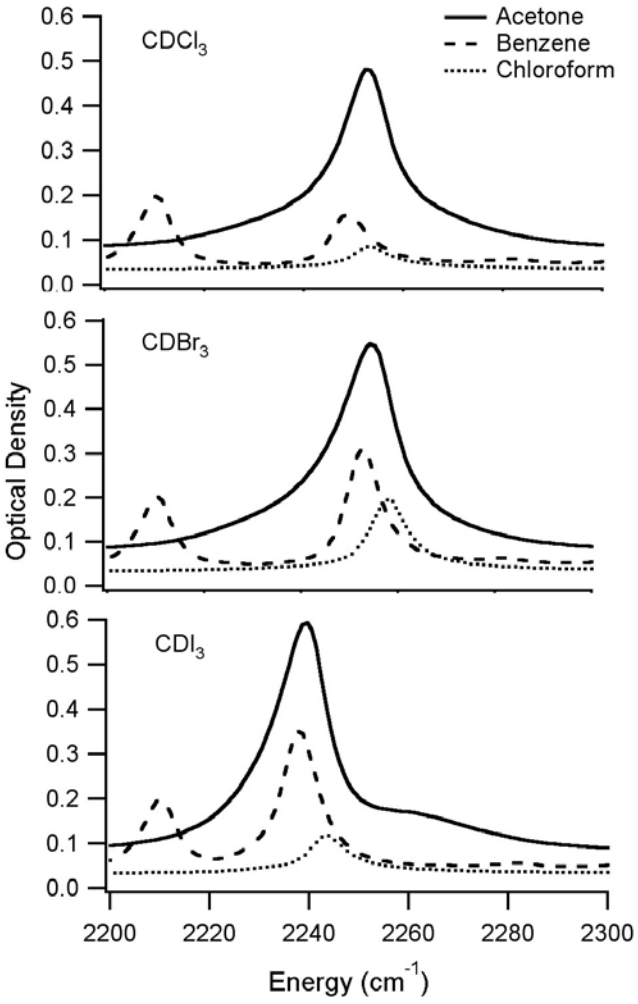

Figure 27. Infrared absorption spectra of deuterated chloroform (top), bromoform (middle), and iodoform (bottom) in acetone (solid line), benzene (dashed line), and chloroform (dotted line).

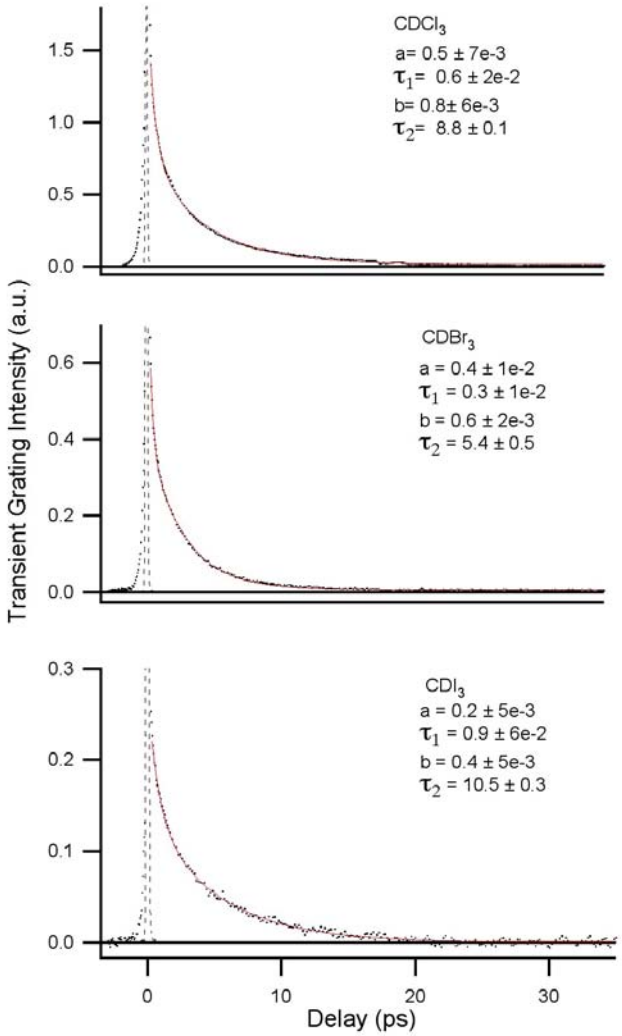

Figure 28. Time-resolved transient grating data for deuterated chloroform (top), bromoform (middle), and iodoform (bottom) in acetone. The solid lines are the fits to the data for which the parameters are given in each figure. The dashed line is the neat solvent response.

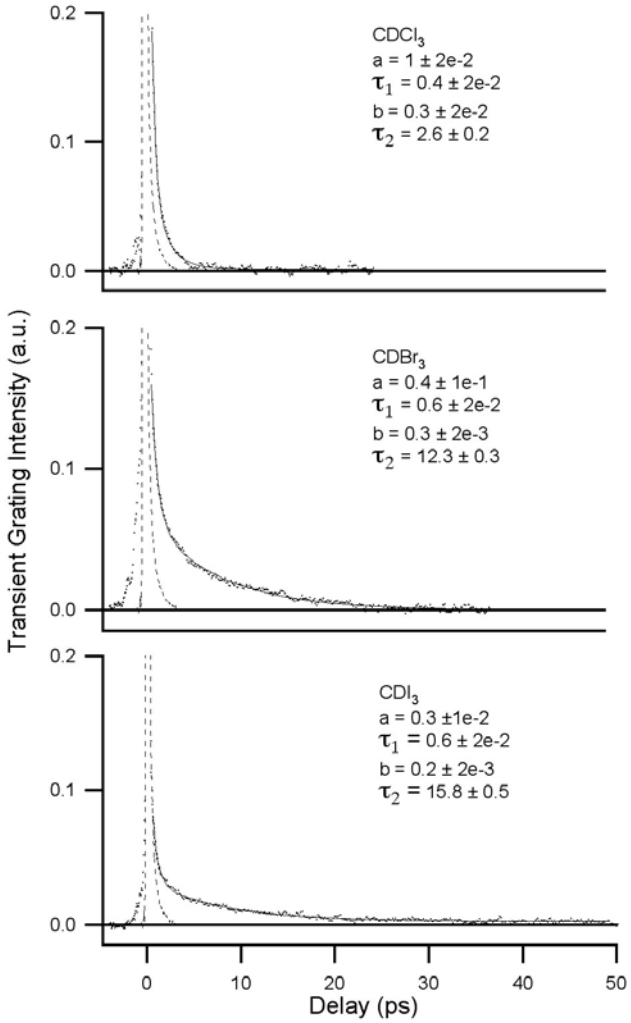

Figure 29. Time-resolved transient grating data for deuterated chloroform (top), bromoform (middle), and iodoform (bottom) in benzene. The solid lines are the fits to the data for which the parameters are given in each figure. The dashed line is the neat solvent response.

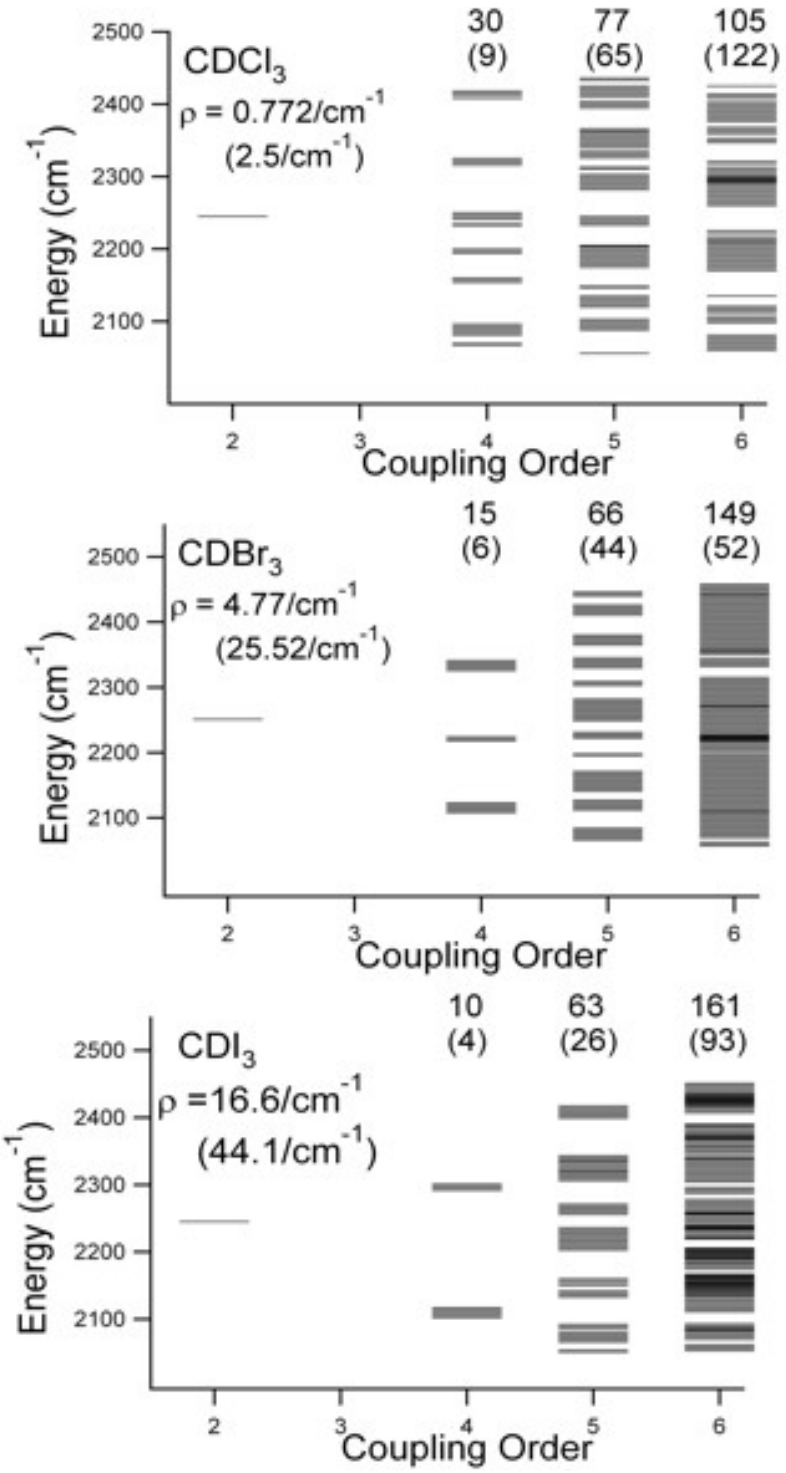

Figure 30. Enumeration of overtone and combination states within 200 cm^{-1} of the C-D stretching state sorted by coupling order based on a harmonic state count for each haloform.

Table 1. Time constant for the IVR process of deuterated haloforms in acetone and benzene.

	Acetone	Benzene
Solvent	IVR time (ps)	IVR time (ps)
$CDCl_3$	8.8 ± 0.1 (6^6)	2.6 ± 0.2 (32^6)
$CDBr_3$	5.4 ± 0.1 (5^6)	12.3 ± 0.3 (36^6)
CDI_3	10.5 ± 0.3 (90^{90})	15.8 ± 0.5 (45^6)

Note: The corresponding time constants for the unlabeled isotopologs are given in parentheses.

Table 2. Symmetries and energies of each of the normal modes of $CDCl_3$, $CDBr_3$, and CDI_3.

		Energies (cm^{-1})			
	Motion	$CDCl_3$	$CDBr_3$	CDI_3[91]	Sym
ν_1	C-D stretch	2266	2251	2245	a_1
ν_2	C*X*$_3$ *s* stretch	659	521	405	a_1
ν_3	C*X*$_3$ *s* deform	369	222	154	a_1
ν_4	CD *d* bend	914	850	765	*e*
ν_5	C*X*$_3$ *d* stretch	749	632	578	*e*
ν_6	C*X*$_3$ *d* deform	262	153	110	*e*

Note: $CDCl_3$ and $CDBr_3$ frequencies are gas phase values. The CDI_3 frequencies are approximate.

Table 3. Energy defects for the fourth-order-coupled states within 200 cm^{-1} of the C-D (H) stretch for each of the haloforms.

	Energy separation (cm^{-1})		
State (degeneracy)	$CDCl_3$	$CDBr_3$	CDI_3
$3\nu_4(4)$			50 (191)
$2\nu_4 + \nu_6(6)$	176		
$2\nu_4 + \nu_3(3)$	69		
$2\nu_4 + \nu_2(3)$	- (99)	30	
$2\nu_4 + \nu_5(6)$	- (193)	81 (65)	137
$\nu_4 + 2\nu_2(2)$	34		
$\nu_4 + \nu_{2+}\nu_5(4)$	56	137	
$\nu_4 + 2\nu_5(6)$	146		
$2\nu_2 + \nu_5(2)$	199		
$\nu_2 + 2\nu_5(3)$	109		
$3\nu_5(4)$	19		

CHAPTER 4: CHARACTERIZATION OF DEUTERATED FORMIC ACID AS A POSSIBLE IR SPECTROSCOPIC PROBE

Introduction

Isotopic substitution is a powerful tool in vibrational spectroscopy for selecting specific vibrational modes to probe as reporters of local structure and dynamics. As such isotope editing, primarily of C=O and O-H stretching modes, has been widely used in recently developed multidimensional spectroscopies such as two-dimensional infrared spectroscopy (2DIR).[26, 40, 52, 55, 94-101] Isotopic substitution of deuterium for hydrogen on carbon atoms has been far less common in 2DIR studies, however, in large part due to the relatively small molar absorptivity of typical C-D stretching vibrations. Previous 2D IR studies that have used C-D stretching modes have been two-color 2D IR experiments that take advantage of the signal enhancement afforded by measuring the cross peak of the weak C-D mode with a strong chromophore like a carbonyl vibration.[10, 102-104] In spite of their weak transition probabilities, C-D vibrations hold promise as versatile spectroscopic probes of local structure and dynamics.

Previous theoretical[105, 106] and experimental[8, 9, 11, 107] studies using infrared absorption spectroscopy of C-D stretching vibrations demonstrate the potential of this chromophore as a weakly perturbing probe of protein and peptide structure and structural distributions. C-D substitution represents a very weak perturbation, which is especially important when considering biological applications. In addition, C-H bonds are ubiquitous in chemistry and biology meaning that deuterium substitution has the potential to be a probe with general applicability. Another advantage of C-D stretching vibrations is that the isotopic substitution shifts the vibrational frequency into a nearly transparent region of the infrared spectrum of proteins and peptides around 2200 cm^{-1} separating them from any other absorbances that might otherwise interfere. These potential

advantages have largely been outweighed, however, by the one major drawback of C-D stretching vibrations: their weak transition moment. In general, C-D stretching vibrations exhibit molar absorptivities that vary between 1 and 100 $M^{-1}cm^{-1}$ depending on the molecular context of the carbon. That is 10 to 100 times weaker than the commonly used amide I mode of peptides. Because the 2DIR signal scales as the square of the molar absorptivity, the anticipated C-D signal is expected to be between 100 and 10,000 times weaker than for amide I. For this reason, little attention has been paid to C-D stretching vibrations as a potential chromophore for 2D IR spectroscopy in spite of their other merits.

Although nonlinear spectroscopic measurements of C-D stretching vibrations are challenging, they are not unprecedented. Seifert and coworkers made the first measurements of the population lifetime of a C-D stretching vibration in neat liquid $CDBr_3$.[82] Their comparison to measurements of the lifetime of the C-H stretch in $CHBr_3$ showed that the isotopic substitution reduced the population lifetime by about a factor of 2. Subsequently, our group studied the population relaxation of the C-D stretching modes of haloforms in benzene and acetone using transient grating spectroscopy.[108] We showed that the reduced lifetime of the C-D mode relative to the C-H mode is a common result of the isotopic substitution, and we explained this result based on the low coupling order of the states nearby in energy to the C-D fundamental suggesting that the coupling matrix elements connecting the C-D to these states should be better than the corresponding coupling matrix elements for the C-H stretching fundamental. More recently, in collaboration with Floyd Romesberg's group, we have also reported a photon echo study of deuterated leucines.[13] Taken together, these studies demonstrate that the nonlinear spectroscopy of C-D stretching vibrations is feasible, but 2D IR measurements of a C-D stretching vibration remain unrealized.

We report the first one color 2D IR measurements of a C-D stretching vibration in the formyl-deuterated formic acid dimer in hexane, $(DCOOH)_2$. Formic acid is an ideal

system in which to test the feasibility of 2D IR spectroscopy of C-D stretching vibrations because the molar absorptivity of the C-D stretching transitions is among the highest of any C-D transition we have seen. In addition, formic acid is a good model system because the vibrational spectroscopy of the gas-phase formic acid dimer in the C-D stretching region is well characterized.[109] Yoon et al. measured the vibrational action spectrum of jet-cooled deuterated formic acid dimers revealing an accidental Fermi resonance between the C-D stretching fundamental and antisymmetric combinations of the C-O stretch and the DCO bend. Their analysis of the spectrum in the gas phase showed that the perturbing dark states couple strongly to the bright C-D stretching state as well as to one another. 2D IR measurements of this Fermi resonance coupled system offers an opportunity to directly compare the vibrational state structure in the gas phase to that in solution to assess the influence of solvent-solute interactions on the zeroth-order frequencies and coupling matrix elements. In addition, we measure the population relaxation of the C-D stretching states using transient grating spectroscopy. This measurement is important in considering potential applications as a probe chromophore for 2D IR spectroscopy because the population lifetime sets an upper limit on the timescale over which the 2D IR spectrum can be measured. Altogether our results demonstrate the feasibility of using 2D IR of C-D stretching vibrations to probe structure and dynamics at least in favorable cases.

Results and Discussion

The top panel of Figure 31 shows the deuterated formic acid dimer structure. The doubly hydrogen bonded dimer forms a planar near-prolate C_{2h} structure. The bottom portion of Figure 31 shows the absorption spectrum of the deuterated formic acid dimer in hexane in the region of the C-D stretching transition. There are two transitions associated with the C-D stretching vibration of the dimer associated the Fermi resonance perturbed C-D stretching vibration: one centered at 2202 cm^{-1} and the other at 2235 cm^{-1}.

The stronger transition at 2202 cm^{-1} has a full width at half maximum (FWHM) of 13 cm^{-1} while the FWHM of the 2235 cm^{-1} transition is 15 cm^{-1}.

Figure 32 shows the decay of the transient grating signal of the C-D stretch of the formic acid dimer in hexane as a function of the time delay between the second and third pulses signified by T. The large peak (off scale) at T=0 is the nonresonant response that arises when all three pulses are both space and time coincident. For positive times, the third pulse is delayed relative to the first two. This portion of the grating signal reflects the dynamics of the states that are coherently excited by the two laser pulses that prepare the grating. A significant feature in the transient grating decay is the damped oscillation riding on the decay. These oscillations, originate from coherent superposition of the two eigenstates prepared by the broadband excitation pulses. As expected, the frequency of these oscillations corresponds to the energy difference between the two peaks in the infrared absorption spectrum, ~36 cm^{-1}.

We fit the grating decay to a biexponential plus a damped oscillation resulting in a fast time constant of 800 fs and a slow time constant of 11 ps. The damped oscillation decays with a 600 fs time constant. The faster decay component mostly likely reflects the rapid equilibration of population between the two eigenstates, which are not excited with equal probability by the laser pulses due to the difference in their transition moments. The long time constant then must reflect the overall population relaxation out of the two eigenstates.

The 11 ps population lifetime for the C-D stretching states of the formic acid dimer is similar to the C-D stretch lifetimes measured in our lab for deuterated haloforms in both acetone and benzene[108] and with that measured for deuterated liquid bromoform.[82] In contrast, most other common spectroscopic probes used in time-resolved vibrational spectroscopy have shorter lifetimes. For example, the antisymmetric stretch of the azide anion relaxes with a time constant of approximately 3 ps when dissolved in a polar protic solvents.[110] Similarly, the lifetime of the amide I vibration of

the peptide backbone is about 1.2 ps.[22] Compared to these more common examples, the C-D stretching lifetime is notably longer. Because 2D IR is a heterodyned spectroscopy, it is frequently possible to measure the 2D spectrum for population times up to five times the lifetime of the vibration being probed.[111] One can imagine, therefore, using the C-D stretch transition for probing solvation or chemical relaxation dynamics into the tens of ps in a region of the IR spectrum that is nearly background free. Thus, based on the lifetime, C-D stretching vibrations are attractive as a spectroscopic probe for time resolved spectroscopy.

Figure 33 shows the 2D IR correlation spectrum of the deuteratued formic acid dimer in hexane at T = 300 fs. The peak positions and amplitudes in the 2DIR spectrum reflect the energies and vibrational character of the molecular eigenstates, and the shapes of the peaks depend on the solvent-solute interactions. The peaks labeled 1, 1', 2, and 2' we refer to as diagonal peaks; while those labeled 3, 3', 4, and 4', are off-diagonal peaks. Peaks 1 and 2 are positive features, indicated by the red contours, and are located at $\{\omega_1, \omega_3\} = \{2204, 2204\}$ cm^{-1}, and $\{2233, 2241\}$ cm^{-1} respectively. These features reflect ground state bleaching of and stimulated emission from the states excited by the interactions with the first two laser pulses in the 2D pulse sequence. These transitions are accompanied by negative features, indicated by the blue contours, that are located at the same frequencies in ω_1 but anharmonically shifted to lower energy in ω_3, 2155 cm^{-1} and 2225 cm^{-1} respectively, corresponding to excited state absorptions from the states prepared by the first two laser pulses. The differences between the center frequencies of the red and the blue diagonal peaks on the ω_3 axis indicate the diagonal anharmonicities of the eigenstates. For the lower energy eigenstate indicated by 1 and 1' the anharmonic shift is 47 cm^{-1}, and for the higher energy eigenstate corresponding to peaks 2 and 2' the anharmonic shift is 17 cm^{-1}.

The cross peaks labeled 3 and 4 and located at $\{\omega_1, \omega_3\} = \{2204, 2238\}$ cm^{-1} and $\{2133, 2204\}$ cm^{-1} respectively reflect the ground state bleach associated with each of the

eigenstates as a result of exciting the other oscillator. Peak 3' located at {2204, 2223} cm^{-1} is an excited state absorption. The expected negative feature 4' is exceptionally weak and is essentially absent from the spectrum because the transition to the eigenstate in the two-quantum manifold at that energy has no oscillator strength.

All of the peaks appear to be circular with the exception of diagonal peak 2. The circular shaped peaks reflect the fact that the transitions are in the motionally narrowed limit so that the line shape is essentially homogeneous. The higher frequency diagonal transition, labeled 2, is not located at the same frequency in both ω_3 and ω_1 axes ({2233, 2241} cm^{-1}). In addition this feature is elongated along the diagonal in contrast to the other peaks in the spectrum. Although we only observe one transition in the infrared absorption spectrum associated with this feature, based on the gas phase spectroscopy done by Yoon et al.,[109] we believe that this peak is composed of two transitions that are not spectroscopically resolved. These two transitions constructively interfere along the diagonal giving rise to the elongated peak shape for both the 2 and 2' diagonal peaks as well as the asymmetry in the peak position ($\omega_1 \neq \omega_3$).

The fact that the line shapes are predominantly motionally narrowed at T = 300 fs suggests that the solvent-solute interactions in this system are weak and that the eigenstates we probe are insensitive to thermal fluctuations of the doubly hydrogen bonded dimer structure. This is consistent with previous studies of C-D stretching vibrations that indicate that C-D bonds are not easily polarized by interaction with their surroundings.[7]

Based on the positions of the features in the 2D IR spectrum, we can uniquely determine the energies of each of the eigenstates in the region of one- and two-quanta of C-D stretching. Figure 34 shows an energy level diagram indicating the energies of the eigenstates probed in our measurements. We take the energy of the ground vibrational state to be zero. There are two energetic manifolds to consider for our measurements. There are the two eigenstates at the energy of one-quantum of C-D stretching excitation.

We identify these as one-quantum states even though they are of mixed character and the perturbing state is a combination band that involves a quantum of C-O stretch and a quantum of DCO bending excitation. Similarly, we indicate the higher energy manifold near the energy of the first overtone of the C-D stretching vibration as the two-quantum states. The energies of the one-quantum states can be determined directly from the positions of the peaks in ω_1 in the 2D spectrum, 2204 cm^{-1} and 2235 cm^{-1} or from the infrared absorption spectrum, which are in good agreement. Each of the negative peaks in the 2D spectrum reveals the transition energy between a one-quantum state and one of the two-quantum states. The arrows in Figure 34 identify the energy levels between which there are excited state absorption peaks in the 2D spectrum and which peak corresponds to which transition. Using this information, we can deduce the absolute energies of the two-quantum states by adding the observed transition frequencies in ω_3 of each of these peaks to the appropriate one-quantum-state energy.

Once we have determined the energies of the one- and two-quantum eigenstates, we can construct a model based on a few simplifying assumptions that will allow us to determine the energies of the zeroth-order states and the coupling between them. The most significant approximation we must make is that we will treat our system as involving only two oscillators. We know based on the previous gas phase studies that there are actually three one-quantum eigenstates, but, in our measurements, we cannot resolve the third state or any of the two-quantum states that might be associated with it. As a result, we are forced to reduce the problem to two oscillators. In addition, we will treat the combination band as a single oscillator and assume that its energy scales anharmonically as we climb the vibrational manifold. Finally, we will assume that the coupling matrix elements scales harmonically going to the two-quantum states. Based on these approximations, we can write zeroth-order Hamiltonian matrices for the one- and two-quantum states as,

Equation 20. Matrices for Deperturbation Calculation

$$\mathbf{H_1} = \begin{pmatrix} \varepsilon_1 & \beta_{12} \\ \beta_{12} & \varepsilon_2 \end{pmatrix} \quad \text{and} \quad \mathbf{H_2} = \begin{pmatrix} 2\cdot\varepsilon_1 - A_1 & 0 & \sqrt{2}\cdot\beta_{12} \\ 0 & 2\cdot\varepsilon_2 - A_2 & \sqrt{2}\cdot\beta_{12} \\ \sqrt{2}\cdot\beta_{12} & \sqrt{2}\cdot\beta_{12} & \varepsilon_1 + \varepsilon_2 \end{pmatrix}$$

where ε_1 and ε_2 are the one-quantum energies of the zeroth-order states, β_{12} is the coupling matrix element between the oscillators, and A_1 and A_2 are the anharmonicities of the oscillators. Altogether, this model contains five unknowns. The eigenvalue problems associated with these two matrices will result in 5 eigenvalues that correspond to the 5 energy levels we deduce from our 2D IR data. Using these 5 energy levels, we can set up a system of 5 coupled equations, where each equation is of the form,

Equation 21. The 2 State Hamiltonian

$$\left|\mathbf{H} - E_n \cdot \mathbf{I}\right| = 0$$

where **H** is the appropriate one- or two-quantum state Hamiltonian matrix, E_n is one of the eigenstate energies, and **I** is the identity matrix. We then solve this system of equations for the five unknowns numerically. The resulting parameters are $\varepsilon_1 = 2210$ cm^{-1}, $\varepsilon_2 = 2230$ cm^{-1}, $\beta_{12} = 12$ cm^{-1}, $A_1 = 56$ cm^{-1}, and $A_2 = 14$ cm^{-1}. Based on the anharmonicities, we conclude that the lower energy state ate 2210 cm^{-1} is the bright C-D stretching state and the 2230 cm^{-1} state is the optically dark combination band. One of the advantages to the 2D IR method is that it allows us to uniquely determine these values from the experimentally measured 2D IR spectrum alone.

The 12 cm^{-1} coupling matrix element that we determine for the coupling between the zeroth-order C-D stretching state and the combination band is in good agreement with the coupling determined by Yoon et al. for the gas phase dimer. Our values for the zeroth

order energies of the states do not agree as well, particularly for the C-D stretching state, which they place at 2227 cm^{-1}. Some of that difference can be attributed to a shift in the energies of the states as a result of solvation consistent with the differences in the eigenstate energies that, in solution are both shifted to lower frequency, 2210 cm^{-1} and ~2245 cm^{-1}. In addition, our calculation differs from theirs in that they are able to resolve the third eigenstate state and, therefore, make a three-state model. Although we see the evidence of this third state in our spectrum, because we cannot resolve it or any of the excited-state absorption features associated with it, we can only construct a two state model for our data. In a three-state model where both of the dark states couple to the bright state with a similar coupling matrix element, we would expect the zeroth-order energy of the bright state to be somewhat higher than it is in our two-state model. In spite of these differences, however, the agreement between our results based on the 2D IR spectroscopy in hexane and those of Yoon et al. based on the gas-phase action spectroscopy is remarkable and clearly shows that the accidental Fermi resonance responsible for this perturbation is not significantly altered by the solvent-solute interactions.

Figure 35 shows a simulated 2D IR spectrum for T = 300 fs based on our two-state model. While calculating this spectrum we assume simple Lorentzian lineshapes of the same width for all of the peaks. We also assume that the zeroth-order bright state carries most of the oscillator strength, but, in order to accurately model the spectral intensities of all of the transitions, we do have to allow for some transition probability to the combination band. In this simulation, the transition probability for exciting the combination band is assumed to be 7% of the transition probability for exciting the C-D stretching fundamental. Although this is a modest contribution, it is significant. Quite likely, the need for this contribution reflects the breakdown of our two-state model to accurately describe the state mixing. In addition, peak 3' that we observe in our experimentally measured 2D spectrum appears much weaker in the simulated spectrum.

The reason for the small amplitude in the simulation is that the transition probability to the appropriate two-quantum state that gives rise to this feature in the 2D spectrum is too low in the simulation. Once again, this must reflect the fact that our two state model is not accurate enough in its description of the state mixing to be able to correctly describe the peak intensities for all of the transitions in the 2D spectrum. In spite of these differences, the gross features of the simulated spectrum agree with the experimental result quite well.

Summary

The potential of nonlinear spectroscopy to contribute to a wide range of problems in chemistry and biology is limited by the range of spectroscopic probes that can be incorporated selectively into the system of interest without perturbing that system significantly. C-D vibrations are an attractive option. We report the nonlinear vibrational spectroscopy of the C-D stretch of formyl deuterated formic acid dimer in hexane. We have characterized the population lifetime of the C-D stretching state, 11 ps. We have also measured and analyzed the 2D IR spectrum. This spectrum is complicated by the observation of an accidental Fermi resonance, which had been identified previously in gas phase studies. We show that the effect of solvation on the spectroscopy is minor, and that the 2D IR spectrum can be analyzed to determine the frequencies of and the couplings between the zeroth-order states of the system. Our results suggest that C-D stretching vibrations are, in fact, viable probes for nonlinear spectroscopy that should be explored more extensively.

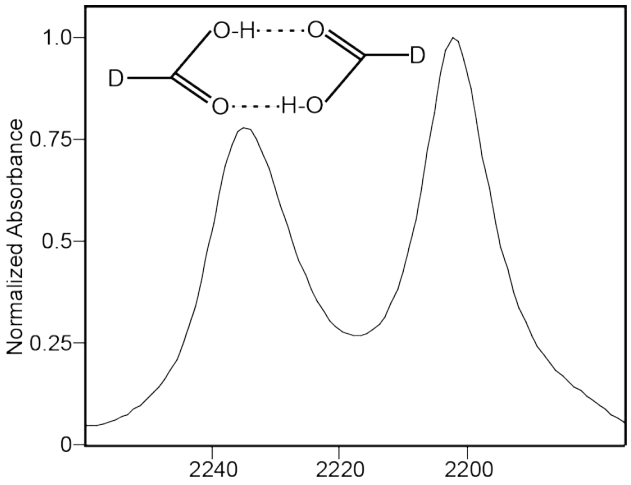

Figure 31. Cartoon of the formic acid dimer (inset). Infrared absorption spectrum of the C-D stretching transition of deuterated formic acid dimers dissolved in hexane. The spectrum shows two peaks located at 2202 cm^{-1} and 2234 cm^{-1}.

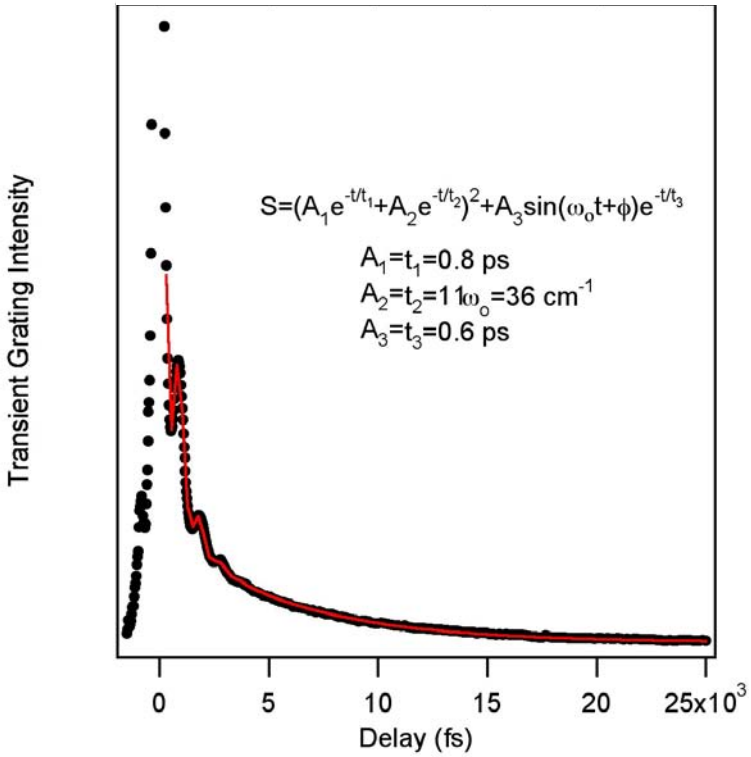

Figure 32. Infrared transient grating spectrum of the C-D stretching vibration of deuterated formic acid-d dimers in hexane. The black line is the experimental data and the red is the fit to a damped oscillator.

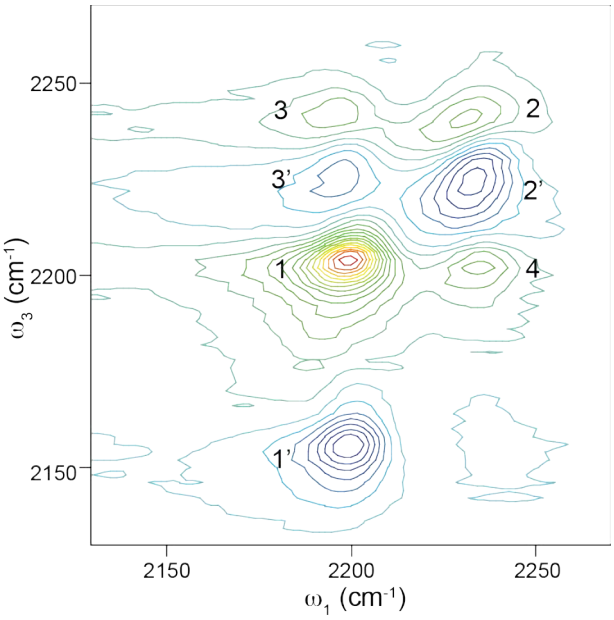

Figure 33. 2DIR spectrum of deuterated formic acid dimers dissolved in hexane at waiting time, T=300 fs.

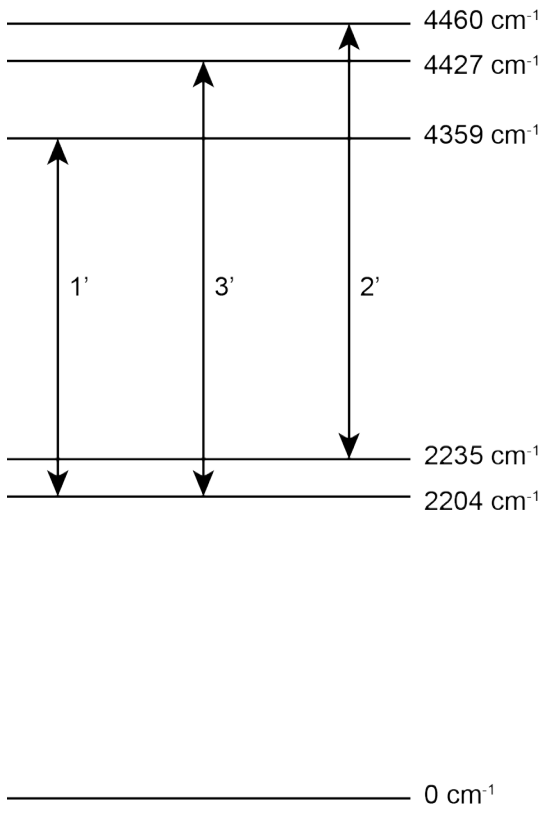

Figure 34. Cartoon showing the energy level diagram for formic acid-d.

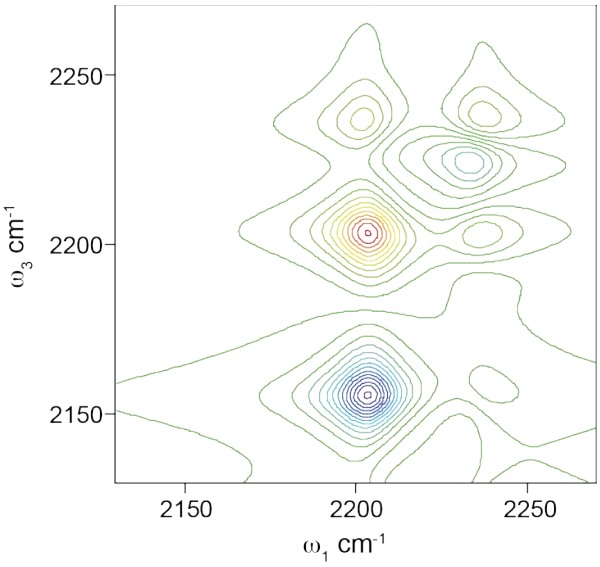

Figure 35. A simulated 2D IR spectrum for T = 300 fs based on our two-state model.

CHAPTER 5: 3-AZOPYRIDINE AS A PROBE FOR ACID-BASE INTERACTIONS

Introduction

Spectroscopic probes in the mid-infrared play a critical role in reporting local structure and dynamics. Ideally the system of interest would have an intrinsic chromophore that makes it spectroscopically accessible. For example, the amide I mode of proteins and peptides has been used extensively to probe protein and peptide structure and dynamics using two-dimensional infrared (2D IR) spectroscopy.[30, 31, 42, 94, 95, 112-119] Similarly, the O–H(D) stretching vibration of water, alcohols, and acids has been used to probe hydrogen-bond dynamics.[120-129] In other cases, external probes can be introduced to the system. Ideally, these external probes can be chosen to interact with the system under study in a desirable way and also report on the local structural or chemical dynamics. For example, the pseudohalide anions have been used to report both solvation dynamics[17, 130-134] and protein dynamics.[18, 21, 135] These anions are nearly ideal spectroscopic probes because they exhibit strong transition moments, and their vibrational transitions, which are located between 2000 and 2200 cm^{-1}, are well separated from the spectral regions in which most organic molecules absorb. As a result, these anions exhibit sharp absorption features that are sensitive to the fluctuations of their surroundings. Unfortunately, the anions do not lend themselves to wide application because they interact with a limited range of partners.

Organic derivatives of the pseudohalides could potentially be of broader applicability as spectroscopic probes than the bare anions are. Organic nitriles (RCN) have been used in a variety of protein and peptide studies.[136-138] Unfortunately, the nitrile stretching vibration exhibits a relatively weak transition moment making it a less than ideal probe. Recently, cyanylated cysteine, in which the cysteine thiol is chemically modified to convert it into a thiocyanate, has been the subject of several studies.[139-142]

These studies illustrate that the thiocyanate is very sensitive to its local environement making it an excellent probe of the local dynamics. Furthermore, because it is prepared by modifying cysteine in the protein, the synthetic methods to incorporate the probe site selectively are straightforward. Nevertheless, the thiocyanate transition moment, although better than for nitriles, is still rather modest compared to that for the bare pseudohalide anions. Cyanates have also been considered as potential infrared probes. Recently, Tucker et al.[143] measured 2D IR spectra of phenyl cyanate to characterize the anharmonic couplings associated with accidental Fermi resonances that perturb the -OCN stretching vibration in this compound. Although they are able to unravel the complicating features of this probe, these complications remain undesirable for studying chemical or structural dynamics. Recent work from Minhaeng Cho's group indicates the potential for azido-derivatized compounds as vibrational probes.[144, 145] Organic azides are particularly interesting because they tend to have large transition moments that would make them superior to both nitriles and thiocyanates for nonlinear spectroscopy. Furthermore, they have been shown to be sensitive to changes in the solvation environment making them excellent candidates to report on structural fluctuations. Here, we report 2D IR measurements of 3-azopyridine characterizing its spectroscopy and how that spectroscopy changes upon protonation of the pyridine nitrogen.

Following the chemical reaction dynamics of a system as a function of time is an important application of time-resolved vibrational spectroscopies. Spectroscopically, however, the bonds directly involved in a chemical reaction can be a challenge. The bonds that are part of the reaction coordinate are undergoing dramatic changes in their stretching frequency as they evolve from a normal bound vibration to an unbound degree of freedom and the potential becomes distinctly anharmonic so that the vibrational character of the stretching modes may not remain constant throughout the course of the reaction. As a result of these changes, the spectroscopy of the reactive bond stretching vibration can become significantly complicated and difficult to interpret. Proton transfer

reactions present an excellent example of this behavior where, even in unreactive systems, the proton stretching bands of strongly hydrogen bonded complexes exhibit unusually strong anharmonic couplings of the stretching mode to combination bands and overtones as well as low-frequency hydrogen-bond fluctuations accompanied by the red-shifting of the absorbance as a result of the hydrogen bonding interaction. These effects broaden the vibrational transition and give rise to a complex spectroscopic structure that is difficult to interpret even with the aid of sophisticated nonlinear spectroscopies.[128, 129, 146-149] With such complications, a remote probe of the protonation state of an acid or a base, such as pyridine, would be a powerful tool in studying proton-transfer reactions that would avoid the spectroscopic challenges associated with probing the transferring proton directly. With this idea in mind, we synthesized 3-azopyridine in which the azo group is intended to serve as a spectroscopic reporter of the protonation state of the pyridine ring. Because it is conjugated with the π system of the ring, the azo stretching vibration would be expected exhibit a distinct frequency shift upon protonation of the ring making it a sensitive reporter of the protonation state.

Figure 36 shows the infrared absorption spectrum of 3-azopyridine in CCl_4. Although we anticipate seeing a single transition in this spectral region corresponding to the azo group antisymmetric stretching vibration, it is clear that there are at least two transitions in this spectrum. The two most likely explanations for this spectrum are that 1) there are two conformers present, one with the azide oriented toward the pyridyl nitrogen and one with it oriented away, or 2) that there is a combination or overtone state forming an accidental Fermi resonance with the first excited state of the azo-stretching vibration. Using 2D IR spectroscopy we distinguish these possibilities showing that the second transition, in fact, arises from an accidental Fermi resonance. Furthermore, we measure 2D IR spectra of 3-azopyridine in hydrogen-bonded complexes with both formic acid and trifluoroacetic acid to assess the sensitivity of the vibrational spectrum to hydrogen bonding and protonation of the pyridine nitrogen. Based on our results, we

conclude that not only is the spectroscopy in this region sensitive to the protonation state of the ring, but also it is the azo-stretching state, which provides the oscillator strength of the observed transitions, that shifts upon protonation of the ring. Thus, the azo stretch does, in fact, serve as a sensitive reporter of the protonation state in spite of the spectral complications that arise from the accidental Fermi resonance interactions. These results suggest that, although this particular molecule is unsuitable as a probe of proton-transfer reactions, this strategy holds promise and should be pursued further in future studies.

Materials and Methods

Azopyridine is synthesized as described by Sawanishi *et al*. In short, 3-amino pyridine (8g, 0.08 mols) dissolves in 5M HCl and reacts with a solution of sodium nitrate (10g, 0.15 mols) at ≤5 ºC for 10-15 min. A solution of sodium azide (13g, 0.15 mols) is added drop wise to this mixture for 10-15 minutes. The reaction continues for 30 minutes at room temperature and then is quenched until alkaline by Na_2CO_3. The oily liquid is filtered and extracted with CH_2Cl_2 (3x200 mL). The extract is purified using Silica-Gel chromatography with CH_2Cl_2–EtAc (1:1) to obtain the final product with a yield 5.57g, of pure product.(68.7%, overall yield). ^{1}H-NMR (δ, $CDCl_3$): 7.2-7.4 (2H, m), 8.3-8.4 (2H, m). IR: 2134, 2094 cm^{-1}. UV ; 287 nm. MS ; 120.1. The trifluoroacetic acid and the formic acid were purchased from Aldrich and Fluka, respectively. The acids were used as received.

The acids were each combined with 3-azopyridine to form approximately equimolar ratios (.05 mM) between acid and base in CH_2Cl_2 solvent. The pKa's for trifluoroacetic acid and formic acid are 0.5 and 3.77, respectively. Comparing the pKa's for the acids we expect that in the 3-azopyridine-formic acid complex the proton remains covalently attached to the acid. For the 3-azopyridine-trifluoroacetic acid complex, however, we expect that the acid will protonate the pyridine ring resulting in the formation of a charge separated complex. We confirm this behavior by the absence of

the C=O stretch transition in the FTIR spectrum of the 3-azopyridine-TFA complex (data not shown).

Results

Figure 37 shows the absorption spectra of the 3-azopyridine (3AP) complexes with formic acid (FA) in blue and with trfluoroacetic acid (TFA) in red dissolved in dichloromethane. For comparison, we also show the spectrum of free 3-azopyridine in black. The absorption spectrum of free 3-azopyridine exhibits two strong transitions and at least one weaker feature in between them. The two main peaks are located at 2095 cm^{-1} and 2135 cm^{-1} and have nearly equal intensities. This basic pattern is conserved upon forming the hydrogen bonded complex with formic acid with a slight blue shift of the lower frequency transition. The two strongest features for the 3-azopyridine-FA complex are at 2103 cm^{-1}, and 2136 cm^{-1}. In both of these spectra, it is clear that there is at least one more feature in between the two main peaks, and there may be additional broad and weakly coupled transitions as well. The absorption spectrum of the 3-azopyridine –TFA complex, however, shows more significant changes compared to the other two. There is one strong transition in this spectrum centered at 2116 cm^{-1} with a weaker transition at 2138 cm^{-1} and a much weaker shoulder at 2103 cm^{-1}.

Clearly, there are significant changes to the absorption profile upon protonation of the pyridine ring. To understand those changes, we must first clarify the origins of the spectral complexity. There are two possibilities for the multiple peaks that appear in these spectra: 1) there could be multiple conformations of the azo group each of which exhibits a distinct azo stretching frequency, or 2) there could be accidental Fermi resonances, combination band and overtones of the ring vibrations that strongly couple to the azo stretch giving rise to additional transitions in this region. Using 2D IR spectroscopy we can uniquely distinguish these possibilities because at early waiting times we would not expect to see any cross peaks in the spectrum if there are multiple

conformers that give rise to the absorption structure, but Fermi resonance couplings would give rise to a distinct pattern of cross peaks even at the earliest waiting times. Furthermore, if Fermi resonances are responsible for the spectral complexity, 2D IR spectroscopy allows us to characterize the eigenstate structure and thereby determine the energies of the zeroth-order states and the couplings between them.

Figure 38 shows 2D IR spectra of 3-azopyridine in complexes with formic acid (top) and trifluoroacetic acid (bottom) dissolved in CH_2Cl_2 at a waiting time of T = 200 fs. Because the absorption spectra of the free 3-azopyridine and the 3-azopyridine–formic acid complex are qualitatively similar, we do not report the 2D IR spectrum of the free base and focus instead on comparisons of the two hydrogen-bonded complexes. It is immediately apparent from these two spectra that there are distinct cross peaks in each case even at this early waiting time. This observation shows that the complex absorption profile of 3-azopyridine results from anharmonic couplings of overtone and combination bands that lie nearby in energy and borrow oscillator strength by mixing with the azo-group antisymmetric stretching vibration.

The red (positive) peaks in each spectrum correspond to increased transmission as a result of ground state bleaching and stimulated emission. The blue (negative) peaks reflect decreased transmission as a result of excited-state absorptions. The positive diagonal peaks for the 3-azopyridine-FA complex, labeled 1 and 2, are located at $\omega_1 = \omega_3 = 2103$ cm^{-1} and 2136 cm^{-1}. The corresponding excited-state absorptions are located at $(\omega_1, \omega_3) = (2103, 2081)$ cm^{-1} and (2136, 2127) cm^{-1}. Based on these observed frequencies, we calculate that the diagonal anharmonicities of these two transitions are 22 cm^{-1} and 9 cm^{-1}, respectively. The positive cross peaks for the 3-azopyridine–formic acid complex are located at (2103, 2136) cm^{-1} and (2136, 2103) cm^{-1}, respectively. A negative cross peak at lower energy in ω_3 accompanies each of these cross peaks. Those features, which help to identify the energies of states in the two-quantum manifold, are located at (2103, 2119) cm^{-1} and (2136, 2086) cm^{-1}, respectively. The 2D IR spectrum

for the 3-azopyridine–trifluoroacetic acid complex also shows a distinct two-oscillator pattern, but the peak positions and intensities are quite different yet, consistent with the differences seen in the absorption spectrum. For this complex, the positive diagonal peaks are located at $\omega_1 = \omega_3 = 2116$ cm^{-1} and 2138 cm^{-1}. The negative peaks along the diagonal are at $(\omega_1, \omega_3) = (2116, 2096)$ cm^{-1} and $(2138, 2125)$ cm^{-1}. The positive cross peaks have positions $(\omega_1, \omega_3) = (2103, 2138)$ cm^{-1} and $(2138, 2103)$ cm^{-1}. Finally, the negative cross peaks are located at $(\omega_1, \omega_3) = (2103, 2111)$ cm^{-1} and $(2138, 2089)$ cm^{-1}. Together these peak positions uniquely identify the energies of all of the eigenstates in a two-oscillator model. Based on the infrared absorption spectra, the assumption of a two-oscillator model is a drastic oversimplification as there is at least one additional state present in each of the absorption spectra and the broad band structures suggest that there may be additional transitions buried within the lineshape. Nevertheless, the 2D IR data are only able to clearly resolve transitions consistent with two oscillators. This suggests that there is one state that is strongly coupled to the azo antisymmetric stretch and that the rest of the structure must arise from additional weaker couplings. As a result, we will make the simplifying approximation of a two-oscillator model to describe the 2D IR spectra recognizing that this is only the first order of coupling that contributes to the spectrum. In spite of this approximation, we anticipate that the model will adequately account for the variations in the energies and coupling of the zero-order states to characterize the effect that protonating the pyridine ring has on the vibrational frequency of the azo stretching vibration.

The shapes of the peaks in the 2D IR spectra reveal information about the system-bath (solvent) interactions. At T = 200 fs, the peaks are elongated along the diagonal. The differences in the transition frequencies for the free 3-azopyridine and the 3-azopyridine–formic acid complex clearly show that the transitions in this spectral region are sensitive to hydrogen bonding. Thus, it is reasonable to conclude that the elongation of the peaks most likely reflects the distribution of hydrogen bond distances. Figure 39

shows the 2D IR spectra of the 3-azopyridine–formic acid complex for increasing waiting times: T = 200 fs, 500 fs, and 5 ps. The two major changes observed with increasing waiting times are that the line shapes become elongated parallel to the ω_1 axis and the relative amplitude of the cross peaks increases considerably even as the absolute amplitudes of the peaks in the 2D spectra decrease. The evolution of the line shape reflects the sampling of the distribution of hydrogen bonding structures, which is complete within 2 ps. The increase in the relative intensity of the cross peaks results from population exchange between the two eigenstates at the fundamental level. These states are excited in proportion to their transition moments, but the states themselves are separated by a small energy gap and would be expected to have very similar populations at equilibrium. Thus, the nonequilibrium population that results from the initial excitation undergoes rapid population exchange leading to the growth of the cross peaks. This evolution is nearly complete within a picosecond. The overall intensity decays over a much longer time scale, however, extending beyond 5 ps.

Modeling

From the observed transition frequencies in the 2D IR spectra of the two complexes we can determine the energies of the one- and two-quantum eigenstates in a simple two-oscillator model. The model used for the 3-azopyridine acid complexes is the same as for the formic acid-d dimers in chapter 4. Using these eigenenergies and a few simplifying assumptions we can determine the energies of the zeroth-order states and the coupling between them. The most significant approximation we must make is that we will treat our system as involving only two oscillators. We know based on the absorption spectra that there are at least three one-quantum eigenstates and perhaps more, but, in our 2D IR measurements, we cannot resolve a third state or any of the two-quantum states that might be associated with it because the transition moment for this state is too weak and the transitions are positioned so close to larger features in the spectrum that they are

not identifiable in the spectrum. As a result, we are forced to reduce the problem to two oscillators. In addition, we will treat the Fermi resonance state that mixes with the azo stretch as a single oscillator and assume that its energy scales anharmonically as we climb the vibrational manifold. Finally, we will assume that the coupling matrix element that mixes the states scales harmonically going to the two-quantum states. Based on these approximations, the zeroth-order Hamiltonian matrices for the one- and two-quantum states as in equation 20.

As in the case of the formic acid-d dimer, this model contains five unknowns. The eigenvalue problems associated with these two matrices will result in 5 eigenvalues that correspond to the 5 energy levels we deduce from our 2D IR data. Using these 5 energy levels, we can set up a system of 5 coupled equations, where each equation is of the form of equation 21. We then solve this system of equations for the five unknowns numerically.

Figure 40 shows energy level diagrams for the eigenstates in the one-quantum and two-quantum manifolds for the two complexes. Each state is labeled by an energy that we determine from the transition frequencies we observe in the 2D IR spectra. Table 4 shows the parameters that result from the numerical solution of the system of equations outlined above using each of these sets of eigenenergies. Upon protonation, both of the zeroth-order states shift up in energy, and the coupling matrix element between them decreases somewhat, though this latter effect is of minor significance. The results of this calculation also suggest that the apparent anharmonicity of the perturbing state increases by a factor of two. Although such an increase is possible, it is unlikely and probably indicates that the state structure in the region of two-quanta of azo stretching excitation is more complicated than our model assumes in which case the anharmonicity of the perturbing state is of limited physical significance.

Figure 41 shows simulated 2D IR spectra for the 3-azopyridine-formic acid (top) and 3-azopyridine–trifluoroacetic acid (bottom) complexes. To calculate these spectra,

we use the parameters for the zeroth order states that come from the deperturbation calculation and assume that the lower frequency zeroth order state in each case is the azo stretching state. In addition we assume that the azo stretching state provides all of the oscillator strength and that the transition dipole moment scales harmonically with vibrational level. We assume a Lorentzian lineshape with a 14 cm^{-1} FWHM. The calculation includes all of the relevant rephasing and nonrephasing Liouville pathways consistent with the 2D IR correlation spectrum for T = 200 fs waiting time.[53, 150] As we would expect, the Lorentian lineshapes that we assume do not capture the details of the 2D IR spectral shapes because it does not account for the distribution of frequencies or the spectral diffusion that occurs during the waiting time. Nevertheless, in spite of its simplicity, this model for the state structure captures the essential features of the 2D spectra quite well and accurately accounts for both the peak positions and the intensity pattern of the features in the 2D IR spectrum. Thus, these spectral simulations affirm the reasonableness of our simplified model for the Fermi resonance interaction that gives rise to the eigenstates in this system.

Discussion

Comparing 3-azopyridine to the azide anion, there are three major differences in the spectroscopy of the azo antisymmetric stretching vibration. The first is that the transition probability for 3-azopyridine decreases considerably relative to azide anion. Secondly, the spectrum shifts by approximately 100 cm^{-1} to higher frequency. Third, the spectral transition of 3-azopyridine is anharmonically coupled to one or more combination or overtone states. The large molar absorptivity of the azide anions from the charge flow as a result of the symmetry breaking excitation of the antisymmetric stretch that changes the contributions of the two valence bond structures that contribute to the overall electronic structure of the anion. Bonding the azo group to the pyridine ring breaks the symmetry so that excitation of the antisymmetric stretch does not result in

significant charge flow because the electronic structure already exhibits broken symmetry due to the bonding to the ring. In addition, the pi system of the ring is conjugated to the azo pi bonds, and this mixing also contributes to the reduced molar absorptivity as evidenced by the fact that an azo group bonded to a methylene spacer exhibits a much higher molar absorptivity than one directly bound to the aromatic ring.[7] This same change in the electronic structure of the azo group upon binding to the ring is also responsible for the shift to higher frequency as there is more single-bond/triple-bond character to the bonding structure. In spite of these differences, the extinction coefficient remains strong enough, approximately 250 M^{-1} cm^{-1}, and the transition frequency is still located in a suitable spectral region so that the 3-azopyridine is still a suitable chromophore for 2D IR. The most complicating feature of the azo stretch of 3-aopyridine is the anharmonic coupling of the azo stretch to the nearby combination bands that gives rise to the complex absorption profile of the free base in solution. This complication raises significant questions about the suitability of this compound as a spectroscopic probe.

In spite of the concerns, the spectroscopy of 3-azopyridine in hydrogen bonded complexes with acids, such as formic acid and trifluoroacetic acid does show that the azo stretch is a sensitive reporter of the protonation state of the pyridine ring. First, the infrared absorption spectra show that qualitatively the spectral features are sensitive to hydrogen bonding and protonation state since there are distinct shifts in the spectral features of the complex azo stretching band upon forming the hydrogen bond with formic acid. Furthermore, the spectral pattern changes qualitatively upon protonation of the pyridine ring in the complex with trifluoroacetic acid. These qualitative results, however, do not clearly indicate whether the spectral sensitivity we observe is a result of changes in the azo stretching frequency or changes in the frequencies of the anharmonically coupled states that complicate the spectroscopy. In fact there are two possible explanations for the changes to the absorptions spectra that we observe. One possibility

is that the bright state, the azo antisymmetric stretch, shifts in response to protonation of the pyridine nitrogen. This shift would make sense because the azo group is conjugated to the π system of the ring. When the pyridine ring becomes protonated it causes significant changes to the electronic distribution of the pyridine ring resulting in a significant perturbation of the π electronic structure that would be expected to shift the azo stretching frequency considerably. An alternative explanation for the observed spectroscopic shifts is that the dark states that couple to the bright state could shift in frequency upon protonation of the ring. Gaussian calculations of the harmonic vibrational states at the DFT-B3LYP level of theory for each of the 3-azopyridine complexes predict that there are 8 combination bands that lie within 10 cm^{-1} of the azo antisymmetric stretching fundamental. These states all involve combinations of in-plane C-H bending and ring stretching modes. These modes all shift in frequency considerably upon protonation of the pyridine ring. In addition, a change in the coupling matrix element between the bright state and dark state could also result in the changes in the frequencies and intensities of the peaks in the FTIR spectra.

The results of the modeling of the 2D IR spectra are able to unravel the various contributions to the changes in the vibrational state structure. The zeroth-order azo stretching state shifts up in frequency by approximately 8 cm^{-1}, the dark state shifts up in frequency by 7 cm^{-1} and the coupling matrix element decreases by 6 cm^{-1}. Together these shifts are responsible for the dramatic changes observed in the infrared absorption spectrum. The lower frequency eigenstate retains more of the bright state character upon protonation of the pyridine ring, and, as a result, this state, which shifts up in frequency because both the bright and dark state do as well, increases in intensity relative to the neutral complex with formic acid. Although this model probably does not capture the quantitative details of the eigenstate structure and its changes upon protonation, it does accurately describe the most significant features as evidenced by the excellent agreement between the simulated and experimental 2D IR spectra.

Conclusion

Our results suggest that the azo stretching vibration of 3-azopyridine possesses many characteristics that would make it an excellent reporter vibration for 2D IR spectroscopy. It exhibits a relatively strong transition moment, 250 M^{-1} cm^{-1} at the peak. In addition it has a population lifetime of several picoseconds meaning that the dynamics of interest could be probed to nearly 20 ps. It is also clear that the azo stretching vibration is a sensitive reporter of the protonation state of the pyridine ring in 3-azopyridine. Such a remote reporter vibration holds significant potential for efforts to probe the kinetics and dynamics of hydrogen bonded complexes and proton transfer reactions. Unfortunately, the accidental Fermi resonance interactions that complicate the infrared absorption spectrum would make it very difficult to employ this probe for such studies because the population dynamics involving these states would be difficult to separate from the chemical dynamics of interest. Such strong anharmonic couplings as are observed in 3-azopyridine have been seen in other chromophores in this spectral region before.[109, 143] These results suggest that strong anharmonic couplings could be a common complication in this spectral region. That is reasonable because any overtone or combination state in this energy region is likely to involve only a few quanta of excitation. All of the candidates for the perturbing dark states in 3-azopyridine, for example, are combination states that involve two quanta of excitation. These low-order-coupled states are likely to have large coupling matrix elements. Thus, if they lie nearby in energy to a bright fundamental, as in the azo antisymmetric stretching vibration, this coupling will result in eigenstates with strongly mixed vibrational character. This phenomenon should be considered in developing new vibrational probes that absorb in this spectral region.

Table 4. Parameters for the zeroth-order states derived from the two-oscillator deperturbation analysis using the eigenstate energies deduced from the experimental 2D IR spectra.

Complex	ε_1 (cm^{-1})	ε_2 (cm^{-1})	β_{12} (cm^{-1})	A_1 (cm^{-1})	A_2 (cm^{-1})
3AP-FA	2113	2125	15	28	16
3AP-TFA	2121	2132	9	25	34

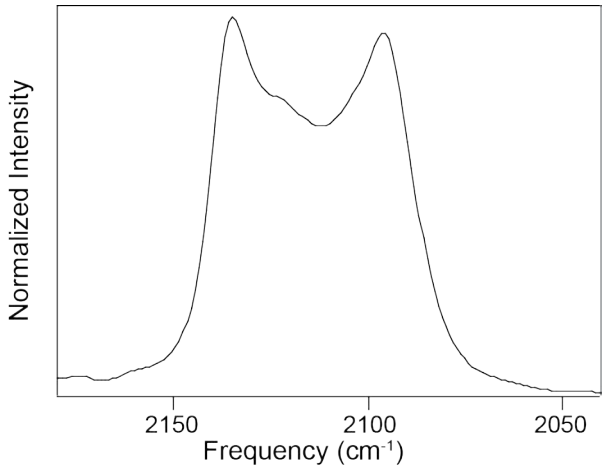

Figure 36. The infrared absorption spectrum of 3-azopyridine in CH_2Cl_2 in the region of the azo antisymmetric stretching vibration.

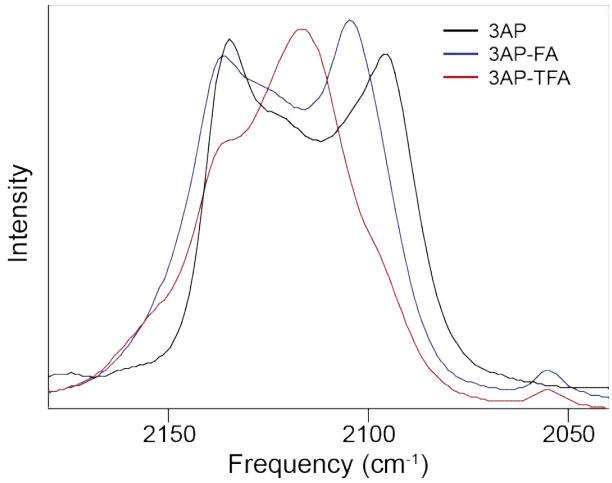

Figure 37. The infrared absorption spectra of free 3-azopyridine (3AP), the 3-azopyridine–formic acid complex (3AP-FA), and the 3-azopyridine–trifluoroacetic acid complex (3AP-TFA), each dissolved in CH_2Cl_2.

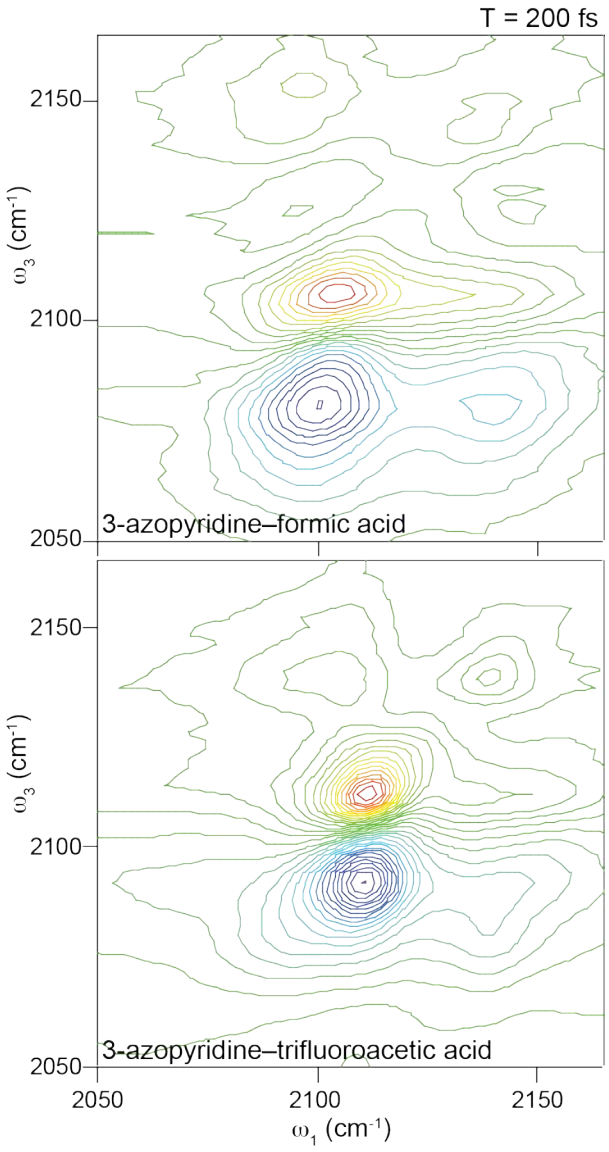

Figure 38. 2D IR spectra of 3-azopyridine–formic acid (top) and 3-azopyridine-trifluoacetic acid (bottom) dissolved in CH_2Cl_2 at a waiting time of T = 200 fs.

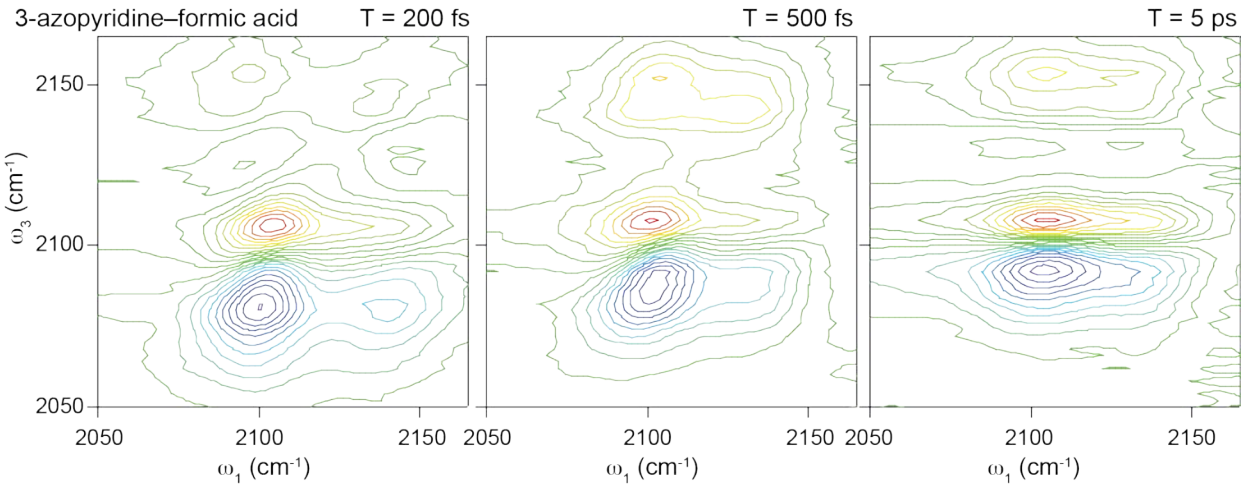

Figure 39. 2D IR spectra of the 3-azopyridine–formic acid complex at three waiting times: T = 200 fs (left), T = 500 fs (center), and T = 5 ps (right).

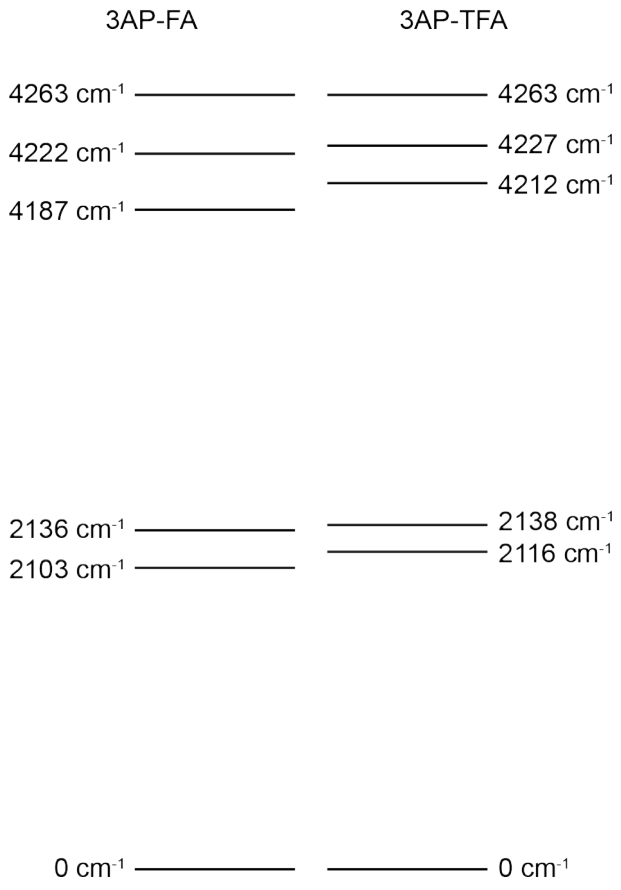

Figure 40. Energy level diagrams indicating the energies of the eigenstates in the one- and two-quantum manifolds of the azo stretching vibration for the 3-azopyridine–formic acid complex (left) and the 3-azopyridine–trifluoroacetic acid complex (right).

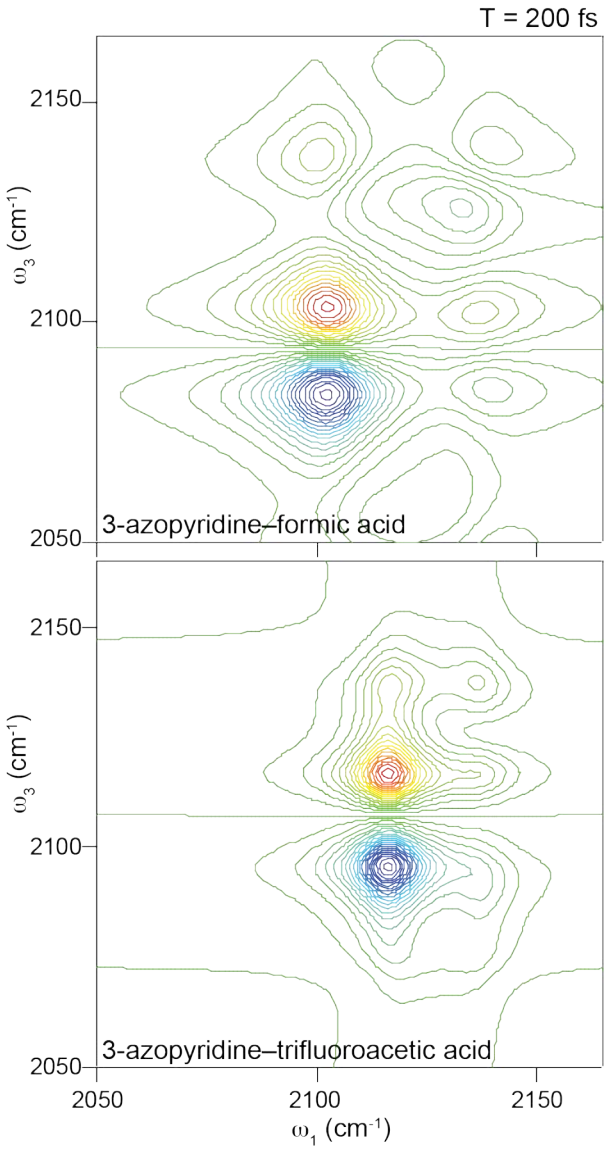

Figure 41. Simulated 2D IR spectra for T = 200 fs using the parameters in Table 1 that result from the deperturbation analysis of the experimental 2D IR spectra for the 3-azopyridine–formic acid complex (left) and the 3-azopyridine–trifluoroacetic acid complex (right).

CHAPTER 6 SUMMARY, IMPACT AND FUTURE DIRECTIONS

The main goal for this research was to characterize new chromophores for possible probes in 2DIR experiments. Ideal chromophores would be sensitive to the solvent environment to report the solvent dynamics that occur. Equally important the chomophore must possess a long lifetime. The lifetime of the chromophore should be long enough to sample all of the solvent configurations that construct the environment. The lifetime and sensitivity to the environment are not mutually exclusive. The interaction of the solvent on the chromophore affects the chromophore's lifetime. The effect of the solvent onto the lifetime of the chromophore is important because if the probe is to used to relay information about the solvent dynamics. For example, the lifetime of the C≡O stretching mode of acetylacetonato-dicarbonylrhodium(I), $Rh(CO)_2(C_5H_7O_2)$, RDC differs when dissolved in the non polar solvent, hexane, compared to being dissolved in a polar solvent such as chloroform, $CHCl_3$.[54] The motionally-narrowed or homogeneous limit describes the line shape when RDC is dissolved in hexane and yields a lifetime in the 100's of ps.[54] When RDC dissolved in $CHCl_3$, the lifetime is approximately 10 ps.[54]

The ideal chromophore would also possess a large transition dipole moment generating a large signal to be detected whose transitions should occur in a convenient part of the spectrum that is background free. The (2000-2300) cm^{-1} region of the spectrum described a background free region. Very few transitions are in this region ensuring that the observed mode is desired.

A large anharmonicity provides a clean lineshape. When comparing the 2DIR spectra of the formic acid-d dimer with that of the 3-azopyridine acid complexes, the peaks of the formic acid are less distorted due to the large anharmonicity in the system. Having a clean lineshape is important because the shape of the peak reveals information

on the solvent-solute interaction. The large anharmonicity, $\Delta = 47$ cm^{-1}, separate the $\nu = 0 \rightarrow \nu = 1$ transition from the $\nu = 1 \rightarrow \nu = 2$ mode. The overtone does not interfere with the fundamental transition for the formic acid-d dimer. The anharmonicity for the 3azopyridine acid complexes are 20 cm^{-1} smaller. For both the formic acid and trifluoroacetic acid complexes, the overtone transition interferes with the fundamental transition, producing a flattened shape on the low frequency portion of the peak.

The ideal IR probe would not perturb the system. The use of isotopes does not change the number of vibrational modes for the system. For example, the deuterated haloforms of formic acid contains the same number of vibrational modes as does the proteated forms. However when azide was attached to the pyridine ring, the number of atoms increased from 11 to 13. Likewise the number of allowed transitions increased from 25 for the pyridine to 33 vibrational modes for the 3-azopyridine.

The occurrence of Fermi Resonances have been shown to be problematic for probes. Both deuterated formic acid-d dimers in hexane and the two 3azopyridine acid complexes dissolved in dichloromethane formed unexpected additional peaks originating from Fermi Resonances that complicated the 2DIR spectra. The idea IR probe would produce a simple 2DIR spectra with a peak resulting from the fundamental transition and another peak from the overtone transition.

For the experiments contained in this dissertation, we choose to study the C-D stretching transitions for deuterated haloforms and formic acid-d dimers as well as the antisymmetric stretch of 3-azopyridine acid complexes. The first experiment, the C-D stretching mode for deuterated chloroform, bromoform and iodoform dissolved in the non polar solvent benzene and a polar solvent, acetone. This series of deuterated haloforms was chosen because the C-H stretching transition has been well studied for proteated haloforms. Transient grating experiment measures the vibrational relaxation rate for the deuterated haloforms. The C-D stretch transition possesses a faster vibrational relaxation rate than the C-H transitions. The deuterated haloforms contain a larger number of low

ordered coupled states within 200 cm^{-1} of the C-D stretching mode compared to the C-H stretch of the proteated forms. The 800 cm^{-1} red shift of the C-D stretch compared to the C-H stretch resulted in a large number of low ordered coupled states results in a faster vibrational relaxation rate for the deuterated haloforms as opposed to the proteated haloforms.

Once again a transient grating experiment measured an 11 ps lifetime or vibrational relaxation rate for the C-D stretching mode of formic acid- d dimer dissolved in hexane. The first one color 2DIR spectrum at T = 300 fs showed Fermi Resonances by the evidence of cross peaks. A depurturbation calculation calculated the bright state, dark state and the coupling matrix element between bright and dark states as well as the anharmonicities for the two fundamentals. The bright state was calculated to occur at 2210 cm^{-1} while 2235 cm^{-1} was the energy for the dark state. The calculated anharmonicities for the two fundamental transitions were 56 cm^{-1} and 27 cm^{-1} which are in good agreement with the experimental values of 47 cm^{-1} and 17 cm^{-1}, respectively. The calculated coupling matrix element was 13 cm^{-1} and was in perfect agreement with published results.[109] Published results identified a combination of the C-O stretch and CDO bend as the dark state.[109] The coupling of the C-D stretch to the dark state complicates the spectrum making te C-D stretch of the formic acid- d dimer an unlikely candidate for measuring chemical exchanges processes such as proton transfer. Our results indicate that the C-D stretching transition is a feasible probe for 2D IR spectroscopy.

3 azopyridine was synthesized by Samrat Dutta and was reacted with a weak acid, formic acid and with a strong acid, trifluoroacetic acid. The azide reported hydrogen bonding dynamics differences between the acids. The formic acid hydrogen bonded to the amine present on the pyridine ring while the trifluoroacetic acid and 3azopyridine formed charge separated species. The 2DIR spectra displayed the anitsymmetrc stretch of the azide for both acid complexes. Crosspeaks at early times in the 2D IR spectra

indicate the formation Fermi Resonances. The Fermi Resonances are formed from the antisymmetric stretch of the azide and modes from the pyridine ring. A 16 cm^{-1} and 12 cm^{-1} coupling matrix elements were determined by the deperturbation calculations method described in chapters 4 and 5 for formic acid-d dimers, 3-azopyridine acid complexes, respectively. The energy of the bright state, the antisymmetric azide stretch, was calculated to be 2115 cm^{-1} for the 3-azopyridine-FA and 2120 cm^{-1} for the 3-azopyridine- TFA. The energy of the dark states was calculated to be 2130 cm^{-1} for both 3-azopyridine-FA and 3-azopyridine-TFA. The energy of the bright state changes depending on the bonding conditions. From Spartan and Gaussian calculations the dark state for both complexes contains C-H in and out of plane bends or wags which are sigma bonds and are responsible for the movement of the bright state energy.

For both the deuterated formic acid dimers and the 3-azopyridine complexes their vibrational modes occur in the background free region of the spectrum. However, both cases contain Fermi Resonances that have very large coupling matrix elements which as a surprise to us. Isotopically labeling would be possible solution for disrupting the Fermi Resonances. For example, changing the oxygen in the deuterated formic acid to O^{18} may shift the CDO bend and C-O stretch enough so as to not couple with the C-D stretch; possibly resulting in a disruption of the Fermi Resonance producing a simpler spectrum. This same strategy may work with the 3azopyridine by changing the nitrogens to ^{15}N. To determine if these strategies will work, calculations should be performed first before because isotopically labeled molecules are expensive and setting up the 2DIR experiment is costly in time.

APPENDIX

Enumerating States Code

```
// density of states with made up values.

#include <iostream.h>
#include <fstream.h>

int main ()

{
        int
n1,n2,n3,n4,n5,n6,n7,n8,n9,n10,n11,n12,n13,n14,n15,n16,n17,n18,n19,n20,e1,e2,e3,e4,e
5,e6,e7,e8,e9,e10,e11,e12,e13,e14,e15,e16,e17,e18,e19,e20,et,em;      //start with n1
being the quantum number for the lowest energy oscillator.
                n1=0;      //Requires an n for every mode.
                n2=0;                                   //n2 should be for the next
lowest number and so on.
                n3=0;
                n4=0;
                n5=0;
                n6=0;
                n7=0;
                n8=0;
                n9=9;
                n10=0;
                n11=0;
```

```
n12=0;
n13=0;
n14=0;
n15=0;
n16=0;
n17=0;
n18=0;
n19=0;
n20=0;
e1=79;  //Requires and energy for every mode.
e2=163;
e3=177;
e4=217;
e5=238;
e6=285;
e7=690;
e8=722;
e9=906;
e10=904;
e11=994;
e12=1019;
e13=1023;
e14=1037;
e15=1272;
e16=1275;
e17=1436;
e18=1489;
```

```
                e19=1678;
            e20=1757;
                em=2471;       //em is the maximum energy, so it is the maximum
Q.N. oscillator*Energy.

                ofstream fout("fad2.txt");   //creats the file which is named formic
acid-d dimer
              while (n20<35)
              {
               n19=0;
               while (n19<35)
               {
                n18=0;
                while (n18<35)
                {
                 n17=0;
                 while (n17<35)
                 {
                      n16=0;
                      while (n16<35)
                      {
                       n15=0;
                       while (n15<35)
             {
              n14=0;
                   while (n14<35)
                   {
```

```
n13=0;
while (n13<35)
{
        n12=0;
        while (n12<35)
        {
         n11=0;
         while (n11<35)
         {
          n10=0;
          while (n10<35)
          {
                  n9=0;
                  while (n9<35)
                  {
                   n8=0;
                   while (n8<35)
//Requires a while statement for every oscillator.
                   {
                          n7=0;
                          while (n7<35)
                          {
                           n6=0;
                           while (n6<35)
                           {
                n5=0;
                            while (n5<35)
```

```
                                        {
                                        n4=0;
                                              while (n4<35)
                                              {
                                              n3=0;
                                              while (n3<35)
                                              {
                                              n2=0;
                                               while (n2<35)
                                               {
                                               n1=0;
                        while (n1<35)
                                                    {

        et=((n1*e1)+(n2*e2)+(n3*e3)+(n4*e4)+(n5*e5)+(n6*e6)+(n7*e7)+(n8*e8)+(n9*
e9)+(n10*e10)+(n11*e11)+(n12*e12)+(n13*e13)+(n14*e14)+(n15*e15)+(n16*e16)+(n1
7*e17)+(n18*e18)+(n19*e19)+(n20*e20));    //Calculation for total energy, Q.N.*Energy
summ over all oscillators.
                                                                        fout
<<n1<<"\t"<<n2<<"\t"<<n3<<"\t"<<n4<<"\t"<<n5<<"\t"<<n6<<"\t"<<n7<<"\t"<<n8<<
"\t";
                                                                        fout
<<n9<<"\t"<<n10<<"\t"<<n11<<"\t"<<n12<<"\t"<<n13<<"\t"<<n14<<"\t"<<"\t"<<n15<
<"\t"<<n16<<"\t"<<n17<<"\t"<<n18<<"\t";
                                                                        fout
<<n19<<"\t"<<n20<<"\t"<<et<<endl;   //Writes to the file cdbr3.
```

```
                                        n1++;
                                        if
(((n1*e1)+(n2*e2)+(n3*e3)+(n4*e4)+(n5*e5)+(n6*e6)+(n7*e7)+(n8*e8)+(n9*e9)+(n10
*e10)+(n11*e11)+(n12*e12)+(n13*e13)+(n14*e14)+(n15*e15)+(n16*e16)+(n17*e17)+(
n18*e18)+(n19*e19)+(n20*e20))>em)
                                        {n1=36;}
                                        }
                                        n2++;
                                        if
(((n2*e2)+(n3*e3)+(n4*e4)+(n5*e5)+(n6*e6)+(n7*e7)+(n8*e8)+(n9*e9)+(n10*e10)+(n
11*e11)+(n12*e12)+(n13*e13)+(n14*e14)+(n15*e15)+(n16*e16)+(n17*e17)+(n18*e18)
+(n19*e19)+(n20*e20))>em)
                                        {n2=36;}
                                        }
                                    n3++;
                                    if
(((n3*e3)+(n4*e4)+(n5*e5)+(n6*e6)+(n7*e7)+(n8*e8)+(n9*e9)+(n10*e10)+(n11*e11)+
(n12*e12)+(n13*e13)+(n14*e14)+(n15*e15)+(n16*e16)+(n17*e17)+(n18*e18)+(n19*e1
9)+(n20*e20))>em)
                                     {n3=36;}
                                     }
                                    n4++;
                                    if
(((n4*e4)+(n5*e5)+(n6*e6)+(n7*e7)+(n8*e8)+(n9*e9)+(n10*e10)+(n11*e11)+(n12*e12
)+(n13*e13)+(n14*e14)+(n15*e15)+(n16*e16)+(n17*e17)+(n18*e18)+(n19*e19)+(n20*
e20))>em)
                                    {n4=36;}
```

```
                                                    }
                                                    n5++;
                                                    if
(((n5*e5)+(n6*e6)+(n7*e7)+(n8*e8)+(n9*e9)+(n10*e10)+(n11*e11)+(n12*e12)+(n13*e
13)+(n14*e14)+(n15*e15)+(n16*e16)+(n17*e17)+(n18*e18)+(n19*e19)+(n20*e20))>e
m)
                                                    {n5=236;}

                                                    }
                                                    n6++;
                                                    if
(((n6*e6)+(n7*e7)+(n8*e8)+(n9*e9)+(n10*e10)+(n11*e11)+(n12*e12)+(n13*e13)+(n14
*e14)+(n15*e15)+(n16*e16)+(n17*e17)+(n18*e18)+(n19*e19)+(n20*e20))>em)
//Requires and if statement for every mode.
                                                    {n6=36;}
                                            }
                                                    n7++;
                                                    if
(((n7*e7)+(n8*e8)+(n9*e9)+(n10*e10)+(n11*e11)+(n12*e12)+(n13*e13)+(n14*e14)+(n
15*e15)+(n16*e16)+(n17*e17)+(n18*e18)+(n19*e19)+(n20*e20))>em)
                                                    {n7=36;}

                                                    }
                                                    n8++;
                                                    if
(((n8*e8)+(n9*e9)+(n10*e10)+(n11*e11)+(n12*e12)+(n13*e13)+(n14*e14)+(n15*e15)
+(n16*e16)+(n17*e17)+(n18*e18)+(n19*e19)+(n20*e20))>em)
```

```
                                    {n8=36;}
                                    }
                                    n9++;
                                    if
(((n9*e9)+(n10*e10)+(n11*e11)+(n12*e12)+(n13*e13)+(n14*e14)+(n15*e15)+(n16*e1
6)+(n17*e17)+(n18*e18)+(n19*e19)+(n20*e20))>em)
                        {n9=36;}
                                    }
                                    n10++;
                                    if
(((n10*e10)+(n11*e11)+(n12*e12)+(n13*e13)+(n14*e14)+(n15*e15)+(n16*e16)+(n17*
e17)+(n18*e18)+(n19*e19)+(n20*e20))>em)
                                    {n10=36;}
                                    }
                                n11++;
                                if
(((n11*e11)+(n12*e12)+(n13*e13)+(n14*e14)+(n15*e15)+(n16*e16)+(n17*e17)+(n18*
e18)+(n19*e19)+(n20*e20))>em)
                                    {n11=36;}
                                                        }
                                n12++;
                                if
(((n12*e12)+(n13*e13)+(n14*e14)+(n15*e15)+(n16*e16)+(n17*e17)+(n18*e18)+(n19*
e19)+(n20*e20))>em)
                                    {n12=36;}
                                    }
                                n13++;
```

```
                                    if
(((n13*e13)+(n14*e14)+(n15*e15)+(n16*e16)+(n17*e17)+(n18*e18)+(n19*e19)+(n20*
e20))>em)
                                    {n13=36;}
                                    }
                                   n14++;
                                   if
(((n14*e14)+(n15*e15)+(n16*e16)+(n17*e17)+(n18*e18)+(n19*e19)+(n20*e20))>em)
                                    {n14=36;}
                                    }
                                  n15++;
                                  if
(((n15*e15)+(n16*e16)+(n17*e17)+(n18*e18)+(n19*e19)+(n20*e20))>em)
                                   {n15=36;}
                                   }
                                  n16++;
                                  if
(((n16*e16)+(n17*e17)+(n18*e18)+(n19*e19)+(n20*e20))>em)
                                   {n16=36;}
                                   }
                                 n17++;
                                 if ((n17*e17)+(n18*e18)+(n19*e19)+(n20*e20))>em)
                                 {n17=36;}
                                 }
                                n18++;
                               if (((n18*e18)+(n19*e19)+(n20*e20)>em)
                               {n18=36;}
```

```
                    }
                n19++;
                if (((n19*e19)+(n20*e20))>em)
                {n19=36;}
                }
               n20++;
               if ((n20*e20)>em)
               {n20=36;}
               }
          fout.close(); //Closes the file.
        return 0;
}
```

The Igor Code for working up data

```
#pragma rtGlobals=1          // Use modern global access method.


Function timefreq2(inp1, inp2)// in1 is the rephasing data; in2 is the nonrephasing data!!
        Wave inp1, inp2
        Duplicate/O inp1 resp1
        Duplicate/O inp2 resp2
        DeletePoints 0,2, resp1
```

```
DeletePoints 0,2, resp2
Variable tau1_0 = 0
Variable tau1_step = 19 // Step size in T1 axis
Variable w3_0 = 2166 // Start of the monochromater, minus 4 due to error of the monochromater!!
Variable w3_step = -2 // Step size of the monochromater, it is minus because we collect from largest wavenumber to lower.
Variable low = 2050 // For plotting data
Variable high = 2170 // For plotting data
SetScale/P x tau1_0,tau1_step,"",resp1;DelayUpdate
SetScale/P y w3_0,w3_step,"",resp1
SetScale/P x tau1_0,tau1_step,"",resp2;DelayUpdate
SetScale/P y w3_0,w3_step,"",resp2
Variable l1 =  DimSize (resp1,0)
Variable w1 = Dimsize(resp1,1)
Variable l2 =  DimSize (resp2,0)
Variable w2 = Dimsize(resp2,1)
Duplicate/O resp1 win1 temp1
Duplicate/O resp2 win2 temp2
win1 = Cos(pi*x/(2*l1*tau1_step))
win2 = Cos(pi*x/(2*l2*tau1_step))
resp1*=win1
resp2*=win2
if (l1<1024)
        Redimension/N=(1024,w1) resp1 //Assuming that the data file will
        l1 = 1024                     //typically be fewer than 1024 points
```

```
		endif 					//we want to zero pad
up to that size
		if (l2<1024)
			Redimension/N=(1024,w2) resp2 //Assuming that the data file will
			l2 = 1024 				//typically be fewer than
1024 points
		endif 					//we want to zero pad
up to that size
		FFT/OUT=1/Cols/DEST=reph resp1
		FFT/OUT=1/Cols/DEST=nreph resp2
		Make/O/N = ((l1/2)+1,w1)/D rephre rephim rephabs
		Make/O/N = ((l2/2)+1,w2)/D nrephre nrephim nrephabs
		Variable dfreq1 = 1/(tau1_step*l1*.00003)
		Variable freq1offset = 1/(tau1_step*.00003)
		Variable dfreq2 = 1/(tau1_step*l2*.00003)
		SetScale/P x freq1offset, dfreq1, rephre, rephim, reph, rephabs
		SetScale/P y w3_0,w3_step,"", rephre, rephim, reph, rephabs
		SetScale/P x freq1offset, dfreq2, nrephre, nrephim, nreph, nrephabs
		SetScale/P y w3_0,w3_step,"", nrephre, nrephim, nreph, nrephabs
		rephre = real(reph)
		rephim = imag(reph)
		rephabs = cabs(reph)
		nrephre = real(nreph)
		nrephim = imag(nreph)
		nrephabs = cabs(nreph)
		KillWaves  resp2, resp1, win1, win2
		Make/O/N=513/D diag
```

```
SetScale/P x freq1offset,dfreq1,"", diag
diag=x
Display;AppendMatrixContour rephre
SetAxis left low,high ;DelayUpdate
SetAxis bottom low,high
ModifyContour rephre
ctabLines={*,*,Rainbow,1},labels=4,labelFSize=10,autoLevels={*,*,21}
//ModifyContour rephre manLevels={-.5,0.0254,42}
AppendToGraph/VERT diag
Display;AppendMatrixContour rephim
SetAxis left low,high ;DelayUpdate
SetAxis bottom low,high
ModifyContour rephim
ctabLines={*,*,Rainbow,1},labels=4,labelFSize=10,autoLevels={*,*,21}
//ModifyContour rephre manLevels={-.5,0.0254,42}
AppendToGraph/VERT diag
Display;AppendMatrixContour nrephre
SetAxis left low,high ;DelayUpdate
SetAxis bottom low,high
ModifyContour nrephre
ctabLines={*,*,Rainbow,1},labels=4,labelFSize=10,autoLevels={*,*,21}
//ModifyContour nrephre manLevels={-.5,0.0254,42}
AppendToGraph/VERT diag
Display;AppendMatrixContour nrephim
SetAxis left low,high ;DelayUpdate
SetAxis bottom low,high
```

```
		ModifyContour nrephim
ctabLines={*,*,Rainbow,1},labels=4,labelFSize=10,autoLevels={*,*,21}
		//ModifyContour nrephim manLevels={-.5,0.025,42}
		AppendToGraph/VERT diag
	End
```

BIBLIOGRAPHY

1. Bonn, M.; Brugmans, M. J. P.; Bakker, H. J., Solvent-dependent vibrational relaxation pathways after successive resonant IR excitation to [upsilon] = 2. Chemical Physics Letters 1996, 249 (1-2), 81-86.

2. De‡k, J. C.; Iwaki, L. K.; Dlott, D. D., When vibrations interact: ultrafast energy relaxation of vibrational pairs in polyatomic liquids. Chemical Physics Letters 1998, 293 (5-6), 405-411.

3. Iwaki, L. K.; De‡k, J. C.; Rhea, S. T.; Dlott, D. D., Vibrational energy redistribution in liquid benzene. Chemical Physics Letters 1999, 303 (1-2), 176-182.

4. Laenen, R.; Rauscher, C., Time-resolved infrared spectroscopy of ethanol monomers in liquid solution: molecular reorientation and energy relaxation times. Chemical Physics Letters 1997, 274 (1-3), 63-70.

5. Laenen, R.; Simeonidis, K., Energy relaxation and reorientation of the OH mode of simple alcohol molecules in different solvents monitored by transient IR spectroscopy. Chemical Physics Letters 1999, 299 (6), 589-596.

6. Bakker, H. J., Effect of intermolecular interactions on vibrational-energy transfer in the liquid phase. The Journal of Chemical Physics 1993, 98 (11), 8496-8506.

7. Suydam, I. T.; Boxer, S. G., Vibrational Stark Effects Calibrate the Sensitivity of Vibrational Probes for Electric Fields in Proteins,Ä†. Biochemistry 2003, 42 (41), 12050-12055.

8. Chin, J. K.; Jimenez, R.; Romesberg, F. E., Direct Observation of Protein Vibrations by Selective Incorporation of Spectroscopically Observable Carbon,àíDeuterium Bonds in Cytochrome c. Journal of the American Chemical Society 2001, 123 (10), 2426-2427.

9. Kinnaman, C. S.; Cremeens, M. E.; Romesberg, F. E.; Corcelli, S. A., Infrared Line Shape of an Œ±-Carbon Deuterium-Labeled Amino Acid. Journal of the American Chemical Society 2006, 128 (41), 13334-13335.

10. Naraharisetty, S. R. G.; Kasyanenko, V. M.; Zimmermann, J.; Thielges, M. C.; Romesberg, F. E.; Rubtsov, I. V., C,àíD Modes of Deuterated Side Chain of Leucine as Structural Reporters via Dual-frequency Two-dimensional Infrared Spectroscopy. The Journal of Physical Chemistry B 2009, 113 (14), 4940-4946.

11. Thielges, M. C.; Case, D. A.; Romesberg, F. E., Carbon,àíDeuterium Bonds as Probes of Dihydrofolate Reductase. Journal of the American Chemical Society 2008, 130 (20), 6597-6603.

12. Weinkam, P.; Zimmermann, J.; Sagle, L. B.; Matsuda, S.; Dawson, P. E.; Wolynes, P. G.; Romesberg, F. E., Characterization of Alkaline Transitions in Ferricytochrome c Using Carbon,àíDeuterium Infrared Probes,Ä†. Biochemistry 2008, 47 (51), 13470-13480.

13. Zimmermann, J.; Gundogdu, K.; Cremeens, M. E.; Bandaria, J. N.; Hwang, G. T.; Thielges, M. C.; Cheatum, C. M.; Romesberg, F. E., Efforts toward Developing Probes of Protein Dynamics: Vibrational Dephasing and Relaxation of Carbon,ÄìDeuterium Stretching Modes in Deuterated Leucine. The Journal of Physical Chemistry B 2009, 113 (23), 7991-7994.

14. Dutta, S.; Cook, R.; Kohen, A.; Cheatum, C. M., A novel mid-IR probe of enzymes active sites. Analytical Biochemistry 2010, In Preparation.

15. Ohta, K.; Tominaga, K., Vibrational population relaxation of thiocyanate ion in polar solvents studied by ultrafast infrared spectroscopy. Chemical Physics Letters 2006, 429 (1-3), 136-140.

16. Li, M.; Owrutsky, J.; Sarisky, M.; Culver, J. P.; Yodh, A.; Hochstrasser, R. M., Vibrational and rotational relaxation times of solvated molecular ions. The Journal of Chemical Physics 1993, 98 (7), 5499-5507.

17. Ohta, K.; Maekawa, H.; Saito, S.; Tominaga, K., Probing the Spectral Diffusion of Vibrational Transitions of OCN- and SCN- in Methanol by Three-Pulse Infrared Photon Echo Spectroscopy. The Journal of Physical Chemistry A 2003, 107 (30), 5643-5649.

18. Hill, S. E.; Bandaria, J. N.; Fox, M.; Vanderah, E.; Kohen, A.; Cheatum, C. M., Exploring the Molecular Origins of Protein Dynamics in the Active Site of Human Carbonic Anhydrase II. The Journal of Physical Chemistry B 2009, 113 (33), 11505-11510.

19. Bandaria, J. N.; Dutta, S.; Hill, S. E.; Kohen, A.; Cheatum, C. M., Fast Enzyme Dynamics at the Active Site of Formate Dehydrogenase. Journal of the American Chemical Society 2007, 130 (1), 22-23.

20. Garcia-Viloca, M.; Nam, K.; Alhambra, C.; Gao, J., Solvent and Protein Effects on the Vibrational Frequency Shift and Energy Relaxation of the Azide Ligand in Carbonic Anhydrase. The Journal of Physical Chemistry B 2004, 108 (35), 13501-13512.

21. Lim, M.; Hamm, P.; Hochstrasser, R. M., Protein fluctuations are sensed by stimulated infrared echoes of the vibrations of carbon monoxide and azide probes. Proceedings of the National Academy of Sciences of the United States of America 1998, 95 (26), 15315-15320.

22. Hamm, P.; Lim, M.; Hochstrasser, R. M., Structure of the Amide I Band of Peptides Measured by Femtosecond Nonlinear-Infrared Spectroscopy. The Journal of Physical Chemistry B 1998, 102 (31), 6123-6138.

23. Asplund, M. C.; Zanni, M. T.; Hochstrasser, R. M., Two-dimensional infrared spectroscopy of peptides by phase-controlled femtosecond vibrational photon echoes. Proceedings of the National Academy of Sciences of the United States of America 2000, 97 (15), 8219-8224.

24. Bagchi, S.; Charnley, A. K.; Smith Iii, A. B.; Hochstrasser, R. M., Equilibrium Exchange Processes of the Aqueous Tryptophan Dipeptide. The Journal of Physical Chemistry B 2009, 113 (24), 8412-8417.

25. Bagchi, S.; Falvo, C.; Mukamel, S.; Hochstrasser, R. M., 2D-IR Experiments and Simulations of the Coupling between Amide-I and Ionizable Side Chains in Proteins: Application to the Villin Headpiece. The Journal of Physical Chemistry B 2009, 113 (32), 11260-11273.

26. Fang, C.; Hochstrasser, R. M., Two-Dimensional Infrared Spectra of the 13C18O Isotopomers of Alanine Residues in an Œ±-Helix. The Journal of Physical Chemistry B 2005, 109 (39), 18652-18663.

27. Finkelstein, I. J.; Ishikawa, H.; Kim, S.; Massari, A. M.; Fayer, M. D., Substrate binding and protein conformational dynamics measured by 2D-IR vibrational echo spectroscopy. Proceedings of the National Academy of Sciences 2007, 104 (8), 2637-2642.

28. Kim, Y. S.; Hochstrasser, R. M., Chemical exchange 2D IR of hydrogen-bond making and breaking. Proceedings of the National Academy of Sciences of the United States of America 2005, 102 (32), 11185-11190.

29. Kim, Y. S.; Hochstrasser, R. M., Dynamics of Amide-I Modes of the Alanine Dipeptide in D2O,Ä†. The Journal of Physical Chemistry B 2005, 109 (14), 6884-6891.

30. Kim, Y. S.; Hochstrasser, R. M., Applications of 2D IR Spectroscopy to Peptides, Proteins, and Hydrogen-Bond Dynamics,Ä†. The Journal of Physical Chemistry B 2009, 113 (24), 8231-8251.

31. Kim, Y. S.; Liu, L.; Axelsen, P. H.; Hochstrasser, R. M., 2D IR provides evidence for mobile water molecules in Œ≤-amyloid fibrils. Proceedings of the National Academy of Sciences 2009, 106 (42), 17751-17756.

32. Krummel, A. T.; Zanni, M. T., DNA Vibrational Coupling Revealed with Two-Dimensional Infrared Spectroscopy:,Äâ Insight into Why Vibrational Spectroscopy Is Sensitive to DNA Structure. The Journal of Physical Chemistry B 2006, 110 (28), 13991-14000.

33. Krummel, A. T.; Zanni, M. T., Evidence for Coupling between Nitrile Groups Using DNA Templates: A Promising New Method for Monitoring Structures with Infrared Spectroscopy. The Journal of Physical Chemistry B 2008, 112 (5), 1336-1338.

34. Massari, A. M.; McClain, B. L.; Finkelstein, I. J.; Lee, A. P.; Reynolds, H. L.; Bren, K. L.; Fayer, M. D., Cytochrome c552 Mutants:,Äâ Structure and Dynamics at the Active Site Probed by Multidimensional NMR and Vibration Echo Spectroscopy,Ä†. The Journal of Physical Chemistry B 2006, 110 (38), 18803-18810.

35. McClain, B. L.; Finkelstein, I. J.; Fayer, M. D., Vibrational echo experiments on red blood cells: Comparison of the dynamics of cytoplasmic and aqueous hemoglobin. Chemical Physics Letters 2004, 392 (4-6), 324-329.

36. Merchant, K. A.; Noid, W. G.; Akiyama, R.; Finkelstein, I. J.; Goun, A.; McClain, B. L.; Loring, R. F.; Fayer, M. D., Myoglobin-CO Substate Structures and Dynamics:,Äâ Multidimensional Vibrational Echoes and Molecular Dynamics Simulations. Journal of the American Chemical Society 2003, 125 (45), 13804-13818.

37. Merchant, K. A.; Xu, Q.-H.; Thompson, D. E.; Fayer, M. D., Frequency Selected Ultrafast Infrared Vibrational Echo Studies of Liquids, Glasses, and Proteins. The Journal of Physical Chemistry A 2002, 106 (38), 8839-8849.

38. Mukherjee, P.; Kass, I.; Arkin, I. T.; Zanni, M. T., Picosecond dynamics of a membrane protein revealed by 2D IR. Proceedings of the National Academy of Sciences of the United States of America 2006, 103 (10), 3528-3533.

39. Park, J.; Hochstrasser, R. M., Multidimensional infrared spectroscopy of a peptide intramolecular hydrogen bond. Chemical Physics 2006, 323 (1), 78-86.

40. Paul, C.; Wang, J.; Wimley, W. C.; Hochstrasser, R. M.; Axelsen, P. H., Vibrational Coupling, Isotopic Editing, and Œ≤-Sheet Structure in a Membrane-Bound Polypeptide. Journal of the American Chemical Society 2004, 126 (18), 5843-5850.

41. Rubtsov, I. V.; Wang, J.; Hochstrasser, R. M., Dual-frequency 2D-IR spectroscopy heterodyned photon echo of the peptide bond. Proceedings of the National Academy of Sciences of the United States of America 2003, 100 (10), 5601-5606.

42. Strasfeld, D. B.; Ling, Y. L.; Shim, S.-H.; Zanni, M. T., Tracking Fiber Formation in Human Islet Amyloid Polypeptide with Automated 2D-IR Spectroscopy. Journal of the American Chemical Society 2008, 130 (21), 6698-6699.

43. Wang, J.; Chen, J.; Hochstrasser, R. M., Local Structure of Œ≤-Hairpin Isotopomers by FTIR, 2D IR, and Ab Initio Theory. The Journal of Physical Chemistry B 2006, 110 (14), 7545-7555.

44. Anna, J. M.; Ross, M. R.; Kubarych, K. J., Dissecting Enthalpic and Entropic Barriers to Ultrafast Equilibrium Isomerization of a Flexible Molecule Using 2DIR Chemical Exchange Spectroscopy. The Journal of Physical Chemistry A 2009, 113 (24), 6544-6547.

45. Cahoon, J. F.; Sawyer, K. R.; Schlegel, J. P.; Harris, C. B., Determining Transition-State Geometries in Liquids Using 2D-IR. Science 2008, 319 (5871), 1820-1823.

46. Kwak, K.; Zheng, J.; Cang, H.; Fayer, M. D., Ultrafast Two-Dimensional Infrared Vibrational Echo Chemical Exchange Experiments and Theory‚Ä†. The Journal of Physical Chemistry B 2006, 110 (40), 19998-20013.

47. Zheng, J.; Kwak, K.; Chen, X.; Asbury, J. B.; Fayer, M. D., Formation and Dissociation of Intra‚àíIntermolecular Hydrogen-Bonded Solute‚àíSolvent Complexes:‚Äâ Chemical Exchange Two-Dimensional Infrared Vibrational Echo Spectroscopy. Journal of the American Chemical Society 2006, 128 (9), 2977-2987.

48. Zheng, J.; Kwak, K.; Steinel, T.; Asbury, J.; Chen, X.; Xie, J.; Fayer, M. D., Accidental vibrational degeneracy in vibrational excited states observed with ultrafast two-dimensional IR vibrational echo spectroscopy. The Journal of Chemical Physics 2005, 123 (16), 164301-7.

49. Zheng, J.; Kwak, K.; Xie, J.; Fayer, M. D., Ultrafast Carbon-Carbon Single-Bond Rotational Isomerization in Room-Temperature Solution. Science 2006, 313 (5795), 1951-1955.

50. Ishikawa, H.; Kwak, K.; Chung, J. K.; Kim, S.; Fayer, M. D., Direct observation of fast protein conformational switching. Proceedings of the National Academy of Sciences 2008, 105 (25), 8619-8624.

51. Fayer, M. D., Dynamics of Liquids, Molecules, and Proteins Measured with Ultrafast 2D IR Vibrational Echo Chemical Exchange Spectroscopy. Annual Review of Physical Chemistry 2009, 60 (1), 21-38.

52. Zheng, J.; Kwak, K.; Asbury, J.; Chen, X.; Piletic, I. R.; Fayer, M. D., Ultrafast Dynamics of Solute-Solvent Complexation Observed at Thermal Equilibrium in Real Time. Science 2005, 309 (5739), 1338-1343.

53. Sung, J.; Silbey, R. J., Four wave mixing spectroscopy for a multilevel system. The Journal of Chemical Physics 2001, 115 (20), 9266-9287.

54. Khalil, M.; Demirdoven, N.; Tokmakoff, A., Coherent 2D IR Spectroscopy: Molecular Structure and Dynamics in Solution. The Journal of Physical Chemistry A 2003, 107 (27), 5258-5279.

55. Fecko, C. J.; Loparo, J. J.; Roberts, S. T.; Tokmakoff, A., Local hydrogen bonding dynamics and collective reorganization in water: Ultrafast infrared spectroscopy of HOD/D[sub 2]O. The Journal of Chemical Physics 2005, 122 (5), 054506-18.

56. Nesbitt, D. J.; Field, R. W., Vibrational Energy Flow in Highly Excited Molecules: Role of Intramolecular Vibrational Redistribution. The Journal of Physical Chemistry 1996, 100 (31), 12735-12756.

57. Cheatum, C. M.; Heckscher, M. M.; Bingemann, D.; Crim, F. F., CH[sub 2]I[sub 2] fundamental vibrational relaxation in solution studied by transient electronic absorption spectroscopy. The Journal of Chemical Physics 2001, 115 (15), 7086-7093.

58. Graener, H.; Zurl, R.; Hofmann, M., Vibrational Relaxation of Liquid Chloroform. The Journal of Physical Chemistry B 1997, 101 (10), 1745-1749.

59. Hill, J. R.; Chronister, E. L.; Chang, T.-C.; Kim, H.; Postlewaite, J. C.; Dlott, D. D., Vibrational relaxation and vibrational cooling in low temperature molecular crystals. The Journal of Chemical Physics 1988, 88 (2), 949-967.

60. Yoo, H. S.; DeWitt, M. J.; Pate, B. H., Vibrational Dynamics of Terminal Acetylenes: I. Comparison of the Intramolecular Vibrational Energy Redistribution Rate of Gases and the Total Relaxation Rate of Dilute Solutions at Room Temperature. The Journal of Physical Chemistry A 2004, 108 (8), 1348-1364.

61. Yoo, H. S.; DeWitt, M. J.; Pate, B. H., Vibrational Dynamics of Terminal Acetylenes: II. Pathway for Vibrational Relaxation in Gas and Solution. The Journal of Physical Chemistry A 2004, 108 (8), 1365-1379.

62. Yoo, H. S.; McWhorter, D. A.; Pate, B. H., Vibrational Dynamics of Terminal Acetylenes: III. Comparison of the Acetylenic C,àíH Stretch Intramolecular Vibrational-Energy Redistribution Rates in Ultracold Molecular Beams, Room-Temperature Gases, and Room-Temperature Dilute Solutions. The Journal of Physical Chemistry A 2004, 108 (8), 1380-1387.

63. Bakker, H. J.; Planken, P. C. M.; Kuipers, L.; Lagendijk, A., Ultrafast infrared saturation spectroscopy of chloroform, bromoform, and iodoform. The Journal of Chemical Physics 1991, 94 (3), 1730-1739.

64. Bakker, H. J.; Planken, P. C. M.; Lagendijk, A., Role of solvent on vibrational energy transfer in solution. Nature 1990, 347 (6295), 745-747.

65. Bakker, H. J.; Planken, P. C. M.; Lagendijk, A., Ultrafast vibrational dynamics of small organic molecules in solution. The Journal of Chemical Physics 1991, 94 (9), 6007-6013.

66. Elles, C. G.; Bingemann, D.; Heckscher, M. M.; Crim, F. F., Vibrational relaxation of CH[sub 2]I[sub 2] in solution: Excitation level dependence. The Journal of Chemical Physics 2003, 118 (12), 5587-5595.

67. Alfano, R. R.; Shapiro, S. L., Establishment of a Molecular-Vibration Decay Route in a Liquid. Physical Review Letters 1972, 29 (25), 1655.

68. Laubereau, A.; von der Linde, D.; Kaiser, W., Direct Measurement of the Vibrational Lifetimes of Molecules in Liquids. Physical Review Letters 1972, 28 (18), 1162.

69. von der Linde, D.; Laubereau, A.; Kaiser, W., Molecular Vibrations in Liquids: Direct Measurement of the Molecular Dephasing Time; Determination of the Shape of Picosecond Light Pulses. Physical Review Letters 1971, 26 (16), 954.

70. Assmann, J.; Benten, R. v.; Charvat, A.; Abel, B., Vibrational Energy Relaxation of Selectively Excited Aromatic Molecules in Solution: The Effect of a Methyl Rotor and Its Chemical Substitution. The Journal of Physical Chemistry A 2003, 107 (12), 1904-1913.

71. Assmann, J.; von Benten, R.; Charvat, A.; Abel, B., Intra- and Intermolecular Vibrational Energy Relaxation of C‚àíH Overtone Excited Benzonitrile, para-Difluorobenzene, and Pyrazine in Solution. The Journal of Physical Chemistry A 2003, 107 (27), 5291-5297.

72. Bingemann, D.; King, A. M.; Crim, F. F., Transient electronic absorption of vibrationally excited CH[sub 2]I[sub 2]: Watching energy flow in solution. The Journal of Chemical Physics 2000, 113 (12), 5018-5025.

73. Graener, H.; Patzlaff, T.; Kadarisman, N.; Seifert, G., Observation of intensity dependent, non-exponential vibrational relaxation in liquid bromoform. Chemical Physics Letters 2001, 348 (5-6), 403-410.

74. Hartl, I.; Zinth, W., Redistribution and Relaxation of Vibrational Excitation of CH-Stretching Modes in 1,1-Dichloroethylene and 1,1,1-Trichloroethane. The Journal of Physical Chemistry A 2000, 104 (18), 4218-4222.

75. Deak, J. C.; Iwaki, L. K.; Dlott, D. D., Vibrational Energy Redistribution in Polyatomic Liquids: Ultrafast IR‚àíRaman Spectroscopy of Acetonitrile. The Journal of Physical Chemistry A 1998, 102 (42), 8193-8201.

76. Boyarkin, O. V.; Rizzo, T. R.; Perry, D. S., Intramolecular energy transfer in highly vibrationally excited methanol. II. Multiple time scales of energy redistribution. The Journal of Chemical Physics 1999, 110 (23), 11346-11358.

77. Iwaki, L. K.; Dlott, D. D., Ultrafast vibrational energy redistribution within C-H and O-H stretching modes of liquid methanol. Chemical Physics Letters 2000, 321 (5-6), 419-425.

78. Bruehl, M.; Hynes, J. T., Vibrational relaxation times for a model hydrogen-bonded complex in a polar solvent. Chemical Physics 1993, 175 (1), 205-221.

79. Ramesh, S. G.; Sibert Iii, E. L., Combined perturbative-variational investigation of the vibrations of CHBr[sub 3] and CDBr[sub 3]. The Journal of Chemical Physics 2004, 120 (23), 11011-11025.

80. Sibert Iii, E. L.; Reinhardt, W. P.; Hynes, J. T., Intramolecular vibrational relaxation and spectra of CH and CD overtones in benzene and perdeuterobenzene. The Journal of Chemical Physics 1984, 81 (3), 1115-1134.

81. Sibert Iii, E. L.; Rey, R., Vibrational relaxation in liquid chloroform following ultrafast excitation of the CH stretch fundamental. The Journal of Chemical Physics 2002, 116 (1), 237-257.

82. Seifert, G.; Zurl, R.; Patzlaff, T.; Graener, H., Time-resolved observation of intermolecular vibrational energy transfer in liquid bromoform. The Journal of Chemical Physics 2000, 112 (14), 6349-6354.

83. Brauner, J. W.; Dugan, C.; Mendelsohn, R., 13C Isotope Labeling of Hydrophobic Peptides. Origin of the Anomalous Intensity Distribution in the Infrared Amide I Spectral Region of Œ≤-Sheet Structures. Journal of the American Chemical Society 2000, 122 (4), 677-683.

84. Sudo, Y.; Furutani, Y.; Wada, A.; Ito, M.; Kamo, N.; Kandori, H., Steric Constraint in the Primary Photoproduct of an Archaeal Rhodopsin from Regiospecific Perturbation of C‚àíD Stretching Vibration of the Retinyl Chromophore. Journal of the American Chemical Society 2005, 127 (46), 16036-16037.

85. Owrutsky, J. C.; Culver, J. P.; Li, M.; Kim, Y. R.; Sarisky, M. J.; Yeganeh, M. S.; Yodh, A. G.; Hochstrasser, R. M., Femtosecond coherent transient infrared spectroscopy of CO on Cu(111). The Journal of Chemical Physics 1992, 97 (6), 4421-4427.

86. Wells, J.-P. R.; Rella, C. W.; Bradley, I. V.; Galbraith, I.; Pidgeon, C. R., Coherent Dynamics of the Localized Vibrational Modes of Hydrogen in CaF2. Physical Review Letters 2000, 84 (21), 4998.

87. Lim, M.; Hochstrasser, R. M., Unusual vibrational dynamics of the acetic acid dimer. The Journal of Chemical Physics 2001, 115 (16), 7629-7643.

88. Maekawa, H.; Ohta, K.; Tominaga, K., Vibrational Population Relaxation of the ‚àíNCN‚àí Antisymmetric Stretching Mode of Carbodiimide Studied by the Infrared Transient Grating Method. The Journal of Physical Chemistry A 2004, 108 (44), 9484-9491.

89. Zanni, M. T.; Asplund, M. C.; Hochstrasser, R. M., Two-dimensional heterodyned and stimulated infrared photon echoes of N-methylacetamide-D. The Journal of Chemical Physics 2001, 114 (10), 4579-4590.

90. Heckscher, M. M.; Sheps, L.; Bingemann, D.; Crim, F. F., Relaxation of the C--H stretching fundamental vibrations of CHI[sub 3], CH[sub 2]I[sub 2], and CH[sub 3]I in solution. The Journal of Chemical Physics 2002, 117 (19), 8917-8925.

91. The chloroform-d and bromoform-d frequenceies are gas phase values from http://webbook.nist.gov. For iodoform-d, the fundamental frequencies are not available. Therefore, we use the experimental value for the C-D stretch frequency and, for the other modes, we analyze the frequency shifts upon deuteration in chloroform and bromoform and scale the iodoform frequencies accordingly.

92. Corradi, E.; Meille, S. V.; Messina, M. T.; Metrangolo, P.; Resnati, G., Halogen Bonding versus Hydrogen Bonding in Driving Self-Assembly Processes13. Angewandte Chemie International Edition 2000, 39 (10), 1782-1786.

93. Metrangolo, P.; Neukirch, H.; Pilati, T.; Resnati, G., Halogen Bonding Based Recognition Processes:‚Äâ A World Parallel to Hydrogen Bonding‚Ä†. Accounts of Chemical Research 2005, 38 (5), 386-395.

94. Woys, A. M.; Lin, Y. S.; Reddy, A. S.; Xiong, W.; dePablo, J. J.; Skinner, J. L.; Zanni, M. T., 2D IR Line Shapes Probe Ovispirin Peptide Conformation and Depth in Lipid Bilayers. Journal of the American Chemical Society 2010, 132 (8).

95. Shim, S. H.; Gupta, R.; Ling, Y. L.; Strasfeld, D. P.; Raleigh, D. P.; Zanni, M. T., Two-dimensional IR spectroscopy and isotope labeling defines the pathway of amyloid formation with residue-specific resolution. Proceedings of the National Academy of Sciences 2009, 106 (16).

96. Eaves, J. D.; Tokmakoff, A.; Geisler, P. L., Journal of Physical Chemistry A 2005, 109 (42).

97. Asbury, J. B.; Steinel, T.; Fayer, M. D., Journal of Luminescence 2004, 107.

98. Asbury, J. B.; Steinel, T.; Fayer, M. D., Journal of Physical Chemistry B 2004, 108 (21).

99. Asbury, J. B.; Steinel, T.; Kwak, K.; Corcelli, S. A.; Lawerence, C. P.; Skinner, J. L.; Fayer, M. D., Journal of Chemical Physics 2004, 108 (7).

100. Asbury, J. B.; Steinel, T.; Stromberg, C.; Corcelli, S. A.; Lawrence, C. P.; Skinner, J. L.; Fayer, M. D., Journal of Physical Chemistry A 2004, 108 (7).

101. Steinel, T.; Asbury, J. B.; Corcelli, S. A.; Lawrence, C. P.; Skinner, J. L.; Fayer, M. D., Chemical Physics Letters 2004, 384, 295.

102. Ha, J.-H.; Kim, Y. S.; Hochstrasser, R. M., Vibrational dynamics of N--H, C--D, and C[Double Bond]O modes in formamide. The Journal of Chemical Physics 2006, 124 (6), 064508-10.

103. Kumar, K.; Sinks, L. E.; Wang, J. P.; Kim, Y. S.; Hochstrasser, R. M., Chemical Physics Letters 2006, 432, 122.

104. Naraharisetty, S. R. G.; Kurochkin, D. V.; Rubtsov, I. V., Chemical Physics Letters 2007, 437.

105. Miller, C. S.; Corcelli, S. A., Jpurnal of Physical Chemistry B 2009, 113 (24).

106. Miller, C. S.; LPloetz, E. A.; Cremeens, M. E.; Corcelli, S. A., Journal Chemical Physics 2009, 130 (12).

107. Cremeens, M. E.; Zimmermann, J.; Yu, W.; Dawson, P. E.; Romesberg, F. E., Journal of the American Chemical Society 2009, 113 (16).

108. Gundogdu, K.; Nydegger, M. W.; Bandaria, J. N.; Hill, S. E.; Cheatum, C. M., Vibrational relaxation of C--D stretching vibrations in CDCl[sub 3], CDBr[sub 3], and CDI[sub 3]. The Journal of Chemical Physics 2006, 125 (17), 174503-8.

109. Yoon, Y. H.; Hause, M. L.; Case, A. S.; Crim, F. F., Vibrational action spectroscopy of the C--H and C--D stretches in partially deuterated formic acid dimer. The Journal of Chemical Physics 2008, 128 (8), 084305-6.

110. Owrutsky, J. C.; Kim, Y. R.; Li, M.; Sarisky, M. J.; Hochstrasser, R. M., Determination of the vibrational energy relaxation time of the azide ion in protic solvents by two-color transient infrared spectroscopy. Chemical Physics Letters 1991, 184 (5-6), 368-374.

111. Finkelstein, I. J.; Zheng, J. R.; Ishikawa, H.; Kim, S.; Kwak, K.; Fayer, M. D., Physical Chemistry Chemical Physics 2007, 9 (13).

112. DeFlores, L. P.; Ganim, Z.; Nicodemus, R. A.; Tokmakoff, A., Amide I'-II" 2D IR Spectroscopy Provides Enhanced Protein Secondary Structure Sensitivity. Journal of the American Chemical Society 2009, 131 (9).

113. Ganim, Z.; Chung, H. S.; Smith, A. W.; DeFlores, L. P.; Jones, K. C.; Tokmakoff, A., Amide I two-dimensional infrared Spectroscopy of proteins. Accounts of Chemical Research 2008, 41 (3).

114. Kim, Y. S.; Liu, L.; Axelsen, P. H.; Hochstrasser, R. M., Two-dimensional infrared spectra of isotopically diluted amyloid fibrils from A beta 40. Proceedings of the National Academy of Science 2008, 105 (22).

115. Maekawa, H.; De Poli, M.; Moretto, A.; Toniolo, C.; Ge, N. H., Toward Detecting the Formation of a Single Helical Turn by 2D IR Cross Peaks between the Amide-I and -II Modes. Journal of Physical Chemistry B 2009, 113 (34).

116. Maekawa, H.; De Poli, M.; Toniolo, C.; Ge, N. H., Couplings between Peptide Linkages across a 3(10)-Helical Hydrogen Bond Revealed by Two-Dimensional Infrared Spectroscopy. Journal of the American Chemical Society 2009, 131 (6).

117. Sengupta, N.; Maekawa, H.; Zhuang, W.; Toniolo, C.; Mukamel, S.; Tobias, D. J.; Ge, N. H., Sensitivity of 2D IR Spectra to Peptide Helicity: A Concerted Experimental and Simulation Study of an Octapeptide. Journal of Physical Chemistry B 2009, 113 (35).

118. Strasfeld, D. B.; Ling, Y. L.; Gupta, R.; Raleigh, D. P.; Zanni, M. T., Strategies for Extracting Structural Information from 2D IR Spectroscopy of Amyloid: Application to Islet Amyloid Polypeptide. Journal of Physical Chemistry B 2009, 113 (47).

119. Sul, S.; Feng, Y.; Le, U.; Tobias, D. J.; Ge, N. H., Interactions of Tyrosine in Leu-Enkephalin at a Membrane-Water Interface: An Ultrafast Two-Dimensional Infrared Study Combined with Density Functional Calculations and Molecular Dynamics Simulations. Journal of Physical Chemistry B 2010, 114 (2).

120. Nicodemus, R. A.; Ramasesha, K.; Roberts, S. T.; Tokmakoff, A., Hydrogen Bond Rearrangements in Water Probed with Temperature-Dependent 2D IR. Journal of Physical Chemistry Letters 2010, 1 (7).

121. Roberts, S. T.; Ramasesha, K.; Tokmakoff, A., Structural Rearrangements in Water Viewed Through Two-Dimensional Infrared Spectroscopy. Accounts of Chemical Research 2009, 42 (9).

122. Roberts, S. T.; Petersen, P. B.; Ramasesha, K.; Tokmakoff, A., Observation of a Zundel-like transition state during proton transfer in aqueous hydroxide solutions. Proceedings of the National Academy of Science 2009, 106 (36).

123. Rosenfeld, D. E.; Kwak, K.; Gengeliczki, Z.; Fayer, M. D., Hydrogen Bond Migration between Molecular Sites Observed with Ultrafast 2D IR Chemical Exchange Spectroscopy. Journal of Physical Chemistry B 2010, 114 (7).

124. Moilanen, D. E.; Fenn, E. E.; Wong, D.; Rosenfeld, D. E.; Fayer, M. D., Ion-water hydrogen-bond switching observed with 2D IR vibrational echo chemical exchange spectroscopy. Proceedings of the National Academy of Science 2009, 106 (2).

125. Moilanen, D. E.; Fenn, E. E.; Wond, D.; Fayer, M. D., Water Dynamics at the Interface in AOT Reverse Micelles. Journal of Physical Chemistry B 2009, 113 (25).

126. Moilanen, D. E.; Fenn, E. E.; Wong, D.; Fayer, M. D., Geometry and Nanolength Scales versus Interface Interactions: Water Dynamics in AOT Lamellar Structures and Reverse Micelles. Journal of the American Chemical Society 2009, 131 (23).

127. Fayer, M. D.; Moilanen, D. E.; Wong, D.; Rosenfeld, D. E.; Fenn, E. E.; Park, S., Water Dynamics in Salt Solutions Studied with Ultrafast Two-Dimensional Infrared (2D IR) Vibrational Echo Spectroscopy. Accounts of Chemical Research 2009, 42 (9).

128. Huse, N.; Bruner, B. D.; Cowan, M. L.; Dreyer, J.; Nibbering, E. T. J.; Miller, R. J. D.; Elsaesser, T., Anharmonic Couplings Underlying the Ultrafast Vibrational Dynamics of Hydrogen Bonds in Liquids. Physical Review Letters 2005, 95 (14), 147402.

129. Heyne, K.; Nibbering, E. T.; Elsaesser, T.; Petkovic, M.; Kuhn, O., Cascaded energy redistribution upon O-H stretching excitation in an intramolecular hydrogen bond. Journal of Physical Chemistry A 2004, 108 (29).

130. Kuo, C. H.; Vorobyev, D. Y.; Chen, J. X.; Hochstrasser, R. M., Correlation of the vibrations of the aqueous azide ion with the O-H modes of bound water molecules. Journal of Physical Chemistry B 2007, 111 (50).

131. Kuo, C. H.; Hochstrasser, R. M., Two dimensional infrared spectroscopy and relaxation of aqueous cyanide. Chemical Physics 2007, 341 (1-3).

132. Hamm, P.; Lim, M.; Hochstrasser, R. M., Non-Markovian dynamics of the vibrations of ions in water from femtosecond infrared three-pulse photon echoes. Physics Review Letters 1998, 81 (24).

133. Ohta, K.; Tominaga, K., Dynamical interactions between solute and solvent studied by three-pulse photon echo method. Bulletin of the Chemical Society of Japan 2005, 78 (9).

134. Maekawa, H.; Ohta, K.; Tominaga, K., Spectral diffusion of the anti-symmetric stretching mode of azide ion in a reverse micelle studied by infrared three-pulse photon echo method. Physical Chemistry Chemical Physics 2004, 6 (16).

135. Bandaria, J. N.; Dutta, S.; Hill, S. E.; Kohen, A.; Cheatum, C. M., Fast enzyme dynamics at the active site of formate dehydrogenase. Journal of the American Chemical society 2008, 130 (1).

136. Fang, C.; Bauman, J. D.; Das, K.; Remorino, A.; Arnold, E.; Hochstrasser, R. M., Two-dimensional infrared spectra reveal relaxation of the nonnucleoside inhibitor TMC278 complexed with HIV-1 reverse transcriptase. Proceedings of the National Academy of Science 2008, 105 (5).

137. Waegele, M. M.; Tucker, M. J.; Gai, F., 5-Cyanotryptophan as an infrared probe of local hydration status of proteins. Chemical Physics Letters 2009, 478 (4-6).

138. Tucker, M. J.; Getahun, Z.; Nanda, V.; DeGrado, W. F.; Gai, F., A new method for determining the local environment and orientation of individual side chains of membrane-binding peptides. Journal of the American Chemical Society 2004, 126 (16).

139. McMahon, H. A.; Alfieri, K. N.; Clark, C. A. A.; Londergen, C. H., Cyanylated Cysteine: A Covalently Attached Vibrational Probe of Protein-Lipid Contacts. Journal of Physical Chemistry Letters 2010, 1 (5).

140. Edelstein, L.; Stetz, M. A.; McMahon, H. A.; Londergan, C. H., The Effects of alpha-Helical Structure and Cyanylated Cysteine on Each Other. Journal of Physical Chemistry B 2010, 114 (14).

141. Maienschein-Cline, M. G.; Londergan, C. H., The CN stretching band of aliphatic thiocyanate is sensitive to solvent dynamics and specific solvation. Journal of Physical Chemistry A 2007, 111 (40).

142. Fafarman, A. T.; Webb, L. J.; Chuang, J. I.; Boxer, S. G., Site-specific conversion of cysteine thiols into thiocyanate creates an IR probe for electric fields in proteins. Journal of the American Chemical Society 2006, 128 (41).

143. Tucker, M. J.; Kim, Y. S.; Hochstrasser, R. M., 2D IR photon echo study of the anharmonic coupling in the OCN region of phenyl cyanate. Chemical Physics Letters 2009, 470 (1-3), 80-84.

144. Oh, K.-I.; Lee, J.-H.; Joo, C.; Han, H.; Cho, M., b-Azidoalanine as an IR probe: Application to Amyloid Ab(16-22) Aggregation. Journal of Physical Chemistry B 2008, 112, 10352-10357.

145. Choi, J.-H.; Oh, K.-I.; Cho, M., Azido-derivatized compounds as IR probes of local electrostatic environments: Theoretical studies. Journal of Chemical Physics 2008, 129.

146. Petersen, P. B.; Roberts, S. T.; Ramasesha, K.; Nocera, D. G.; Tokmakoff, A., Ultrafast N-H Vibrational Dynamics of Cyclic Doubly Hydrogen-Bonded Homo- and Heterodimers. Journal of Physical Chemistry B 2008, 112 (42).

147. Dwyer, J. R.; Dreyer, J.; Nibbering, E. T. J.; Elsaesser, T., Ultrafast dynamics of vibrational N-H stretching excitations in the 7-azaindole dimer. Chemical Physical Letters 2006, 432 (1-3).

148. Heyne, K.; Huse, N.; Dreyer, J.; Nibbering, E. T. J.; Elsaesser, T.; Mukamel, S., Coherent low-frequency motions of hydrogen bonded acetic acid dimers in the liquid phase. Journal Chemical Physics 2004, 121 (2).

149. Gundogdu, K.; Bandaria, J.; Nydegger, M.; Rock, W.; Cheatum, C. M., Relaxation and anharmonic couplings of the O--H stretching vibration of asymmetric strongly hydrogen-bonded complexes. The Journal of Chemical Physics 2007, 127 (4), 044501-9.

150. Mukamel, S., Principles of Nonlinear Optical Spectroscopy. Oxford University Press: New York, 1995.